N71-24820

EXPERIMENTAL STUDY OF PLASTIC YIELDING AT THE TIP OF SURFACE FLAW CRACKS

P. H. Francis, et al

Southwest Research Institute
San Antonio, Texas

May 1971

NASA CR-114934

EXPERIMENTAL STUDY OF PLASTIC YIELDING AT THE TIP OF SURFACE FLAW CRACKS

by

P. H. Francis

D. L. Davidson

H. C. Burghard

A. Nagy

FINAL REPORT

Contract NAS 9-9493

Prepared for

NATIONAL AERONAUTICS AND SPACE ADMINISTRATION

Technical Management
NASA Manned Spacecraft Center
Houston, Texas
R. G. Forman

May 1971

SOUTHWEST RESEARCH INSTITUTE

San Antonio, Texas

Requests for copies of this report should be referred to

National Aeronautics and Space Administration
Office of Scientific and Technical Information
Attention. AFSS-A
Washington, D.C 20546

NASA CR-114934

EXPERIMENTAL STUDY OF PLASTIC YIELDING AT THE TIP OF SURFACE FLAW CRACKS

by
P. H. Francis
D. L. Davidson
H. C. Burghard
A. Nagy

FINAL REPORT
Contract NAS 9-9493

Prepared for

NATIONAL AERONAUTICS AND SPACE ADMINISTRATION

Technical Management
NASA Manned Spacecraft Center
Houston, Texas
R. G. Forman

May 1971

SOUTHWEST RESEARCH INSTITUTE
San Antonio, Texas

FOREWORD

This is the final report on a program entitled "Experimental Study of Plastic Yielding at the Tip of Surface Flaw Cracks" conducted under Contract NAS 9-9493 to NASA Manned Spacecraft Center. The project was under the technical cognizance of Mr. Royce G. Forman, NASA, and was managed by Dr. Philip H. Francis, SwRI. The work was performed over the period 14 May 1969 to 30 May 1971. In addition to the authors, others involved in a supporting technical capacity include Dr. R. L. Bond and Mr. S. A. Cerwin (Michelson Interferometry), Messrs. H. M. Green and J. G. Barbee (metallography), A. J. Winfield and B. C. Bolton (Talysurf), and A. F. Muller (programming).

ABSTRACT

An experimental investigation was undertaken to determine the stability, surface deformation characteristics, and extent of plastic yielding associated with semi-elliptical surface cracks in plates subjected to tensile loading. The experiments involved both Fe-3Si and Ti-6Al-4V specimens, and a wide range of crack geometries and applied loads were included in the test matrix. Following loading, the Fe-3Si specimens were subjected to an electrolytic etching treatment to reveal the plastic zones in various planes intersecting the crack. Available analytical models of yield zone size and stress intensity factor were used to correlate the data.

SUMMARY

The study herein undertaken concerned surface cracks in Fe-3Si and Ti-6Al-4V plate specimens loaded in axial tension perpendicular to the notch plane The surface notches were introduced by the EDM process, and were subsequently fatigue cracked to provide a true crack front. The surface cracks were idealized as semi-elliptical in shape, and a wide variety of crack parameters were investigated in the testing program. An electrolytic etching technique was used in conjunction with the Fe-3Si specimens to reveal the configuration of the plastic zone circumscribing the crack front Measurements were also made of the front and back surface dimpling patterns on both specimen materials. The principal conclusions arising from this study are summarized below:

1 The electrolytic strain etching technique used on the Fe-3Si specimens revealed plastic deformation at plastic strain levels of about 0.06% and higher.

2. Among the seven analytical models for stress intensity factor calculations of surface cracks investigated, the ones of Paris & Sih (Ref 7) and Kobayashi & Moss (Ref. 9) were most generally applicable to the range of crack parameters investigated The elastic model of Rice & Levy (Ref. 11) predicts a somewhat lower value, while the Model of Anderson, Holms, and Orange (Ref. 13) predicts a somewhat higher value. The models of Smith (Ref. 8) and Orange (Ref. 10) are modifications of the original model of Irwin (Ref. 6) and yield stress intensity factor predictions in approximately mutual agreement, but are limited to relatively shallow cracks

3. The crack experiences a state essentially of plane strain over most of the crack front, with plane stress prevailing over a region of shallow depth in the vicinity of the front surface crack tips.

4. Visually observed back surface dimpling developed consistently at stress levels well below those predicted by theoretical models of yield zone penetration into the back surface.

5. In tests with deep cracks in Ti-6Al-4V it was found that stress levels required for back surface dimple development were lower than those required for the formation of front surface crack tip dimples

TABLE OF CONTENTS

TABLE OF CONTENTS (Cont'd)

LIST OF FIGURES

LIST OF FIGURES (Cont'd)

LIST OF FIGURES (Cont'd)

LIST OF TABLES

I. INTRODUCTION

Introduction

In 1966, concern over the structural integrity of the tankage for the Apollo system arose when unexpected failures developed during verification testing. Nondestructive testing techniques commonly employed for inspection purposes have generally been successful in isolating surface flaws on tankage equipment. Such flaws appear as a result of material processing, fabrication and handling, and may be sufficiently large to become critical at operating stress levels. At the present time, the technology of fracture mechanics has not matured to the point where accurate estimates can be made of the stress intensity factors and plastic zone fields associated with surface notches over the wide range of flaw parameters observed in inspection and proof testing. Thus, wide nondestructive inspections may be quite capable of isolating cracks of a potentially critical size, a problem arises in defining adequate criteria for acceptance.

The purpose of this program was to learn more about the behavior of surface flaws of the type that occur during proof testing of Ti-6Al-4V titanium alloy characteristic of that used in the Apollo spacecraft pressure vessels. It was felt that if the effect of flaw configuration and stress level on the extent of local plastic deformation and surface deformation patterns could be evaluated, it would be possible to prescribe more realistic limits to NDT acceptance criteria. A companion purpose was to compare and evaluate current analytical models for the determination of stress intensity factors and the extent of local plastic deformation. To achieve these objectives, an experimental program was designed utilizing specimens having a wide range of flat semi-elliptical flaw configurations and applied stress levels. In order to delineate the plastic zones associated with surface flaws, an auxiliary material, iron-3% silicon, was selected for a number of the experiments because of its susceptibility to preferential response to plastic strain using known electrolytic etching and metallographic techniques. While the majority of the specimens were fabricated of Fe-3Si in thicknesses of from 0.1 to 0.5 inch, a number of parallel tests were conducted with Ti-6Al-4V in an attempt to infer the behavior of surface cracked titanium alloy from the detailed knowledge of the Fe-3Si behavior

The program resulted in a rather extensive body of experimental data describing the nature of the plastic deformation fields and surface deformations associated with surface notches in Mode I loading. In this final report, an attempt has been made to relate these data to the crack parameters and external loading. At the same time, seven

different analytical models which exist in the current technical literature for stress intensity factors associated with surface cracks were examined and compared against each other. While predictive models of stress intensity factors and plastic zones are not yet sufficiently developed to provide all the desired information relating to surface flaw stability, much has been learned from this study.

Following the present Introduction, Section II deals with specimen design and preparation. Section III describes the experimental procedures used in loading the specimen, the metallography, and the surface deformation measurements. Section IV summarizes the present state of knowledge regarding stress intensity factors and plastic zone configurations associated with flat, semi-elliptical surface cracks. Section V contains a statement of the principal results of the program. The report concludes with the references in Section VI, and an Appendix which contains a number of additional photomicrographs of etched plastic zones taken from the Fe-3Si specimens.

II. SPECIMEN DESIGN AND PREPARATION

II. A Materials

The experimental program employed two specimen materials, an iron silicon alloy and a titanium aluminum vanadium alloy. The utilization of the iron silicon alloy as a specimen material is particularly advantageous to the purposes of the program in that it is one of the few alloys in which plastic strain can be readily observed and quantified by metallographic techniques. The titanium alloy employed, Ti-6Al-4V, was selected because of its widespread usage in aerospace structural components. In particular, this alloy is the principal material for the tankage of the Apollo space vehicle system.

The particular iron-silicon material employed was a nominal Fe-3Si alloy, AL No. 9 Hot Rolled Silicon Relay Plate* The material was procured in three thicknesses, 0.1 inch, 0.2 inch and 0 5 inch. A single billet of this material was selected from a production run (Heat No. 208268) and specially rolled to the desired thicknesses. The chemical analysis of the iron silicon alloy as indicated by the mill test report is presented in Table II. 1.

TABLE II. 1

MILL TEST REPORT COMPOSITION OF Fe-3Si ALLOY
ALLEGHENY LUDLUM HEAT NO. 208268

Carbon	0.026%
Silicon	3 21%
Manganese	0.056%
Chromium	0.028%
Nickel	0.073%
Phosphorous	0.007%
Sulfur	0.020%

After receipt of the material at SwRI, uniaxial tensile specimens were prepared from the 0.5 inch thick material and tested in a universal testing machine. The test specimens were fabricated with a 2-inch gage length and a test section 0.25 inch thick by 0.50 inch wide. The average

* Purchased from Allegheny Ludlum Steel Corporation, Pittsburgh, Pa.

tensile properties determined from four tests on the 0.5 inch Fe-3Si material were as follows:

Ultimate tensile strength	74,100 psi
Yield strength	57,500 psi
Elongation in 2 inches	9.7%

Metallographic sections of samples of each thickness of Fe-3Si alloy received were prepared and examined to establish the as-received microstructure. Photomicrographs illustrating the typical microstructure of each thickness of material are shown in Figure II. 1.

The 0.1 inch thick material was characterized by extensive grain elongation in the longitudinal direction as is evident in Figure II. 1a. This material exhibited a tendency toward dark etching of some of the grains. The 0.2 inch material exhibited an equiaxed grain structure with a relatively small grain size, Figure II. 1b. The 0.5 inch thick material was characterized by a grain size considerably larger than that of the 0.2 inch material and exhibited a limited degree of grain elongation in the longitudinal direction of the specimen Some evidence of small matrix precipitates was noted, and this specimen group also exhibited a tendency for dark etching of some of the grains

The Ti-6Al-4V material was procured as annealed plate in two thicknesses, 0.1 inch and 0 5 inch*. The chemical analyses and mechanical properties of this material, as indicated by the certification test report, are presented in Tables II. 2 and II. 3.

TABLE II 2

NOMINAL COMPOSITION OF Ti-6Al-4V ALLOY MATERIAL
CERTIFICATION REPORT - ACTIVE METALS INC.

Thickness In.	Heat No.	Composition - Wt. % Al	V	Fe	N_2	O_2	H_2	C
0.50	K-1145	6.0	4.2	0.11	0.010	0.15	0.005	0.022
0 10	G-6733	5 72	4.30	0 05	0.013	0.11	0.006	0.05

* Purchased from Active Alloys, Inc., Elizabeth, New Jersey

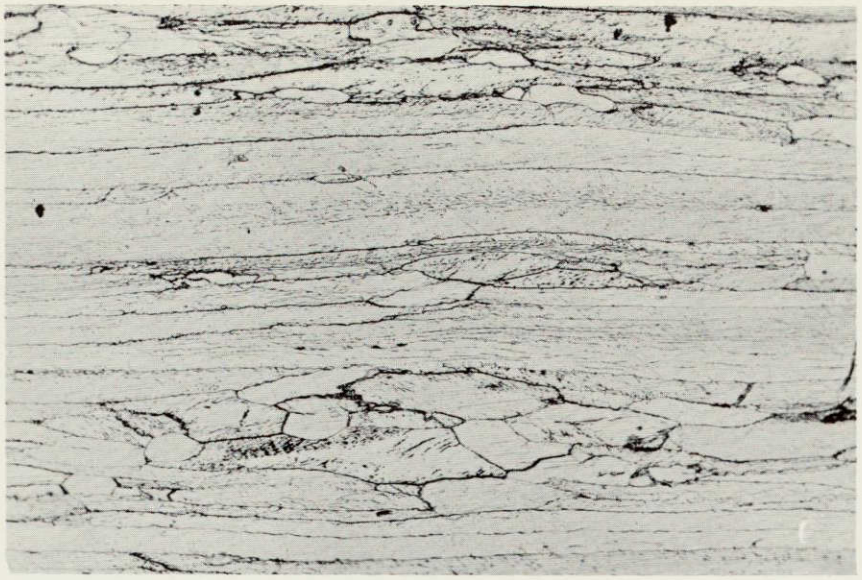

a) 0.1 inch

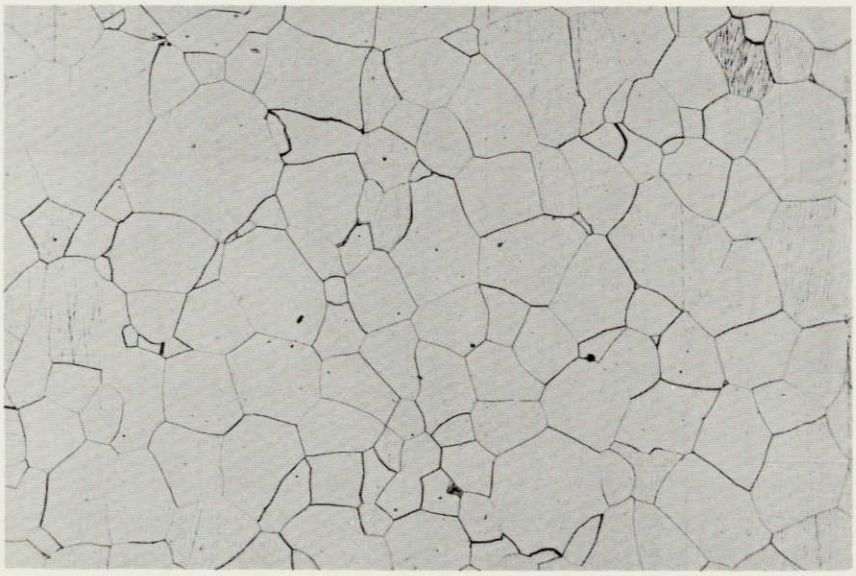

b) 0.2 inch

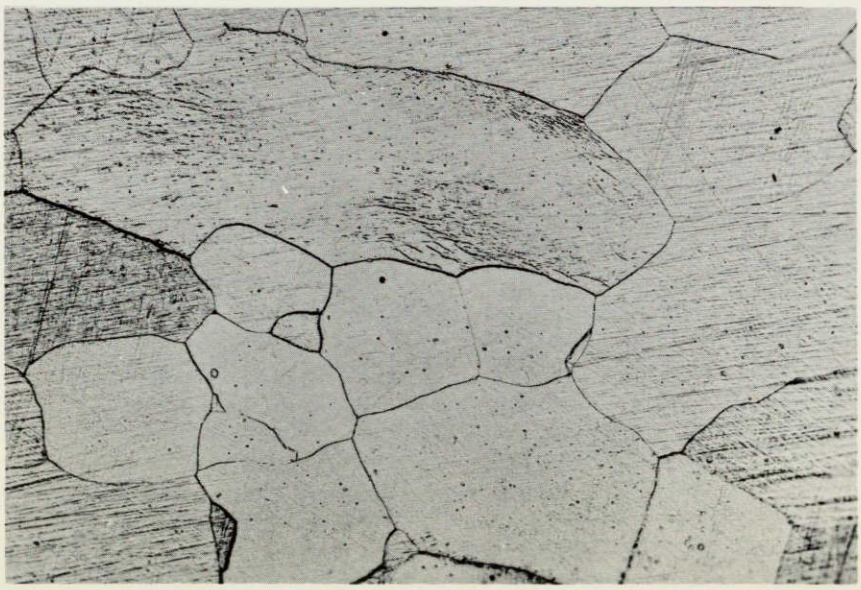

c) 0.5 inch

Figure II.1 As-Received Microstructure of Fe-3Si, 75X

TABLE II. 3

NOMINAL MECHANICAL PROPERTIES OF Ti-6A1-4V ALLOY MATERIAL CERTIFICATION REPORT - ACTIVE METALS, INC.

Thickness in.	Heat No.	U. T. S. psi	Y. S. psi	Elong. % in 2 in
0. 50	K-1145	137, 600	134, 300	17. 5
0. 10	G-6733	139, 000	133, 000	19 0

Uniaxial tensile specimens of the 0. 10 inch thick Ti-6A1-4V alloy material were prepared and tested. These specimens were fabricated with a 2-inch gage length and a test section 0. 10 inch thick by 0 50 inch wide. The average mechanical properties as determined by two tests were as follows:

Ultimate tensile strength	149, 000 psi
Yield strength	144, 100 psi
Elongation in 2 inches	12. 6 percent
Reduction of area	20. 6 percent

II B Test Specimens

Specimens for the test program were fabricated from Fe-3Si with nominal thicknesses of 0. 1, 0. 2, and 0. 5 inch and from Ti-6A1-4V with nominal thicknesses of 0. 1 and 0. 5 inch. The 0. 5 inch Titanium specimens were not tested at full thickness, but were modified by milling them to 0. 2 inch thickness in the test section. Four such specimens were made, two of which were used for determination of K_{Ic}. The general shape of all the specimens was the same as of standard flat tensile specimens, with the length of the test section taken to be three times the neck radius as shown in Figure II. 2. Setting this restriction, it was assumed that the 3R long uniform section was sufficiently long to result in a uniform stress distribution at the center region of the specimen The specimens were saw-cut to size in accordance with the test matrix given in Table II. 4 of Section II. D, and were finish-ground one inch above and below the notch on both front and back surfaces. This was done to facilitate metallographic preparation.

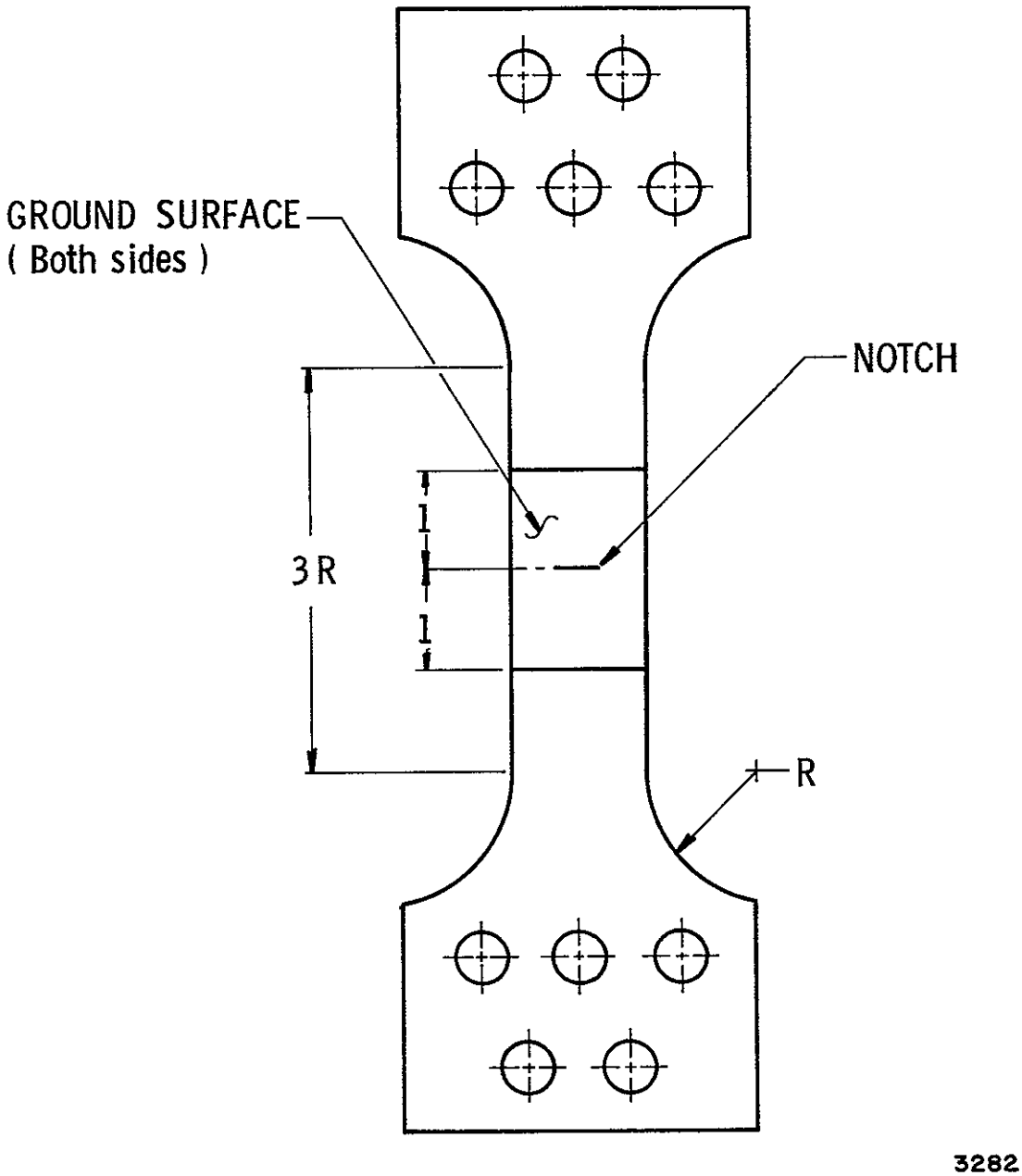

Figure II.2 Test Specimen

II. C EDM

The surface notches were introduced into the specimen by the electric discharge machining (EDM) technique*. Notch widths were nominally held to the following dimensions:

Specimen Material	Nominal Specimen Thickness	Nominal EDM Notch Width
Fe-3Si	0.1"	0.01"
Fe-3Si	0.2"	0.02"
Fe-3Si	0.5"	0.02"
Ti-6Al-4V	0.1"	0.01"
Ti-6Al-4V	0.2"	0.02"

The notch root radius, in all cases, was maintained to a nominal dimension of 0.004 inch Tolerances on the notch length (2c) and depth (a) were, respectively, $\pm$ 0.05 inch and $\pm$ 0.005 inch.

II. D Specimen and Notch Configurations Tested

The specimens were grouped according to material, thickness, and notch configuration as shown in Table II. 4. In the Table, and throughout this report, t refers to the specimen thickness, W to the specimen width, a to the crack depth, and c to the half-length of the surface crack. These parameters are illustrated in Figure IV. 1. In Table II. 4, the crack parameters a and c refer to the notch configuration as introduced by the EDM process, not to the final crack dimensions as achieved through subsequent fatigue cracking

* This work was performed under subcontract to the Institute by Production Die Casting Company, Houston, Texas.

TABLE II. 4

SCHEDULE OF SPECIMENS AND NOTCH CONFIGURATIONS
(BEFORE FATIGUE CRACKING)

Spec. No.	Material	$t^{(1)}$	$W^{(2)}$	$a^{(3)}$	$2c^{(4)}$	a/t	a/2c
102	Fe-3Si	0.115	1.20	0.07	0.17	0.61	0.412
103	Fe-3Si	0.115	1.20	0.07	0.17	0.61	0.412
104	Fe-3Si	0.115	1.20	0.07	0.23	0.61	0.304
105	Fe-3Si	0 115	1.20	0.07	0.23	0.61	0.304
106	Fe-3Si	0.115	1.75	0.07	0.35	0.61	0.200
107	Fe-3Si	0.115	1.75	0.07	0.35	0.61	0.200
108	Fe-3Si	0.115	1.75	0.07	0.35	0.61	0.200
60	Fe-3Si	0.230	1.25	0.10	0.25	0.435	0.400
61	Fe-3Si	0.230	1.25	0.10	0.25	0.435	0.400
62	Fe-3Si	0.230	1.25	0.10	0.25	0.435	0.400
63	Fe-3Si	0.230	1.25	0.10	0.25	0.435	0.400
64	Fe-3Si	0.230	1.70	0.10	0.33	0.435	0.303
65	Fe-3Si	0.230	1.70	0.10	0.33	0.435	0.303
66	Fe-3Si	0.230	1.70	0.10	0.33	0.435	0.303
67	Fe-3Si	0.230	1.70	0.10	0.33	0.435	0.303
68	Fe-3Si	0.230	2.50	0.10	0.50	0.435	0.200
69	Fe-3Si	0.230	2.50	0.10	0.50	0.435	0.200
70	Fe-3Si	0.230	2.50	0.10	0.50	0.435	0.200
71	Fe-3Si	0.230	2.50	0 10	0.50	0.435	0.200
84	Fe-3Si	0.230	1.75	0.14	0.35	0.609	0.400
85	Fe-3Si	0.230	1.75	0.14	0.35	0.609	0.400
86	Fe-3Si	0.230	1.75	0.14	0.35	0.609	0.400
87	Fe-3Si	0.230	2.30	0.14	0.47	0.609	0.298
88	Fe-3Si	0.230	2.30	0.14	0.47	0.609	0.298
89	Fe-3Si	0.230	2.30	0.14	0.47	0.609	0.298
90	Fe-3Si	0.230	2.50	0.14	0.70	0.609	0.200
91	Fe-3Si	0.230	2.50	0.14	0.70	0.609	0.200
92	Fe-3Si	0.230	2.50	0.14	0.70	0.609	0.200
93	Fe-3Si	0.230	2.10	0.17	0.42	0.740	0.405
94	Fe-3Si	0.230	2.10	0.17	0.42	0.740	0.405
95	Fe-3Si	0.230	2.10	0.17	0.42	0.740	0.405
96	Fe-3Si	0.230	2.50	0.17	0.57	0.740	0.298
97	Fe-3Si	0.230	2.50	0.17	0.57	0.740	0.298
98	Fe-3Si	0.230	2.50	0.17	0.57	0.740	0.298

Spec. No.	Material	t(1)	W(2)	a(3)	2c(4)	a/t	a/2c
99	Fe-3Si	0.230	2.50	0.17	0.85	0.740	0.200
100	Fe-3Si	0.230	2.50	0.17	0.85	0.740	0.200
101	Fe-3Si	0.230	2.50	0.17	0.85	0.740	0.200
77	Fe-3Si	0.535	4.03	0.25	1.25	0.467	0.200
78	Fe-3Si	0.525	4.01	0.25	0.84	0.476	0.298
79	Fe-3Si	0.525	4.01	0.25	0.62	0.476	0.403
109	Ti-6Al-4V	0.104	0.985	0.07	0.17	0 674	0.412
110	Ti-6Al-4V	0.104	1.018	0.07	0.17	0.674	0.412
111	Ti-6Al-4V	0.101	1.023	0.07	0.17	0.694	0.412
112	Ti-6Al-4V	0.105	1.023	0.07	0.23	0.667	0.304
113	Ti-6Al-4V	0.102	1.016	0.07	0.23	0.686	0.304
114	Ti-6Al-4V	0.101	1.040	0.07	0.23	0.694	0.304
115	Ti-6Al-4V	0.103	1.257	0.07	0.35	0.680	0.200
116	Ti-6Al-4V	0.104	1.269	0.07	0.35	0.674	0.200
117	Ti-6Al-4V	0.103	1.249	0.07	0.35	0.680	0.200
151	Ti-6Al-4V	0.200	3.00	.08	0.20	0.400	0.400
152	Ti-6Al-4V	0.200	3.00	.08	0.20	0.400	0.400
153	Ti-6Al-4V	0.200	3.00	.14	0.70	0.700	0.200
154	Ti-6Al-4V	0.200	3.00	.14	0.35	0.700	0.400

Notes:

(1) Specimens 102-108, 151-154: $\pm$ .003"
Specimens 60-101: $\pm$ .005"

(2) Specimens 102-108, 60-101: $\pm$ 1/32"
Specimens 151-154: $\pm$ .003"

(3) $\pm$ .005"

(4) $\pm$ .05"

III. EXPERIMENTAL PROCEDURES

III. A Fatigue Cracking and Test Facilities

The first step in the test program was to initiate a fatigue crack around the notch. This was accomplished through the use of the 50,000-lb load capacity servo-controlled hydraulic test apparatus shown in Figure . The required loads were introduced by the loading plates through five pins at each head of the specimen and were controlled by the load cell mounted below the crosshead of the test apparatus. Amplitudes of the sinusoidal fatigue loads were varied from 25% to 40% of net section yield load down to a minimum of from 300 to 1000 pounds, depending on the geometry of the specimen.

The specimen was periodically checked to determine if crack initiation had occurred. It was observed that in most cases crack initiation occurred at one end of the notch only. The crack generally grew to a length of 0.01-0.02 inch, at which point the growth stopped until a crack with approximately the same length appeared at the opposite end of the notch, after which the two cracks grew at the same rate. On specimens where cracks initiated at both ends of the notch at the same time, the specimen was continued in fatigue loading until simultaneous growth was observed on both cracks (which was not the case immediately after initiation) and was fatigued until sufficient crack length was attained. It was assumed that the time required between initiation and the beginning of simultaneous growth was needed in order to allow the cracks to propagate completely around the notch.

Upon completion of fatigue cracking, the specimens were heat-treated to remove all residual stresses and were metallographically prepared for testing. The specimens were loaded in the test apparatus to various percentages of net cross-sectional yield loads shown in Table III. 1. Surfaces at the notch were replicated under loaded and unloaded conditions, and also photographed in the loaded state if visible dimpling was observed on the back side of specimen.

III. B Metallography of Fe-3Si Test Specimens

Localized zones of plastic deformation in Fe-3Si alloys may be delineated by etching with Morris reagent[1, 2]. This technique depends on the fact that the dislocation density in well annealed, single-phase materials is relatively low and increases rapidly with plastic strain. If, after strain, individual dislocations are decorated by segregated solute atoms, the points of intersection of the dislocations with free surfaces are anodic with respect to the matrix. Thus, the etching response

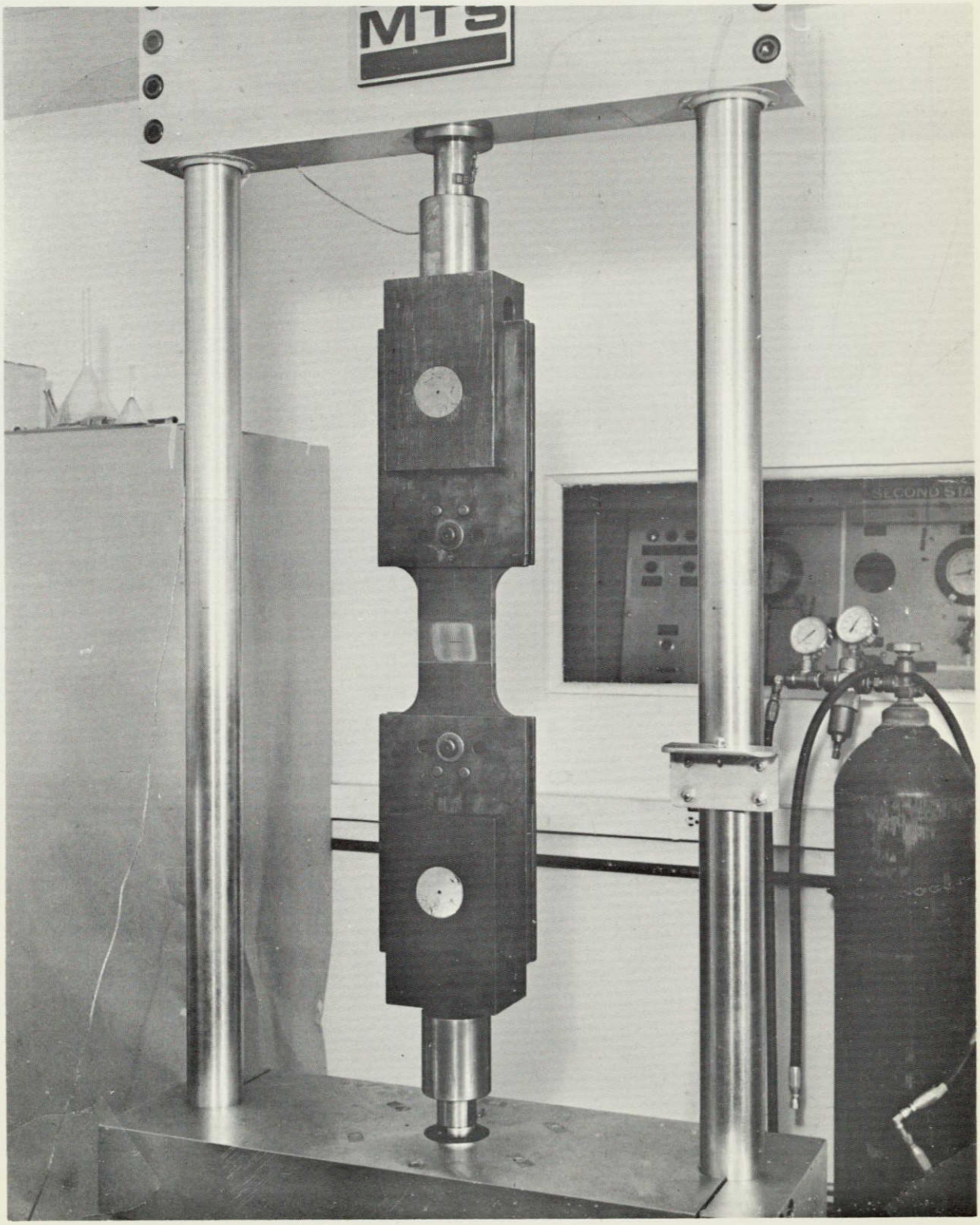

Figure III. 1 Test Apparatus

TABLE III. 1

SCHEDULE OF NOMINAL NET-SECTION LOADS APPLIED TO SPECIMENS (BASED UPON EDM NOTCH, BEFORE FATIGUE CRACKING)

Spec. No.	Material	a/t	a/2c	% Net Section Yield
102	Fe-3Si	0.61	0.412	70
103	Fe-3Si	0.61	0.412	(1)
104	Fe-3Si	0.61	0.304	(1)
105	Fe-3Si	0.61	0.304	(1)
106	Fe-3Si	0.61	0.200	50
107	Fe-3Si	0.61	0.200	(1)
108	Fe-3Si	0.61	0.200	50
60	Fe-3Si	0.435	0.400	50
61	Fe-3Si	0.435	0.400	65
62	Fe-3Si	0.435	0.400	80
63	Fe-3Si	0.435	0.400	85
64	Fe-3Si	0.435	0.303	(2)
65	Fe-3Si	0.435	0.303	70
66	Fe-3Si	0.435	0.303	80
67	Fe-3Si	0.435	0.303	90
68	Fe-3Si	0.435	0.200	70
69	Fe-3Si	0.435	0.200	60
70	Fe-3Si	0.435	0.200	85
71	Fe-3Si	0.435	0.200	80
84	Fe-3Si	0.609	0.400	60
85	Fe-3Si	0.609	0.400	80
86	Fe-3Si	0.609	0.400	70
87	Fe-3Si	0.609	0.298	70
88	Fe-3Si	0.609	0.298	60
89	Fe-3Si	0.609	0.298	80
90	Fe-3Si	0.609	0.200	60
91	Fe-3Si	0.609	0.200	70
92	Fe-3Si	0.609	0.200	80
93	Fe-3Si	0.740	0.405	(3)
94	Fe-3Si	0.740	0.405	70
95	Fe-3Si	0.740	0.405	80
96	Fe-3Si	0.740	0.298	60
97	Fe-3Si	0.740	0.298	70
98	Fe-3Si	0.740	0.298	80

Spec. No.	Material	a/t	a/2c	% Net Section Yield
99	Fe-3Si	0.740	0.200	70
100	Fe-3Si	0.740	0.200	80
101	Fe-3Si	0.740	0.200	60
77	Fe-3Si	0.467	0.200	(4)
78	Fe-3Si	0.476	0.298	(4)
79	Fe-3Si	0.476	0.403	70
109	Ti-6Al-4V	0.674	0.412	70
110	Ti-6Al-4V	0.674	0.412	(5)
111	Ti-6Al-4V	0.694	0.412	(5)
112	Ti-6Al-4V	0.667	0.304	70
113	Ti-6Al-4V	0.686	0.304	(5)
114	Ti-6Al-4V	0.694	0.304	(5)
115	Ti-6Al-4V	0.680	0.200	70
116	Ti-6Al-4V	0.674	0.200	(5)
117	Ti-6Al-4V	0.680	0.200	(5)
151	Ti-6Al-4V	0.400	0.400	(6)
152	Ti-6Al-4V	0.400	0.400	(6)
153	Ti-6Al-4V	0.700	0.200	(6)
154	Ti-6Al-4V	0.700	0.400	(2)

Notes:
(1) Cracked through back surface prematurely
(2) Failed during fatigue loading
(3) Broken in machining operation
(4) Broken during water quench
(5) Loaded only to onset of dimpling
(6) Loaded to fracture

is a function of the dislocation density and a sensitive indication of prior plastic strain. The technique can provide quantitative information on the magnitude of localized strain and has been employed in a number of experimental mechanics studies[3, 4]. In general, metallographic evaluation of localized strain in Fe-3Si involves the following sequence of operations.

1. Anneal specimen to eliminate the effects of prior cold work introduced by machining, polishing, or precracking.

2. Load specimen to appropriate stress level

3. Age specimen to decorate strain generated dislocations.

4. Section and polish specimen and etch electrolytically in Morris reagent.

On the basis of the information available in the technical literature at the outset of the program, and on preliminary tests and examinations, the following sequence of operations was adopted for preparation and metallographic examination of the 0.20 inch thick Fe-3Si specimens.

1. Machine required surface notch and fatigue precrack specimen.

2. Recrystallization anneal at 800°C for 1 hour (inert atmosphere to prevent decarburization). Quench in ambient air.

3. Cut central portion of test section containing notch from the specimen.

4. Age at 150°C; 1/2 - 1 hour.

5. Cut and polish appropriate sections.

6. Etch electrolytically in Morris reagent* and examine sections at 75X.

In order to provide an adequate three dimensional description of the plastic zone formed along the elliptical crack front, the metallographic procedure was standardized (after variations with the first few specimens)

---

* Morris reagent: 25g chromium trioxide, 7 ml H_2O 133ml glacial acetic acid. Etch electrolytically at 8V with stainless steel cathode and specimen-cathode separation of approximately 1 inch; 3 to 8 minutes without agitation.

to examine the sections indicated in Figure III. 2 and described as follows:

1. Specimen surface at each end of the surface crack (Sections 1-1 and 2-2, Figure III. 2).

2. A section normal to the specimen surface at the centerline of the crack (Section 3-3, Figure III. 2).

3. A section oriented normal to the crack front at a point located midway along the arc distance from the crack centerline to the specimen surface. (Section 4-4, Figure III. 2).

It was found necessary to remove 0. 005-0. 010 inch from the surface layer to obtain a satisfactory etch response for Sections 1-1 and 2-2. The surface layer is heavily deformed as a result of machine grinding, and is not representative of the true strain field existing just beneath this thin layer.

In each case the two surface sections and the centerline section (1-1, 2-2, and 3-3, Figure III. 2) were prepared and examined first. Section 4-4 was prepared and examined only for those specimens in which the fatigue crack had truly circumscribed the EDM notch, as determined from Section 3-3. Each of the metallographic sections was etched to reveal the strain zone and sufficient photomicrographs were taken at each section to document the size and shape of the plastic zone. Overlay tracings of the plastic zone boundaries for each of the sections were then prepared from the photomicrographs.

The procedures described above resulted in consistent delineation of the plastic zones in all specimens of the 0. 20-inch material. Photomicrographs illustrating the etching response of these specimens are included in the discussion of the test results, Section V, and also in the Appendix.

Metallographic examination of preliminary test specimens established that the annealing, aging and etching procedures employed for the 0. 20-inch material did not result in adequate definition of the plastic zones for the 0. 10-inch and 0. 50-inch material. For these two thicknesses, etching with Morris reagent after annealing at 800°C and aging at 150°C revealed a dark etching structure for many of the individual grains. Although distinct strain lines were evident in isolated grains, the presence of the dark etching structure prevented adequate delineation of the extent of the plastic zones. A number of preliminary specimens of the 0. 10-inch and 0. 50-inch material were examined with variations of the etching variables

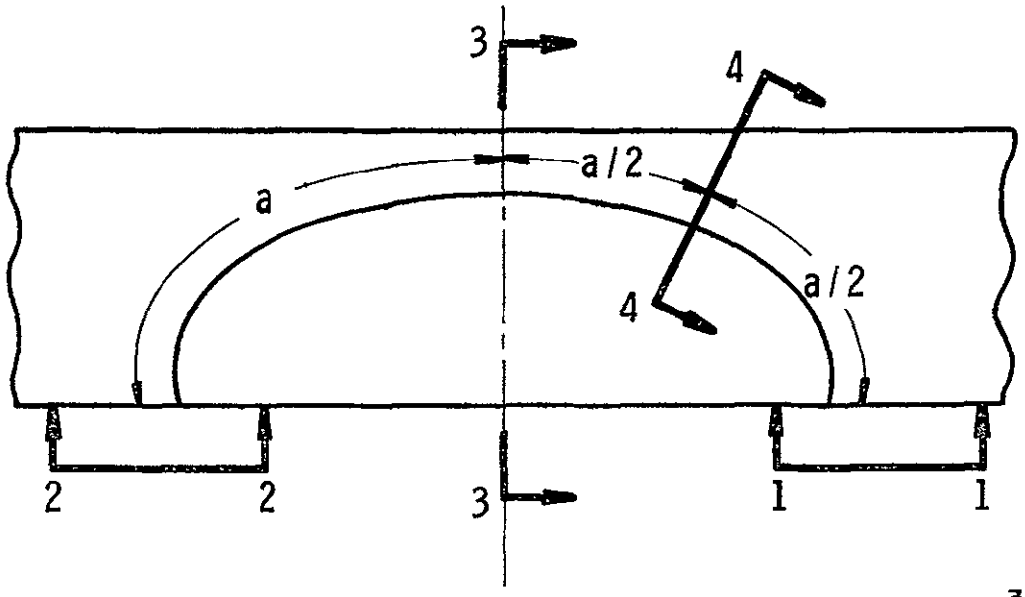

Figure III.2 Schematic Representation of Location of Metallographic Sections of Fe-3Si Specimens

(voltage, time, temperature) quench rate, aging time and temperature In these examinations no consistent definition of plastic strain was observed indicating that the lack of etching response was associated with the material structure rather than with the metallographic procedures. These observations are consistent with the observed differences in the microstructure of the three thicknesses of the material in the as-received condition. Also, recently published information on the metallographic observation of strains in Fe-3Si published by Hahn, Mincer and Rosenfield[5] indicates that the consistent metallographic definition of plastic strain in this material is critically related to the degree of cold work employed in the final steps of fabrication of the specimen material.

Further tests of preliminary specimens of the 0.10-inch and 0.50-inch Fe-3Si material for which the heat treating parameters (annealing temperature and time, and cooling rate) were varied were conducted in an effort to establish procedures for use with these particular specimen materials. In these experiments, successful delineation of plastic strain in the 0.10-inch material was accomplished by employing higher annealing temperatures, longer annealing times and higher quenching rates than those employed for the 0.20 inch material. On the basis of the results of these experiments the following sequence of operations was adopted for the 0.10-inch material.

1. Machine required surface notch and fatigue precrack specimen.

2. Recrystallization anneal at 950°C for 2 1/2 hours in inert atmosphere. Water quench.

3. Cut central portion of test section containing notch from the specimen.

4. Age at 150°C; 1/2 to 1 hour.

5. Cut, polish appropriate sections.

6. Etch electrolytically in Morris reagent and examine section at appropriate magnification.

This particular metallographic procedure was also employed on the limited number of 0.50 inch thick test specimens included in the program.

III. C Calibration of Etch Response

To facilitate data interpretation it is very helpful to have a semi-quantitative estimate as to the magnitude of the plastic strain revealed by the etching procedure actually used. Toward this end, tapered tensile specimens of each of the three thicknesses of Fe-3Si used were prepared in accordance with the drawing shown as Figure III. 3. Each specimen was instrumented with a 1/64" strain gage at three locations as indicated, and loaded so as to place the specimen at yield in the wide end, and near ultimate strength at the narrow end. After loading, each specimen was subjected to the same metallographical and etching procedures used in the regular surface-cracked specimen series as discussed in the previous section.

The results for the 0. 5 inch specimen thickness were inconclusive, as the etching procedure failed to reveal plastic strain lines of any consequence throughout the specimen length. For the 0. 1 and 0. 2 inch material, however, results could be more clearly established. Figures III. 4 and III. 5 show, respectively, the etching response at three locations (at, and 0. 5 inch either side of, the strain gage location at the narrow end of the specimen) for the 0. 1 inch and 0. 2 inch specimen thicknesses. In both cases, light but distinct strain lines are visible in the upper photographs, and the strain line density becomes quite high in the lower photographs. These photomicrographs can be used to estimate the magnitude of the strains revealed under etch for the two Fe-3Si thicknesses. These estimates are given in Table III. 2 which follows, both for the total strain e_t and the plastic strain, e_p .

TABLE III 2

ETCHING CALIBRATION RESULTS

	Threshold		Moderate Density		High Density	
	e_t	e_p	e_t	e_p	e_t	e_p
0. 1"	0. 23%	0. 06%	0. 43%	0. 25%	0. 65%	0. 46%
0. 2"	0. 30%	0. 06%	0. 48%	0. 23%	0. 60%	0. 35%

It is known that for large plastic strains the etching technique used in this investigation fails to reveal the strain pattern. Hahn, Mincer

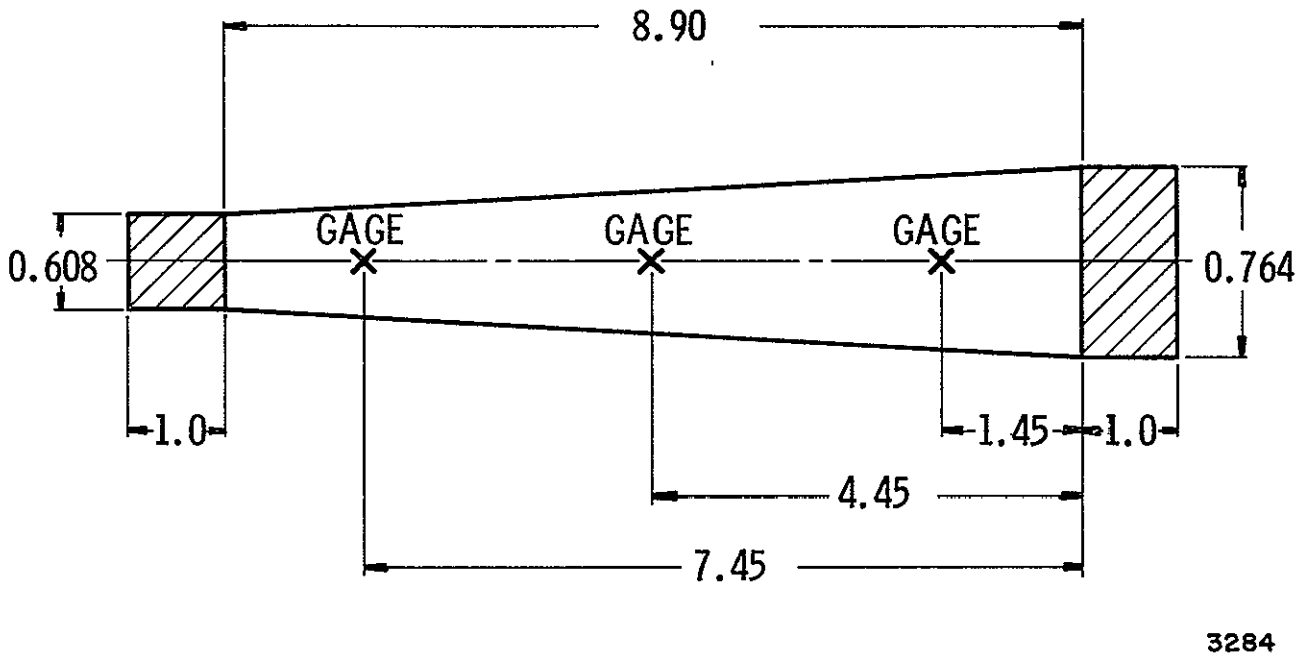

Figure III.3 Calibration Specimen for Etching Response to Strain
(Not to Scale)

$e_t = 0.23\%$

$e_p = 0.06\%$

$e_t = 0.43\%$

$e_p = 0.25\%$

$e_t = 0.65\%$

$e_p = 0.46\%$

Figure III. 4 Etching Calibration of 0. 1 inch Fe-3Si Material, 75X

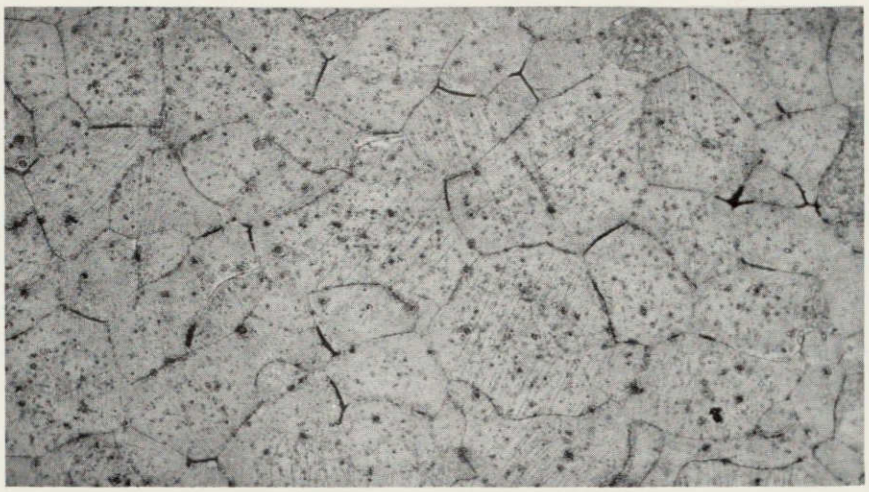

$e_t = 0.30\%$

$e_p = 0.06\%$

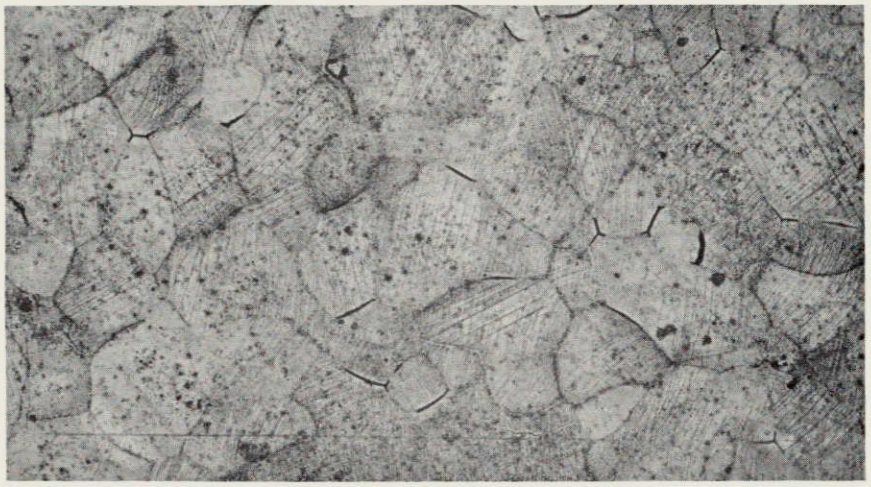

$e_t = 0.48\%$

$e_p = 0.23\%$

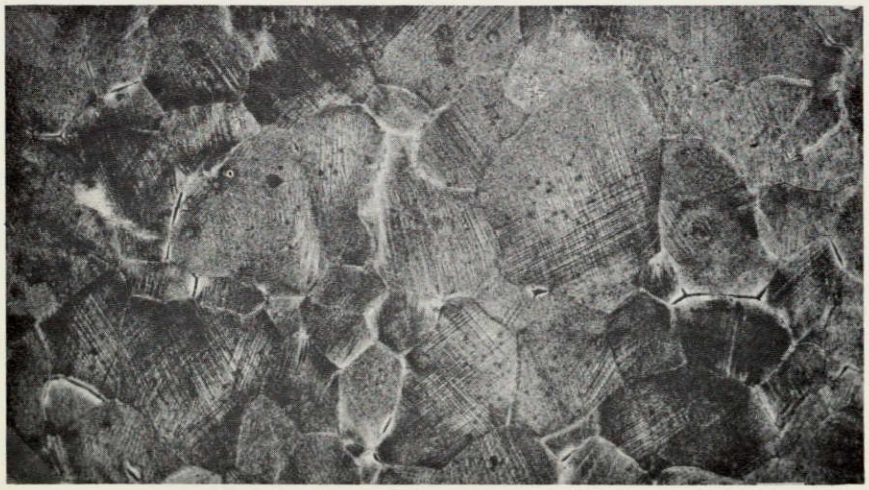

$e_t = 0.60\%$

$e_p = 0.35\%$

Figure III. 5 Etching Calibration of 0.2 inch Fe-3Si Material, 75X

and Rosenfield[5] have shown that this upper limit on etching response is approximately 5-7% in total strain. The results reported by these investigators at low strain levels support the conclusions presented above.

III. D Characterization of Surface Deformation

D-1. Talysurf Measurements

To obtain both qualitative and quantitative information on the surface deformation of the back side of the specimens behind the notches, replicas were taken of those specimens where visible back surface dimpling had developed, under load, and immediately following it, in the unloaded condition These replicas were then analyzed with a Taylor-Hobson Model 3 Talysurf Surface Measuring Instrument. This instrument has a maximum resolution of one microinch. Traces taken at equal intervals perpendicular to the crack direction provided information as to the area size and depth of surface deformation influenced by the notch in the specimen. Samples of these traces are included in Section V of this report. By comparing the deformation patterns corresponding to the loaded and unloaded conditions, it is possible to assess the relative magnitude of elastic and plastic deformations involved

D-2. Interferometric Measurements

In order to characterize the residual surface deformation field in the small regions adjacent to the crack tips, the Michelson interferometric technique was used. This technique provides an interference pattern of the specimen surface by splitting and recollimating light from a laser source The fringe calibration is $1/2\ \lambda$, i.e., adjacent fringes correspond to 0.3164 microns depth on the specimen surface. The interference fringe pattern is magnified and projected onto a screen, and this pattern is then photographed.

The apparatus is shown in Figure III. 6. The distance from the cube beam splitter to the specimen surface was set nominally at 2-15/16 inches, and was adjusted in each case to focus the image. The graticule was placed in position and trans-illuminated by the auxiliary LS-32 laser, together with expanding lenses, for calibration purposes. The graticule used in this apparatus was 1.0 mm long, and was magnified according to the desired magnification of the photographic image.

The specimens, which had a ground and polished surface in the crack-tip regions of interest, were wiped with dry lens tissue before

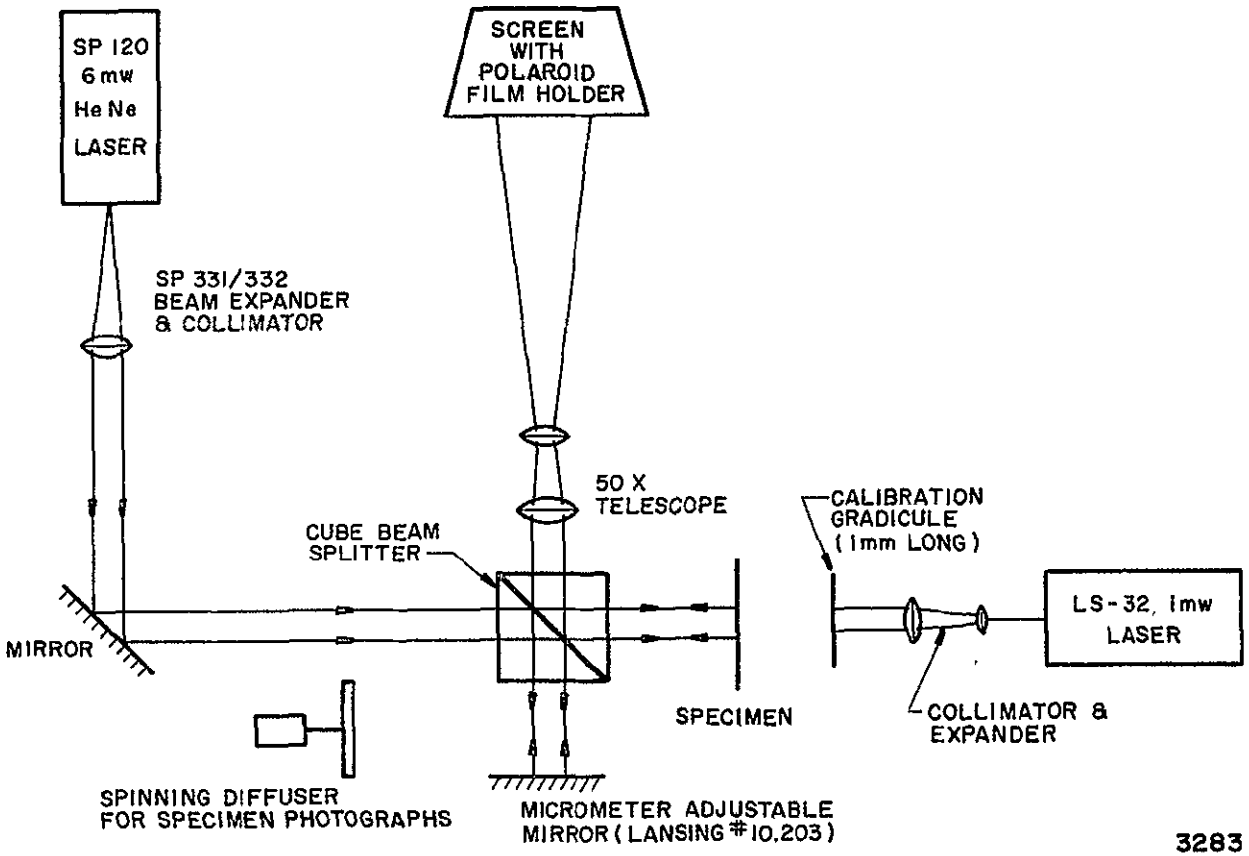

Figure III.6 Diagram of Michelson Interferometry Apparatus

photographing, and sprayed with LPS metal protector afterwards. Each crack tip region was photographed at least twice; once to derive the interference fringe pattern, and again, with diffused laser light, to show the visual surface appearance of the same region. For this latter purpose, a spinning diffuser was introduced into the light path, as shown in the figure.

This technique resulted in excellent characterizations of the local surface deformation resulting from residual plastic deformation near the crack tips. It is particularly attractive for use in connection with highly polished surfaces where the deformation to be measured is small enough that the fringe pattern is countable under the magnifications used Typical results are shown in Figure III. 7 and a more thorough discussion is given in Section V. This figure shows the region of the crack tip in Specimen 98 under uncorrelated laser illumination (upper) and the corresponding interference pattern (lower), under 50X magnification. The interferogram reveals seven fringes from the far-field, giving the dimple depth of about 7/2 (0.6328) microns, or about 87.3 microinches. The distance from the crack tip to the zero-order fringe is about 0.04 inches which compares with a dimension of about 0.067 inches as the characteristic size of the plastic zone as revealed under etch.

D-3. Photography

Each specimen which exhibited dimpling on its back surface under load was photographed with a 35 mm camera equipped with close-up lenses. Although these photographs do not possess any quantitative information about the surface deformations, they do provide visual records of the dimples appearing on the specimens. Some of the dimples were very pronounced even under small loads, sample photographs are included in Section V.

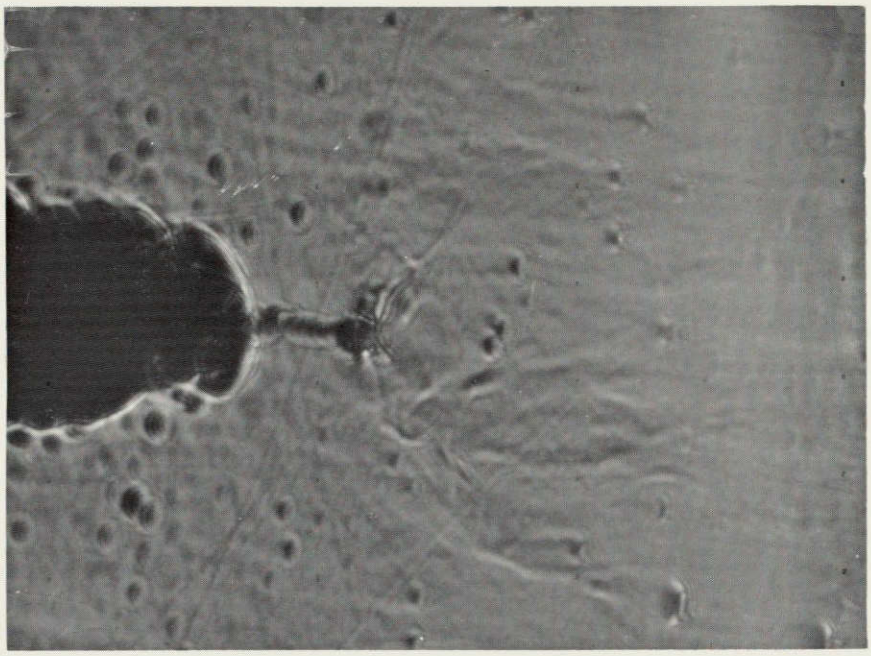

Laser Illuminated Photograph, 50X

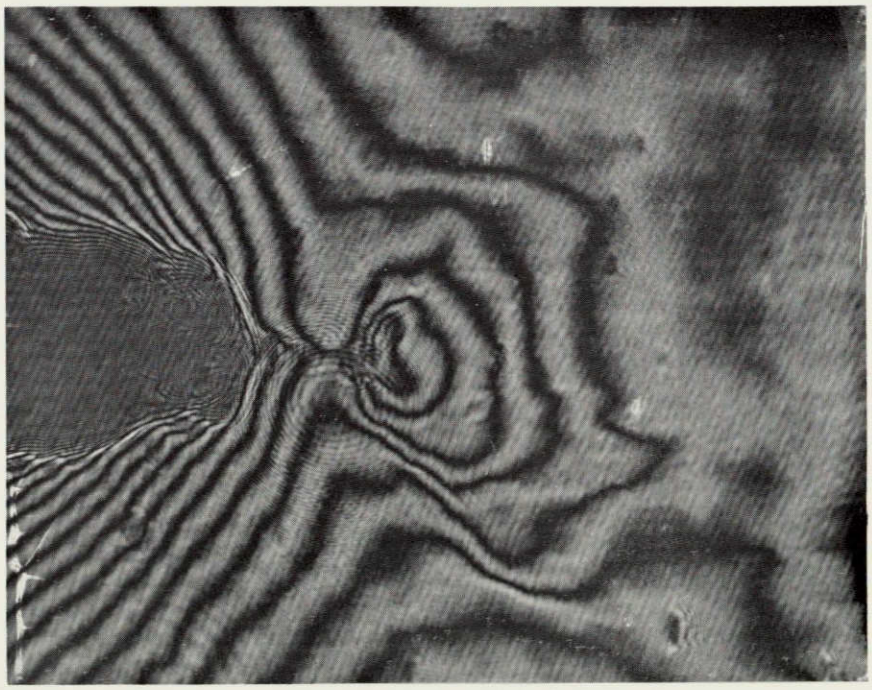

Interferogram, 50X

Figure III. 7 Front Surface of Specimen 98 (0. 2" Fe-3Si) Showing Crack Tip and Dimple

IV. ANALYTICAL PROCEDURES

IV.A Stress Intensity Factors

No exact analytical expressions exist for the stress intensity factors associated with a surface-notched crack geometry. The stress fields introduced by this notch configuration are highly three-dimensional, and are complicated in practical situations by the finite thickness of the specimen and the existence of inelastic strains in the neighborhood of the crack front. Nevertheless, the importance of the surface-notched configuration has motivated a number of investigations which have sought to determine realistic approximations for the stress intensity factors.

The surface-notched specimen geometry is idealized as shown in Figure IV.1. The specimen is of thickness t and wide with respect to the crack length $2c$. The crack is assumed semi-elliptical, characterized by the half-length c and the depth a. The crack is generally assumed to be shallow in the sense that $a/c \leqslant 1$. The stress field remote from the crack is one of pure tension, which loads the specimen in the pure Mode I configuration. The stress intensity factor varies with angular position ϕ around the crack front. The state of deformation is one of plane strain at $\phi = \pi/2$, where lateral constraint is afforded by the adjacent material, and approaches plane stress in the neighborhood of $\phi = 0, \pi$, where no such lateral constraint exists. Since most of the interest in fracture mechanics concerns plane deformation, theoretical stress intensity factor calculations relate, for the most part, to the position $\phi = \pi/2$. Thus, throughout this report, K is understood to be the Mode I plane strain stress intensity factor unless specifically stated otherwise. This factor is defined through the following equations which describe the elastic stress field in the neighborhood of the crack at some point on the crack front:

$$\sigma_x = \frac{K}{\sqrt{2\pi r}} \cos\frac{\theta}{2}\left(1 - \sin\frac{\theta}{2}\sin\frac{3\theta}{2}\right)$$

$$\sigma_y = \frac{K}{\sqrt{2\pi r}} \cos\frac{\theta}{2}\left(1 + \sin\frac{\theta}{2}\sin\frac{3\theta}{2}\right)$$

$$\tau_{xy} = \frac{K}{\sqrt{2\pi r}} \sin\frac{\theta}{2}\cos\frac{\theta}{2}\cos\frac{3\theta}{2}$$

$$\sigma_z = \nu(\sigma_x + \sigma_y), \quad \tau_{xz} = \tau_{yz} = 0 \qquad (4.1)$$

This definition for K is consistent with the standard accepted by the ASTM Special Committee on Fracture Testing (E-24) One sometimes

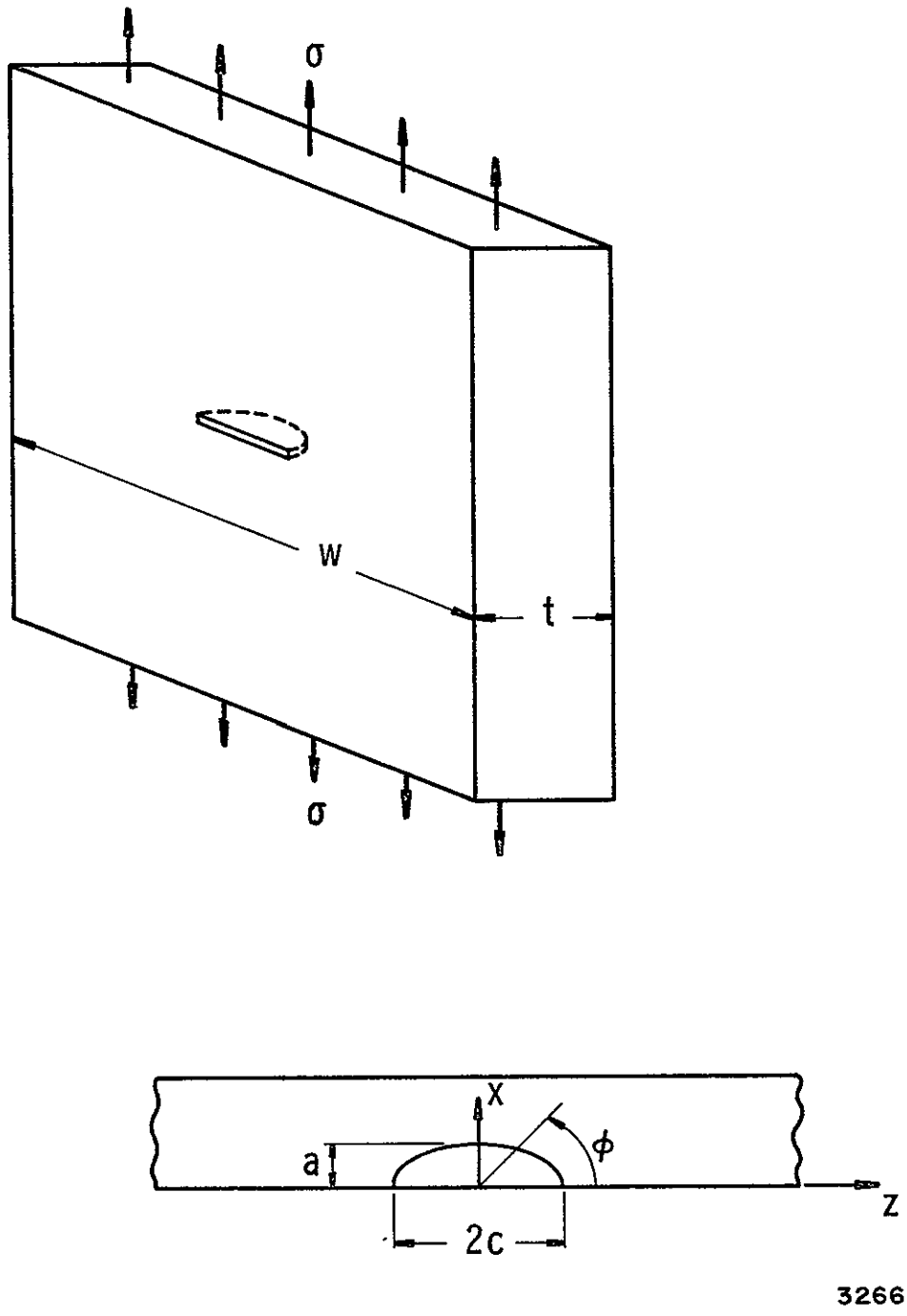

Figure Ⅳ.1 Specimen and Crack Geometry

finds an alternative definition in the literature written usually (but not always) with a script $\mathcal{K}$, and differing from the standard definition by the factor π : $K = \mathcal{K}\sqrt{\pi}$.

In this program seven different expressions for K were applied to the test specimen crack configurations. These expressions for the plane strain stress intensity factor derive from the investigations of the following persons.

Irwin (1962)
Paris & Sih (1965)
Smith (1966)
Kobayashi & Moss (1969)
Orange (1969)
Rice & Levy (1970)
Anderson, Holms & Orange (1970)

The appropriate expressions for K are written below, the reader is referred to the original publications for the methods and derivations. All make use of the elliptic integral:

$$\Phi = \int_0^{\pi/2} \sqrt{1 - (1-a^2/c^2)\sin^2\alpha}\; d\alpha \qquad (4.2)$$

This function is plotted in Figure IV.2 for reference.

Irwin (Ref. 6)

$$K = \sigma\sqrt{\frac{1.2\,\pi a}{\Phi^2 - 0.212\,(\sigma/\sigma_y)^2}}$$

$$a/t < 0.5$$

$$a/c \leq 1.0 \qquad (4.3)$$

Paris & Sih (Ref. 7)

$$K = \left[1 + 0.12\,(1-a/c)\right]\frac{\sigma\sqrt{\pi a}}{\Phi}\sqrt{\frac{2t}{\pi a}\tan\frac{\pi a}{2t}}$$

$a/t < 0.75$ (for claimed accuracy of $\pm$ 10%)
$a/c \leq 1.0$
plastic region contained within half the distance from the crack front to the back surface

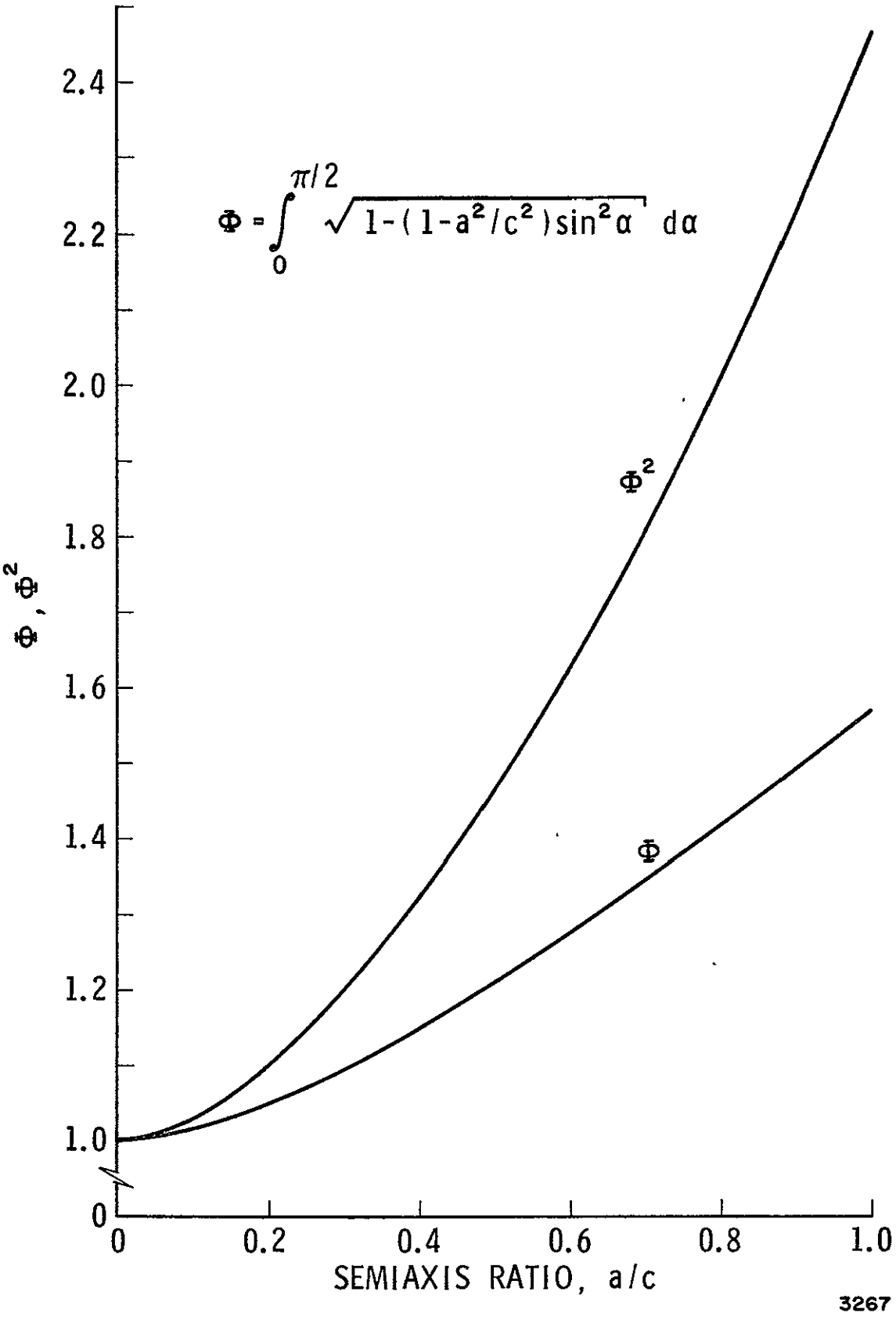

Figure Ⅳ.2 Complete Elliptic Integral of the Second Kind

Smith (Ref. 8)

$$K = \left[1.07 - 0.07 (a/c) \right] \frac{1.03 \sigma \sqrt{\pi a}}{\sqrt{\Phi^2 - 0.212 \left(\sigma / \sigma_y \right)^2}}$$

$a/t < 0.5$

$a/c < 1.0$ (4.5)

Kobayashi & Moss (Ref. 9)

$$K = M_e M_p \frac{\sigma \sqrt{\pi a}}{\Phi}$$

M_e from Figure IV.3 = 1 when yield zone penetrates back surface

M_p from Figure IV.4

$a/t < 1.0$

$a/c \leq 1.0$ (4.6)

Orange (Ref. 10)

$$K = \frac{\sigma}{\Phi} \sqrt{\frac{1.2 \pi a}{1 - \left(\sigma / \sigma_u \right)^2}}$$

$a/t < 0.5$

$a/c \leq 1.0$ (4.7)

Rice & Levy (Ref. 11)

K derived from Figure IV.5, where K_∞ is the Gross & Srawley solution for the edge-notched plate of finite width (Ref. 12).

$c > t$

elastic solution, valid only for very localized yielding

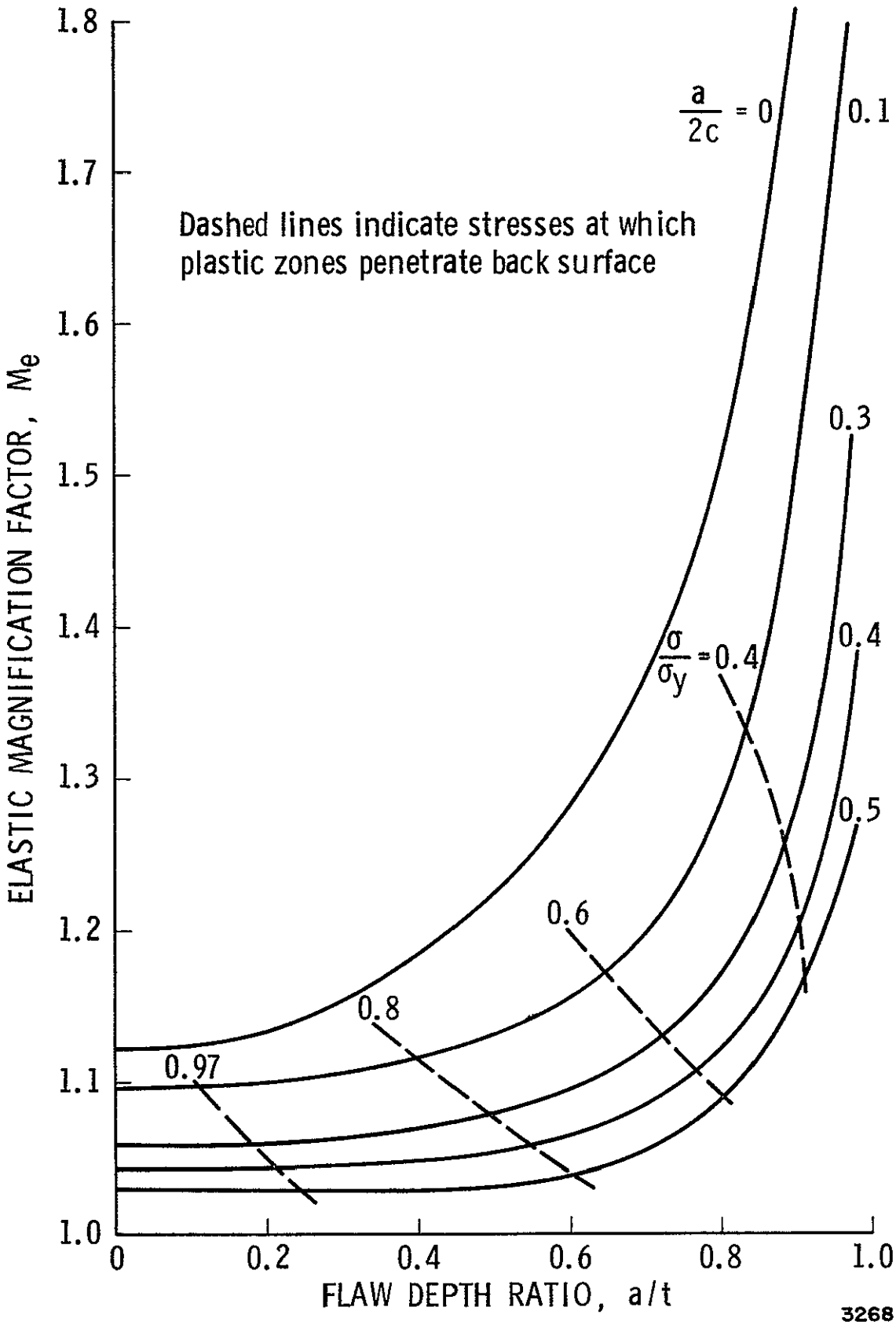

Figure IV.3 Kobayashi & Moss Elastic Stress Intensity Magnification Factor, Ideally Plastic Material (Ref. 9)

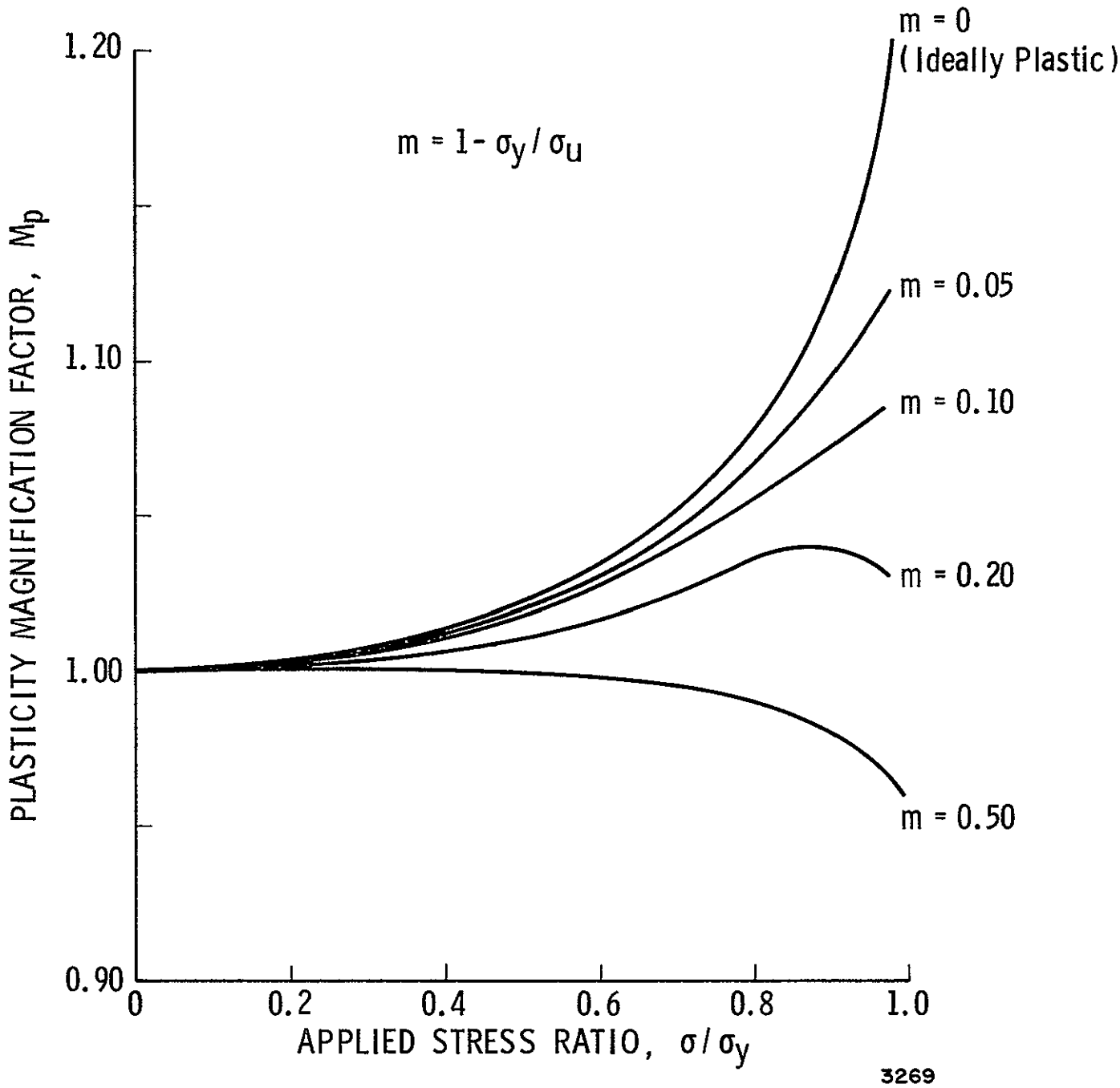

Figure IV.4 Kobayashi & Moss Plasticity Magnification Factor (Ref. 9)

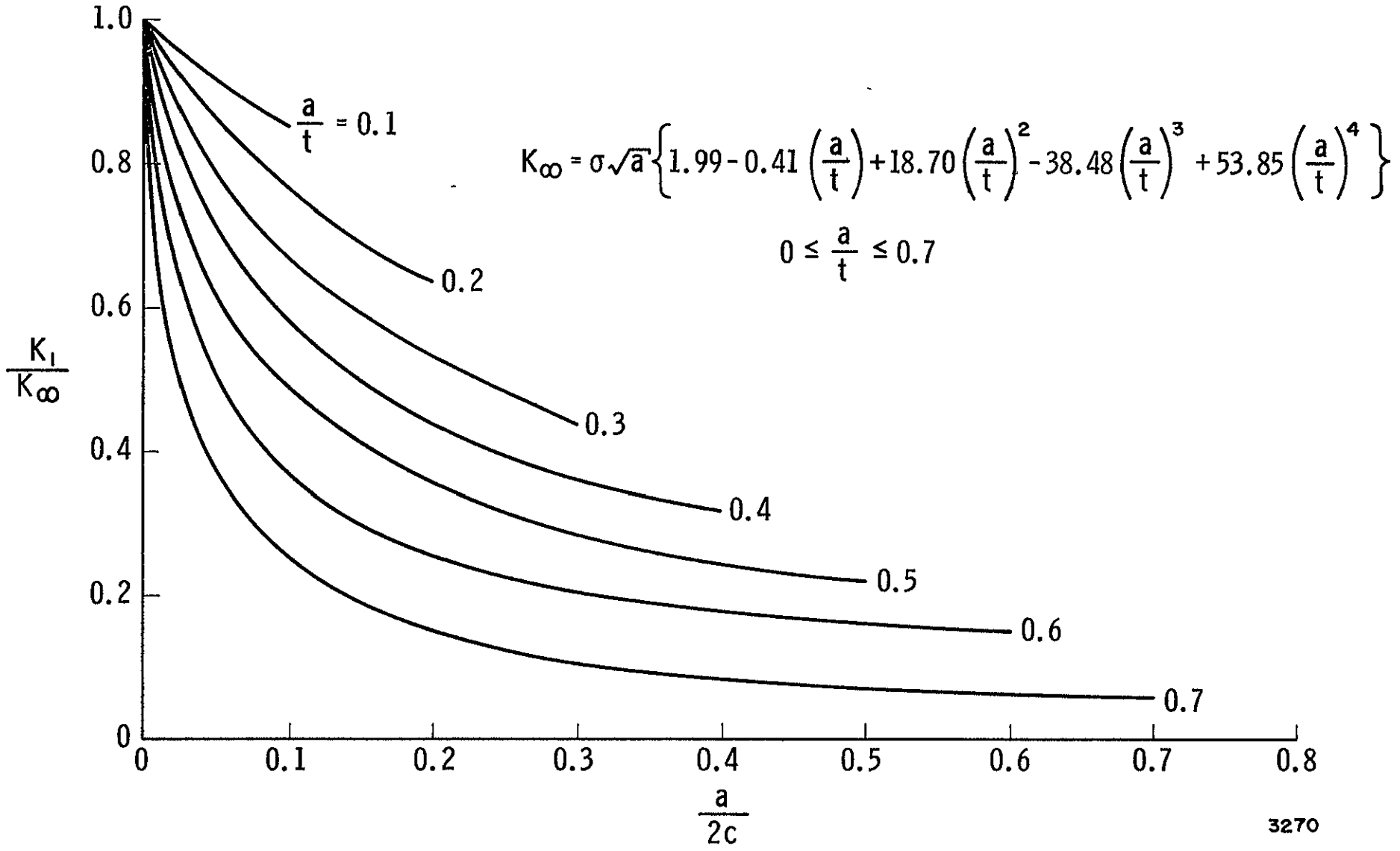

Figure IV.5 Mode I Stress Intensity Factor, Adapted from Rice & Levy (Ref. 11)

Anderson, Holms & Orange (Ref. 13)

$$K = [\,1 + 0.12\ (1 - a/c)]\ \frac{\sigma\sqrt{\pi a}}{\Phi}\sqrt{\frac{2t\Phi^2}{\pi a}\tan\left[\frac{\pi a}{2t\Phi^2}(1+\Omega)\right]}$$

$$\Omega = \frac{2t\Phi^2}{\pi a}\sin^{-1}\left\{\sqrt{1-(\sigma/\sigma_y)^2}\,\sin\left(\frac{\pi a}{2t\Phi^2}\right)\sec\left(\frac{\pi\sigma}{2\sigma_y}\right)\right\} - 1 \qquad (4.8)$$

$a/t < 0.85$

plastic region does not penetrate back surface:

$$\frac{a}{t}\left(1 - \frac{1}{\Phi^2}\right) + \frac{2}{\pi}\sin^{-1}\left[\sin\left(\frac{\pi a}{2t\Phi^2}\right)\sec\left(\frac{\pi\sigma}{2\sigma_y}\right)\right] < 1$$

The foregoing results apply to the semi-minor axis position of the crack front, where state of plane strain prevails. Smith[8] has shown that K is a maximum at this position on the crack front for $a/c < 0.6$, and unstable fracture will therefore initiate in the plane strain region For $1 < a/c < 0.8$ fracture may initiate at the specimen free surface in a state of plane stress The variation in K around the crack front generally is not large. Smith, Emery and Kobayashi[14] have estimated that, for the semi-circular surface crack (ignoring plasticity effects), K varies about 18 percent around the crack front, being highest where the crack intercepts the free surface. These authors also argue that this variation is somewhat less for shallow ($a/c < 1$) surface cracks.

The variation in stress intensity factor around the crack front may be accounted for in an approximate manner by adopting the ϕ -dependent stress intensity factor for the flat elliptical crack imbedded in an infinite solid, as derived by Irwin[6]. The expression is

$$K(\phi) = \frac{\sigma}{\Phi}\sqrt{\frac{\pi a}{c}}\,(a^2\cos^2\phi + c^2\sin^2\phi)^{1/4} \qquad (4.9)$$

where the coordinate system is defined in Figure IV. 1. This result renders the stress intensity factor a maximum at the minor axis, $\phi = \pi/2$. For $0 < \phi < \pi/2$ it may be applied as a reduction factor to the plane strain K, as corrected for front and back surface and plasticity effects, provided the chosen point on the crack front is essentially in a state of plane strain. Its application to the plane stress regions $\phi = 0, \pi$

is questionable at best, and probably underestimates the true value of K. In regions of plane strain, however, the stress intensity factor at position ϕ may be calculated by multiplying the K calculated at the minor axis position by the ratio

$$\frac{K(\phi)}{K(\pi/2)} = \left[\frac{a^2}{c^2} + \left(1 - \frac{a^2}{c^2}\right) \sin^2 \phi\right]^{1/4} \qquad (4\ 10)$$

This function is plotted for convenience in Figure IV 6 and illustrates the reduction in $K(\phi)$ with decreasing a/c.

The various current theories for surface crack stress intensity factors, summarized above, lead to substantial differences for certain ranges of the geometrical parameters. The Kobayashi & Moss formula has a plasticity correction that is five to ten percent higher than Irwin's. The Orange result contains a modification of the Irwin plastic zone correction term so introduced to predict failure at ultimate load for a crack of vanishing depth. It predicts a K always somewhat higher than the Irwin result. Smith has shown that back surface effects for the semicircular crack configuration are small even for very deep ($a/c \approx 0.9$) notches, and are less at the plane stress than at the plane strain locations on the crack front.

IV.B Plane Stress & Plane Strain Plastic Zones

The region of plastic deformation associated with a crack tip exposed to a Mode I loading is generally much greater in plane stress than when a state of plane strain (plane deformation) prevails. In plane stress, the absence of lateral material constraint effectively makes the deviatoric portion of the strain tensor more predominate than in the case of plane strain, and this engenders more extensive yield regions. In the case of the part-through surface crack the state of deformation varies from near plane strain at the deepest part of the crack front to conditions approaching plane stress where the crack front intercepts the free surface. Since the state of deformation varies around the front, the stress intensity factor varies, as does the field of plastic deformation. In order to interpret the experimental data found from this investigation, we will consider some available analytical models for characterizing the plastic zone configuration under conditions of plane stress and plane strain.

A number of models for determining the plastic zone size have been developed on the basis of the stress intensity factor concept. This can be

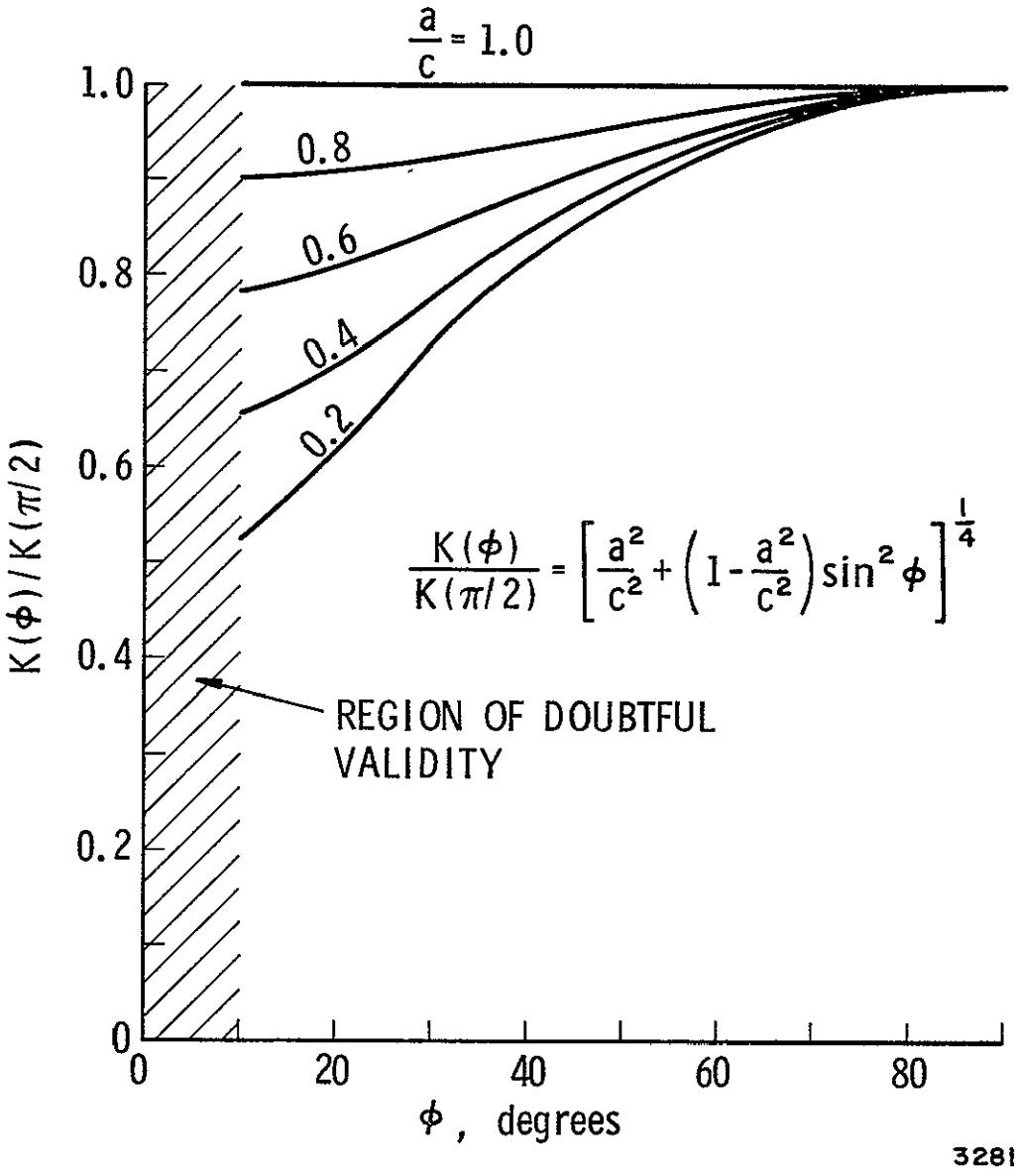

Figure Ⅳ.6 Correction Factor for Reduction in K with Angular Position ϕ

done in an approximate fashion by determining the stress field in the crack tip vicinity, and invoking a yield criterion to estimate the extent of yield.

Rice[15] presents plastic zone estimates under conditions of plane stress and perfect plasticity for the semi-infinite crack and the central through-crack in a large plate stressed in tension. For the semi-infinite crack the characteristic dimension of the plastic zone, R, is found to be

$$R = \frac{\pi}{8} \left(\frac{K}{\sigma_y}\right)^2 \tag{4.11}$$

from the well-known Dugdale-Barenblatt model. For the through-crack, again for a plane stress state, the estimate, as given by Bilby and Swinden[16], is:

$$R = c \left[\sec \left(\frac{\pi \sigma}{2 \sigma_y} \right) - 1 \right] \tag{4.12}$$

where c is the half-length of the crack. Rosenfield et al[3] have extended this problem to the case wherein the material is of the strain-hardening variety. A comparison of the above two models may be made by introducing the stress intensity factor $K = \sigma \sqrt{\pi c}$ into Equation (4.11), thus resulting in

$$R = \frac{\pi^2 c}{8} \left(\frac{\sigma}{\sigma_y}\right)^2 \tag{4.11'}$$

If we examine the ratio of the plastic zone predicted by Equation (4.11') to that predicted by Equation (4.10) we find that the ratio approaches unity for small values of σ / σ_y, and zero for σ / σ_y approaching unity. Thus, Equation (4.11) for the semi-infinite crack predicts a plastic zone smaller than Equation (4.12) for the through-crack, and in increasingly smaller proportion with increased stress level.

Under conditions of plane strain the associated plastic zone is smaller, for a given stress intensity, than the counterpart plane stress problem. The plane strain problem has been approached by Keer and Mura[17] who treat the penny-shaped crack of radius a subjected to a remote uniform tensile stress field σ. The interpretation given to this model, of course, is one of plane strain. The plastic zone which circumscribes the crack front was found to have the linear dimension

$$R = a \left\{ \left[1 - \left(\frac{\sigma}{\sigma_y} \right)^2 \right]^{-1/2} - 1 \right\} \tag{4.13}$$

For this problem, the stress intensity factor is: $K = 2\sigma\sqrt{a/\pi}$, which is smaller than the plane stress value of $\sigma\sqrt{\pi a}$ by a factor of $2/\pi$. Rice[15] has constructed a plane strain model based upon slip line theory. He assumed a "butterfly" plastic zone configuration described by $R(\theta) = R_o \cos[2(\theta - \pi/2)]$ where R_o is the maximum dimension of the plastic zone, occuring at $\theta = \pm \pi/2$. The analysis leads to the result

$$R_o \approx \frac{3(1-\nu)}{8\sqrt{2}(1+\pi/2)} \left(\frac{K}{\tau_o}\right)^2 \qquad (4.14)$$

where τ_o is the yield strength in simple shear. Comparing this result with the plane stress estimate given in Equation (4.11), we find (for $\nu = 0.3$) that the plane strain estimate is 55% of the plane stress value for a Mises material, and 73% for a Tresca material.

A number of other models have been proposed for estimating the extent of the plastic zone under small scale yield, plane strain conditions. Among them are those of Irwin[18]

$$R = 0.053 \left(\frac{K}{\sigma_y}\right)^2 \qquad (4.15)$$

and Liu[19]

$$R = 0.13 \left(\frac{K}{\sigma_y}\right)^2 \qquad (4.16)$$

These models, like those discussed earlier, make certain specific assumptions about the yield zone configuration, and R is to be considered only as a measure of its extent. Such models all are based on a two-dimensional representation of the crack geometry, and hence their applicability to the deep surface crack configuration, where free surface effects are felt, is uncertain a priori

In a recent report Ayres[20] adapted a finite difference technique for the determination of the three-dimensional stress and deformation fields in the neighborhood of a through-crack and a semi-elliptical surface crack in a thick plate in Mode I loading. The material was assumed to be elastic and perfectly plastic, obeying the Mises-Hencky yield condition and the Prandtl-Reuss flow rule in the plastic region. His results are summarized in Figures IV.7 and IV.8. These results correspond to a

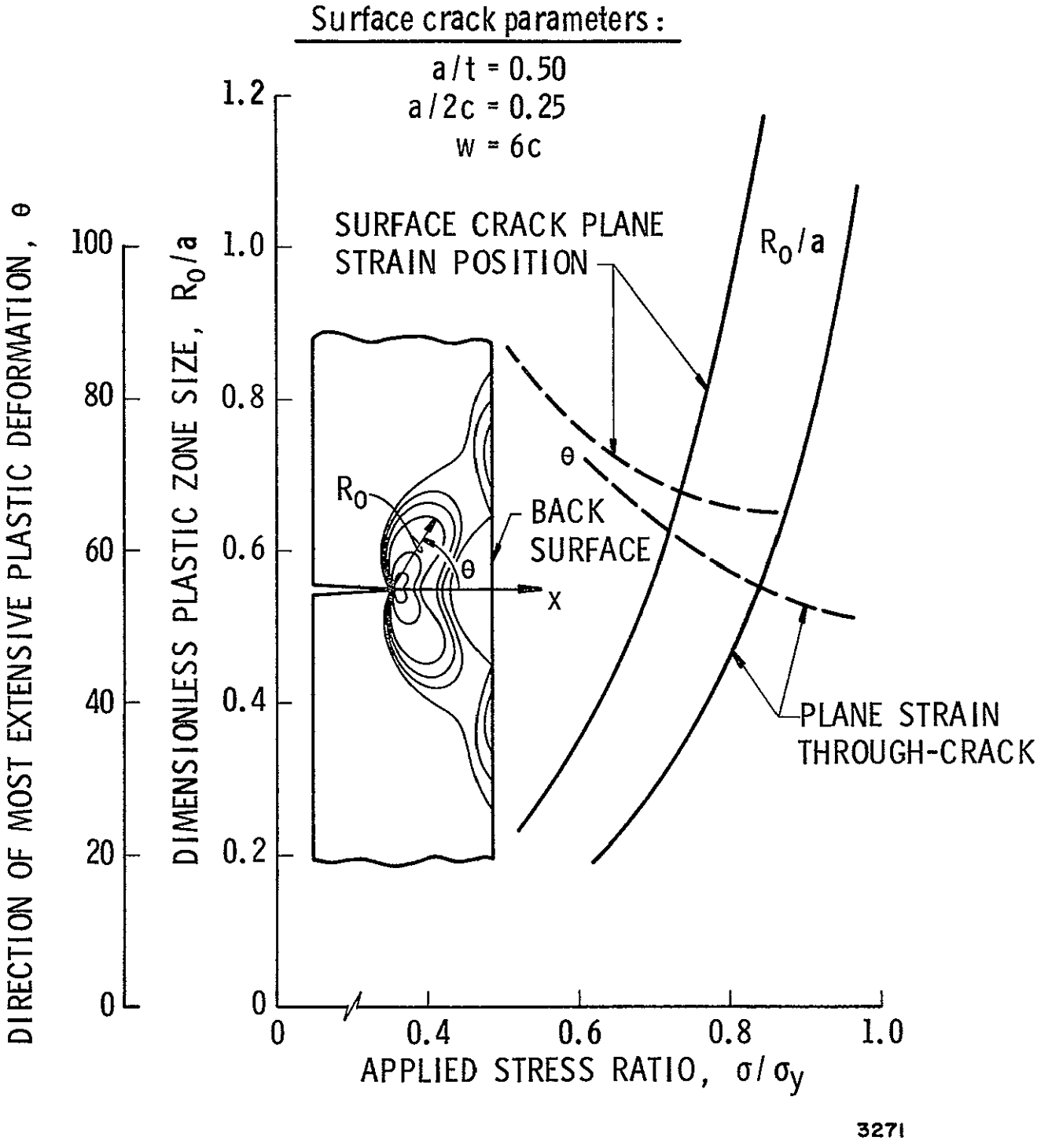

Figure Ⅳ. 7 Characterization of Plane Strain Plastic Zone, Adapted from Ayres (Ref. 20)

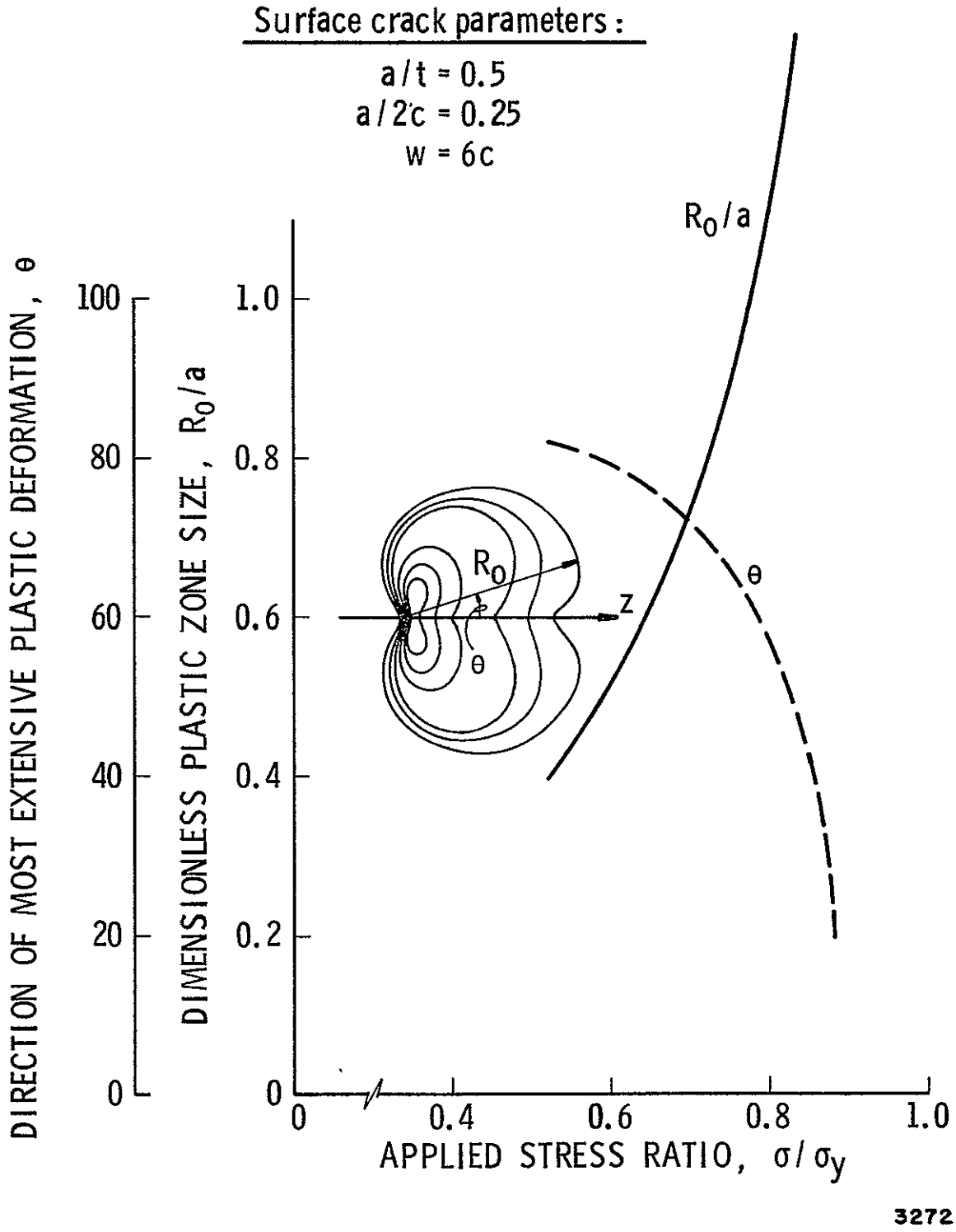

Figure Ⅳ.8 Characterization of Plane Stress Plastic Zone Size, Adapted from Ayres (Ref. 20)

material having a Young's modulus of 30×10^6 psi, a Poisson's ratio of 0.3, and a uniaxial yield strength of 200 ksi. Figure IV.7 characterizes the plastic zones associated with plane strain in terms of the maximum linear dimension and angular direction. The two sets of curves correspond to a plane-strain through-crack, and a surface crack at the minor axis position having the geometric parameters noted. For the surface crack example illustrated the plastic zone penetrated the back surface at a stress ratio σ / σ_y of about 0.8. As seen from the figure, the plastic zone size and its angular orientation both are greater for the surface crack in "plane strain" than for the true through-crack in the plane strain configuration. Figure IV.8 shows corresponding results for the surface crack in plane stress, i.e., where the crack front intercepts the front surface. Comparing Figures IV.7 and IV.8 we see that the angular position to the point of greatest plastic zone size decreases more rapidly with increased applied stress in the plane stress configuration.

V. RESULTS

V.A Test Matrix

Earlier in this report, Table II. 4 was presented to illustrate the nominal specimen notch configurations introduced by the EDM operation. Table III. 1 showed the nominal level to which each specimen was loaded, based upon the notch area, not the actual crack area

Table V. 1, which follows, shows the actual crack dimension parameters as determined during metallographic investigations. These dimensions, together with the applied dimpling and maximum applied loads also shown in the Table, form a proper basis for later data interpretation. In some cases it may be seen that the as-measured crack dimensions are somewhat less than the nominal notch dimensions given in Table II. 4 This is a result of the machining tolerances held on the EDM notches. Also, in some cases the fatigue crack was found not to have circumscribed the notch completely upon metallographic sectioning and analysis. In one specimen, Specimen 102, no evidence of a fatigue crack at all was found In all other cases, however, fatigue cracks were found on either end of the front surface notch, and the crack usually circumscribed the notch completely The fatigue crack was easily measured after metallographic analysis in all cases except for Specimen 154, a 0. 2 inch thick Ti-6A1-4V specimen which failed during fatigue. In this particular specimen there was noted a complex mixture of fatigue striations and plane strain fracture over much of the surface, making it impossible to delineate the crack size at rupture with much precision. The values for a and 2c given in Table V 1 for this specimen are minimum values, as noted.

V.B K and Fracture Toughness

The seven different models for calculation of the stress intensity factor K, described in Section IV. A, were applied to the specimen data under conditions of both back surface dimpling load and maximum load, as appropriate The results of this computation are given in Table V. 2. For purposes of computation the actual as-measured crack parameters a and c, given in Table V. 1, were used, and the stresses were based upon net section stress, as recommended by Randall[21]. Specimen numbers 106, 108, 93, 77, 78, 79 and 154 were not entered into this table as they represented conditions where the crack broke through the back surface under load, or other anomalous behavior which invalidate a calculation for stress intensity factor. Table V. 2 gives a basis for a comparison of the predictions of the various stress intensity factor models as applied to a wide range of surface notch configurations.

TABLE V. 1

SCHEDULE OF APPLIED LOADS AND ACTUAL CRACK CONFIGURATIONS

Spec. No.	t	W	a	2c	Dimpling load, lbs	Maximum load, lbs
102	0.115	1.20	0.053	0.170	2,500	4,720
103	0.115	1.20	0.062	0.240	1,800	(4,050)
104	0.115	1.20	0.023	0.220	790	(2,510)
105	0.115	1.20	0.077	0.288	960	(2,080)
106	0 115	1 75	(a)	(a)	(a)	(4,900)
107	0.115	1 75	0.083	0 491	870	(5,280)
108	0.115	1.75	(a)	(a)	(a)	(4,900)
60	0.230	1.25	0.124	0.314	X	14,500
61	0.230	1.25	0.109	0 285	X	10,900
62	0.230	1.25	0.107	0.262	X	9,100
63	0 230	1.25	0 107	0.282	X	15,500
64	0.230	1.70	0.160	0.484	(b)	8,000
65	0.230	1.70	0.113	0.367	X	11,520
66	0.230	1.70	0.116	0.365	X	13,200
67	0.230	1.70	0.080	0.337	X	14,000
68	0.230	2.50	0.099	0.536	16,930	16,930
69	0.230	2.50	0 145	0.562	10,000	14,520
70	0.230	2.50	0 127	0.531	18,000	20,600
71	0 230	2.50	0 166	0.539	3,500	19,360
84	0.230	1.75	0.126	0.372	X	9,790
85	0.230	1.75	0.122	0.390	11,000	13,060
86	0.230	1.75	0.132	0.379	X	11,420
87	0.230	2.30	0.139	0.511	X	15,000
88	0.230	2.30	0.121	0.513	X	12,830
89	0.230	2 30	0.141	0.512	14,400	17,120
90	0.230	2 50	0.156	0.747	X	13,310
91	0.230	2.50	0.161	0.745	8,600	15,520
92	0.230	2.50	0.128	0.736	X	17,760
93	0.230	2.10	(c)	(c)	(c)	(c)
94	0.230	2.10	0.153	0.472	10,000	13,330
95	0.230	2.10	0.183	0.456	9,200	15,230
96	0.230	2.50	0 153	0.602	13,330	13,330
97	0.230	2.50	0.157	0.726	14,500	15,570
98	0.230	2 50	0.166	0.601	13,100	17,800

Spec. No.	t	W	a	2c	Dimpling load, lbs	Maximum load, lbs
99	0.230	2.50	0.175	0.888	10,000	14,130
100	0.230	2 50	0 180	0.928	8,000	16,000
101	0 230	2.50	0 175	0.855	X	12,110
77	0 535	4.03	(d)	(d)	(d)	(d)
78	0.525	4.01	(d)	(d)	(d)	(d)
79	0.525	4.01			(e)	64,200
109	0.104	0.985	0.086	0.214	1,700	8,220
110	0 104	1.018	0.082	0.225	1,370	1,370
111	0.101	1.023	0.087	0.224	730	730
112	0.105	1 023	0.088	0 278	1,070	8,790
113	0.102	1.016	0.086	0.277	900	900
114	0.101	1.040	0.094	0.295	540	540
115	0 103	1.257	0.094	0.407	870	10,670
116	0.104	1 269	0.095	0 403	375	375
117	0.103	1.249	0.098	0.426	330	330
151	0.200	3 00	0.094	0.259	X	78,100
152	0.200	3.00	0.090	0.243	X	78,100
153	0.200	3 00	0.175	0.741	4,200	58,500
154	0.200	3 00	0.200[f]	0 600[f]	(b)	26,500

Notes:

(a) fatigue crack broke through back surface

(b) specimen failed during fatigue, no dimpling

(c) specimen broken during fabrication

(d) specimen broke during water quench

(e) crack broke through at 14,000 lb, no dimpling

(f) lower estimate due to difficulty in delineating extent of pure fatigue cracking, as discussed in Section V. A

X no dimpling observed

( ) load at which crack broke through to back surface

TABLE V.2

CALCULATED STRESS INTENSITY FACTORS
psi $\sqrt{in}$

Spec	Irwin		Paris & Sih		Smith		Kobayashi & Moss		Orange		Rice & Levy		Anderson, et al	
No.	dimpling	max load	dimpling	max load	dimpling	max load	dimpling	max load	dimpling	max load	dimpling	max load	dimpling	max load
102	6,650	12,770	6,950	13,110	6,410	12,320	6,520	12,640	6,830	14,200	X	X	6,860	15,420
103	X	---	6,300	---	X	---	5,920	---	X	---	5,490	---	5,970	---
104	1,650	---	1,680	---	1,640	---	1,660	---	1,650	---	X	---	1,680	---
105	X	---	4,310	---	X	---	3,560	---	X	---	3,080	---	3,700	---
107	X	---	3,490	---	X	---	2,780	---	X	---	X	---	3,050	---
60	---	X	---	22,800	---	X	---	21,600	---	X	---	X	---	X
61	---	X	---	16,440	---	X	---	15,500	---	X	---	X	---	17,960
62	---	11,880	---	12,190	---	11,310	---	11,500	---	12,560	---	X	---	12,380
63	---	21,320	---	21,550	---	20,380	---	21,320	---	25,800	---	X	---	X
64	---	X	---	17,620	---	X	---	14,510	---	X	---	11,730	---	16,210
65	---	17,170	---	18,010	---	16,570	---	18,680	---	18,740	---	X	---	20,200
66	---	X	---	20,860	---	X	---	21,700	---	X	---	X	---	25,550
67	---	17,950	---	17,780	---	17,500	---	17,910	---	20,120	---	X	---	22,070
68	17,650	17,650	18,380	18,380	17,320	17,320	17,730	17,730	19,010	19,010	17,450	17,450	21,500	21,500
69	X	X	14,220	20,690	X	X	12,250	18,070	X	X	11,140	16,190	13,430	21,900
70	X	X	22,400	25,710	X	X	20,600	24,000	X	X	20,260	23,500	27,150	X
71	X	X	5,610	31,080	X	X	4,690	22,600	X	X	X	X	4,500	X
84	---	X	---	15,310	---	X	---	13,880	---	X	---	X	---	15,430
85	X	X	17,320	20,560	X	X	16,230	19,620	X	X	X	X	18,450	24,010
86	---	X	---	18,970	---	X	---	17,100	---	X	---	X	---	20,200
87	---	X	---	21,750	---	X	---	19,500	---	X	---	18,000	---	24,200
88	---	X	---	17,150	---	X	---	15,830	---	X	---	15,800	---	18,350
89	X	X	21,000	25,000	X	X	18,450	22,300	X	X	16,740	19,930	22,670	X
90	---	X	---	23,470	---	X	---	19,720	---	X	---	18,200	---	X
91	X	X	15,650	28,110	X	X	12,730	23,300	X	X	10,890	19,580	14,480	X
92	---	X	---	25,690	---	X	---	23,800	---	X	---	25,800	---	X
94	X	X	16,960	22,590	X	X	14,620	19,610	X	X	11,190	14,900	15,770	23,650
95	X	X	X	X	X	X	13,500	22,350	X	X	X	X	14,300	X
96	X	X	20,840	20,840	X	X	17,630	17,630	X	X	15,980	15,980	21,530	21,530
97	X	X	25,320	27,160	X	X	19,370	22,800	X	X	18,930	20,300	X	X
98	X	X	22,290	30,300	X	X	18,050	21,800	X	X	X	X	21,600	X
99	X	X	X	X	X	X	17,740	25,200	X	X	X	X	X	X
100	X	X	X	X	X	X	14,580	24,700	X	X	X	X	17,480	X
101	---	X	---	X	---	X	---	19,230	---	X	---	X	---	X

TABLE V.2

CALCULATED STRESS INTENSITY FACTORS (Cont'd)

psi $\sqrt{in}$

Spec	Irwin			Paris & Sih			Smith			Kobayashi & Moss			Orange			Rice & Levy			Anderson, et al	
No	dimpling	max	load	dimpling	max	load	dimpling	max	load	dimpling	max	load	dimpling	max	load	dimpling	max	load	dimpling	max load
109	X	X	X	X	X	X	X	X	X	8,000	35,600	X	X	X	X	X	X	X	7,870	X
110	X	X	X	X	X	X	X	X	X	6,320	---	X	X	X	X	X	X	X	6,300	6,290
111	X	X	X	X	X	X	X	X	X	3,620	---	X	X	X	X	X	X	X	X	X
112	X	X	X	X	X	X	X	X	X	5,850	42,500	X	X	X	X	X	X	X	5,810	X
113	X	X	X	X	X	X	X	X	X	5,120	---	X	X	X	X	X	X	X	5,070	5,070
114	X	X	X	X	X	X	X	X	X	3,600	---	X	X	X	X	X	X	X	X	X
115	X	X	X	X	X	X	X	X	X	5,400	42,900	X	X	X	X	X	X	X	X	X
116	X	X	X	X	X	X	X	X	X	2,360	---	X	X	X	X	X	X	X	X	X
117	X	X	X	X	X	X	X	X	X	2,450	---	X	X	X	X	X	X	X	X	X
151	---	61,900	---	61,490	---		59,310	---		62,000	---		136,900	---		52,700	---		---	X
152	---	59,790	---	58,790	---		57,240	---		59,700	---		129,980	---		50,100	---		---	X
153	X	X	X	X	X	X	X	X	X	6,790	79,100	X	X	X	X	X	X	X	X	X

Notes X = outside valid range for K model

--- = not applicable

In Table V. 2 the entries denoted by X represent conditions under which the restrictions for the particular stress intensity factor model have been violated, as for example, when the ratio a/t exceeds the recommended limit All values for stress intensity factors shown (in units of psi $\sqrt{in}$) are "valid" inasmuch as all stated limitations on the particular model have been fulfilled. One fact that emerges from this table is that in certain cases a "valid" computation for K may in fact exceed the measured fracture toughness value K_{Ic}. In particular, certain stress intensity factor calculations from the models of Irwin, Paris & Sih, Smith, Kobayashi & Moss, Orange, Rice & Levy and Anderson, et al, for Fe-3Si exceed the estimated fracture toughness of 18, 900 psi$\sqrt{in}$, as will be discussed later in this section. Thus, it appears that these models may be subjected to more limiting restrictions than those mentioned by their proposers.

An examination of the table reveals that the models of Paris & Sih, and Kobayashi & Moss lead to the largest number of "valid" K computations, as a consequence of their having relatively weaker restrictions than the other models. The computed stress intensity factors for these two models are in relatively close agreement with one another. The model of Rice & Levy, a purely elastic model, yields values of K generally somewhat less than those of Paris & Sih and Kobayashi & Moss. The models of Smith, and Orange, are modifications of the original model of Irwin, and are subject to the same restrictions, viz, $a/t < 0.5$ and $a/c \leqslant 1\ 0$. The models of Irwin and of Smith generally predict values of K in close mutual agreement, whereas the model of Orange predicts values of K somewhat larger. The model of Anderson, et al consistently overestimates the values of K as computed on the basis of the other models.

The surface notch configuration is seldom used as a fracture toughness specimen, primarily because there is no "exact" method of computing the stress intensity factor short of undertaking an arduous numerical analysis. One of the few discussions on the use of the surface notched specimen for K_{Ic} determination is given by Randall[21]. In the present study a subordinate investigation was made to determine fracture toughness using the surface cracked specimen, and to compare the values as computed from various analytical models of plane strain stress intensity factors for the surface crack Toward this end, two Ti-6Al-4V specimens, 0. 2 inch thickness, were prepared as fracture toughness specimens. In addition, two of the Fe-3Si specimens, which had notch configurations consistent with several of the models studied, failed prematurely during tensile loading, and these specimens can serve to estimate the fracture toughness of the silicon iron.

In conducting the experiments for K_{Ic} determination a small clip gage was placed across the region containing the crack, and the load was plotted against the readout from the strain gage. The clip gage arrangement is shown in Figure V 1. The load-displacement diagram for each specimen was linear over a wide range, and became nonlinear as yielding became more pronounced prior to fracture. In no case was any "pop-in" effect of any significance detected.

The calculated K_{Ic} data are shown in Table V. 3. Those entries intentionally left blank correspond to crack configurations which lie outside of the claimed region of validity for the analytical model. Thus, in the case of specimen 64 the a/t ratio invalidated the Irwin, Smith and Orange models, and the c/t ratio invalidated the Rice & Levy model for Specimen 67. Also, for all specimens except Specimen 67 the Anderson et al model was invalid because it predicted large scale yielding penetrating the back surface of the specimen These results show that the calculated K_{Ic} models for all models are reasonably comparable, except for the Orange model which tends to predict quite large values for high toughness materials. The models of Irwin, Paris & Sih, Smith, and Kobayashi & Moss give values in close correlation with one another. The model of Rice & Levy, which makes no allowance for plasticity effects, tends to underpredict the other models, and would probably serve as a conservative estimate in design practice If we take first four models given in the table as indicative of the true fracture toughness, we find the following averages:

$$\text{Fe-3Si:} \qquad K_{Ic} = 18,900 \text{ psi}\sqrt{\text{in}}$$

$$\text{Ti-6Al-4V:} \qquad K_{Ic} = 60,000 \text{ psi}\sqrt{\text{in}}$$

The value for Ti-6Al-4V alloy is consistent with the value of 65,000 psi$\sqrt{\text{in}}$ cited by Randall[21] as characteristic of these alloys having a yield strength of 154,000 psi.

V.C Characterization of Surface Deformation

C-1. Back Surface Dimpling

During specimen loading the polished back surface was visually observed to detect whether back surface dimpling had occurred. With the aid of appropriate oblique illumination it was possible to see rather clearly the onset of dimpling. In those specimens where dimpling

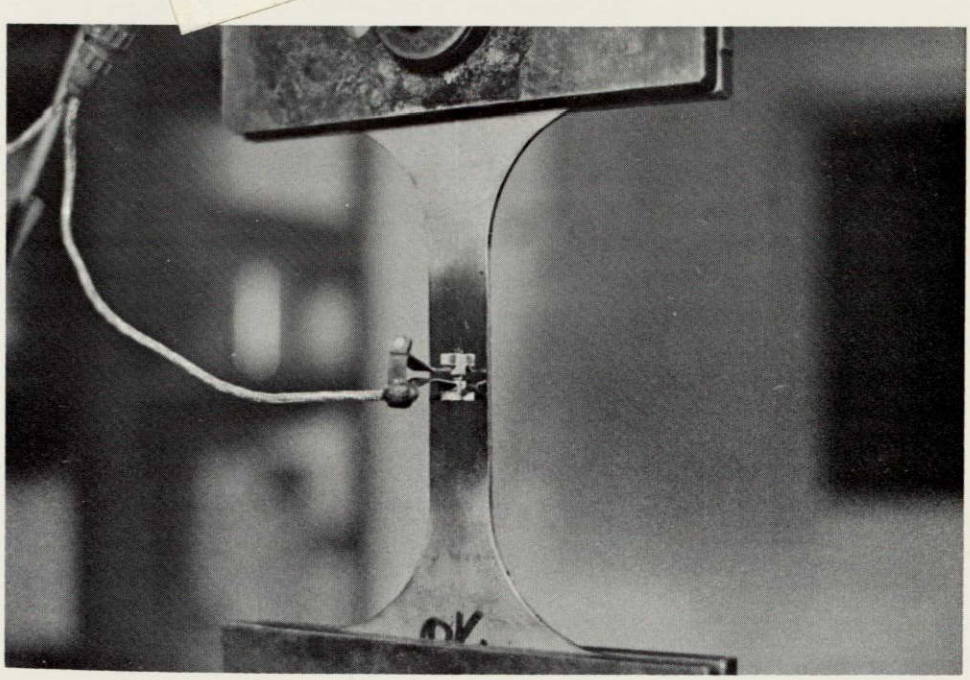

Figure V. 1 Illustration of Clip Gage Used in Connection with Fracture Toughness Measurements

TABLE V.3

COMPUTED VALUES OF K_{Ic} (psi $\sqrt{in}$)

Spec. No.	Mtl	t	a/t	a/2c	Irwin	Paris & Sih	Smith	Kobayashi & Moss	Orange	Rice & Levy
64	Fe-3Si	0.236	0.678	0.331	---	17,620	---	23,500	---	19,140
67	Fe-3Si	0.230	0.348	0.237	17,950	17,780	17,500	17,910	20,120	---
151	Ti-6Al-4V	0.200	0.470	0.363	61,900	61,490	59,310	62,000	136,900	52,700
152	Ti-6Al-4V	0.200	0.450	0.370	59,790	58,790	57,240	59,700	129,980	50,100

Note: For Specimen #67 the Anderson et al model gives K_{Ic} = 22,070 psi$\sqrt{in}$

was observed to occur, an attempt was made to photograph the surface appearance with a 35 mm camera equipped with close-up lenses. Then, plastic replicas were made of the dimpled area under loaded and relaxed conditions. These replicas were then profiled with a Taylor-Hobson Model 3 Talysurf Surface Measuring Instrument, as explained in Section III. D-1.

Figure V. 2 shows the typical appearance of the back surface dimples. Figure V. 2a was taken from Specimen 100, one of the 0. 2 inch Fe-3Si series specimens; Figure V. 2b was from Specimen 115, one of the 0. 1 inch Ti-6Al-4V series, In general, the titanium specimens tended to dimple under smaller net section stresses than did the silicon iron specimens. It should be noted that the dimple shape is a single elongated shallow surface, and differs from the regions where the plastic zone ahead of the interior crack front first penetrates the back surface (see Figure IV. 7). Bixler and Masters[22] have confirmed the surface strain pattern consistent with the results of Ayres[20], from which Figure IV. 7 was taken).

Figure V. 3 shows the results of a typical Talysurf trace, taken perpendicular to the long axis of the dimple through the centerline, in both the loaded and the unloaded states. Typically, significant elastic recovery was evident between the loaded and unloaded conditions. The dimple depth in the 0. 2 inch Fe-3Si specimen series (loaded state) varied from insignificant up to about 260 microinches, depending upon the applied stress level and the crack front geometry. One specimen, Specimen 100 illustrated in Figure V. 2a, had a maximum dimple depth of 830 microinches, but this was not typical of the rest of the series. Figure V. 4 shows the corresponding Talysurf profile for Specimen 115, one of the 0. 1 inch titanium series, and the one which showed the most dramatic dimpling effect (see again Figure V. 1b). Here, it is interesting to note that on unloading, the dimple partially protruded from the reference back surface plane, a result of the severe internal compressive strain field. In no other specimen did this effect manifest itself, since in all other specimens (including the remainder of the titanium series) the dimple depth was less than half (usually much less) this amount. Table V. 4 summarizes the data characterizing the dimple depth in both the loaded and unloaded states.

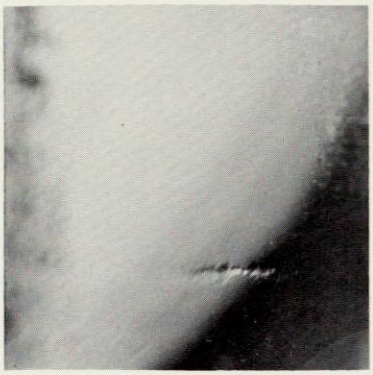

(a) Specimen 100 (0.2" Fe-3Si)

(b) Specimen 115 (0.1" Ti-6Al-4V)

Figure V.2 Visual Appearance of Back Surface Dimples, Loaded Condition (True Size)

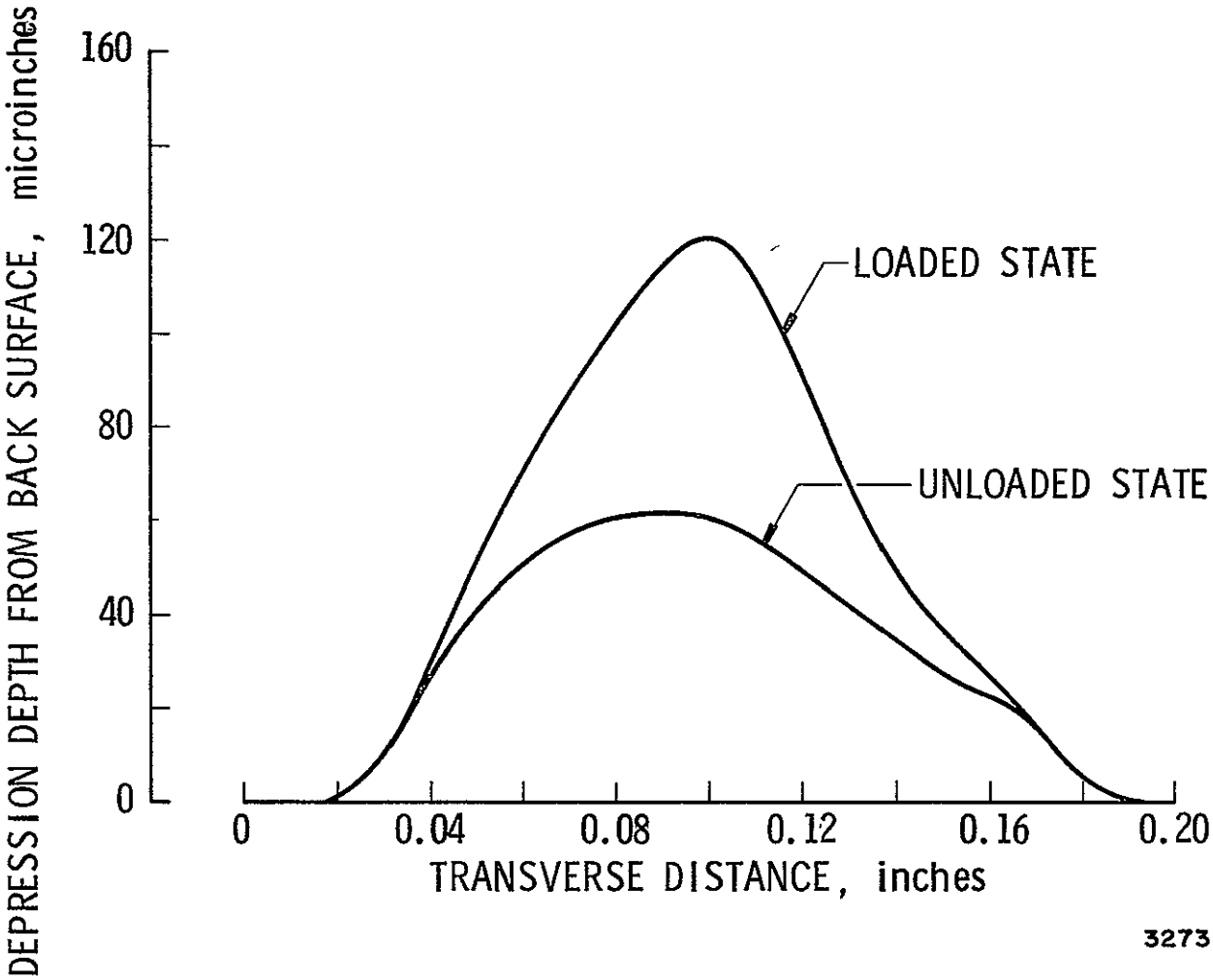

Figure V.3 Back Surface Dimple Configuration, Specimen #95
Transverse Profile Through ℄

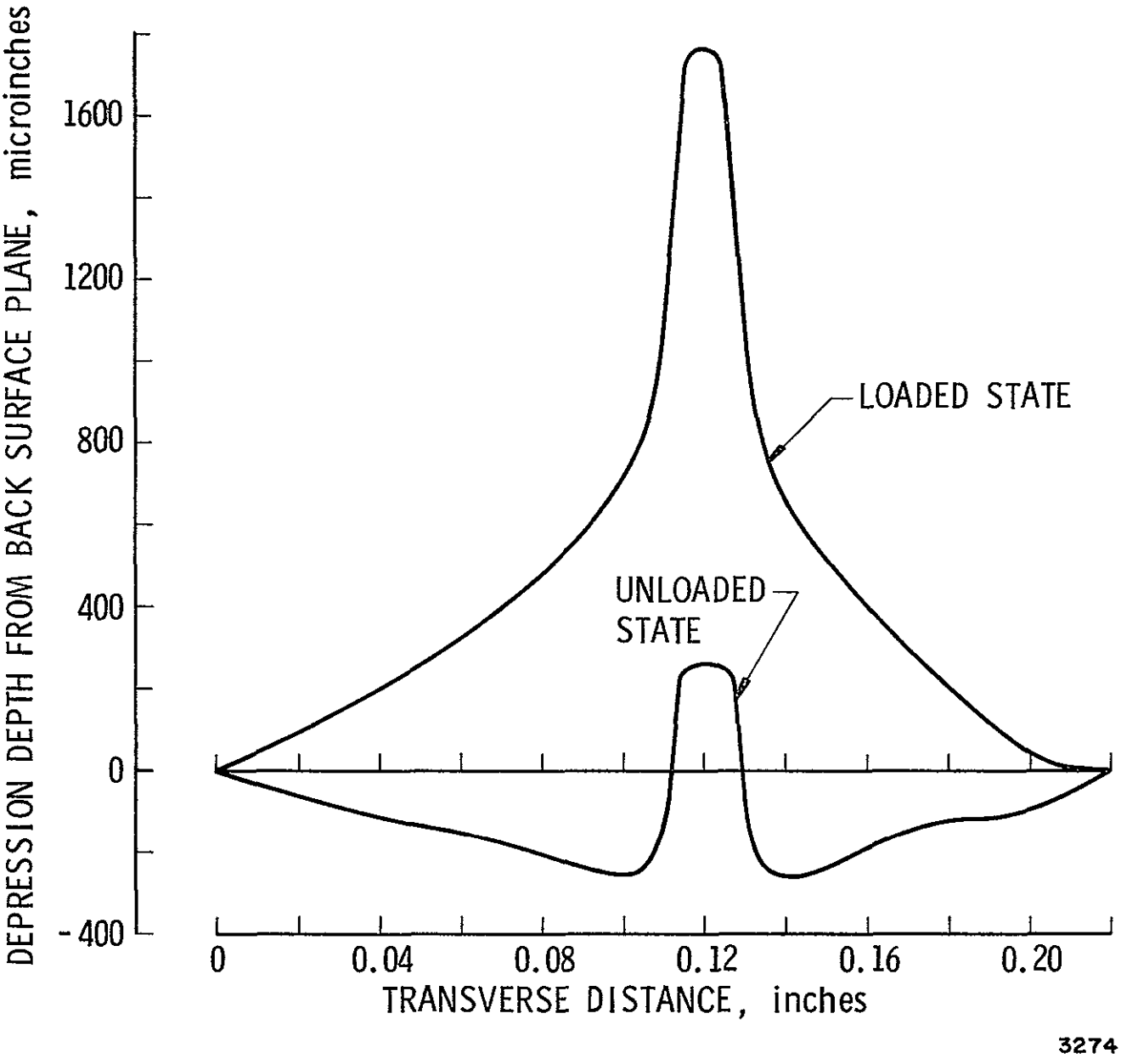

Figure V.4 Back Surface Dimple Configuration, Specimen #115 Transverse Profile Through ℄

TABLE V 4

MEASURED BACK SURFACE DIMPLE DEPTHS

Spec. No	Dimple Depth (microinches) loaded	unloaded
70	100	100
71	150	50
89	72	20
91	180	100
95	130	40
96	-0-	170
97	100	90
98	160	150
99	260	20
100	830	230
112	810	230
115	1780	260

In most cases it was difficult to characterize accurately the surface extent of the dimple, due to the small and smoothly varying displacements involved, and the instrument "noise" arising from the replica surface. In view of this, and due also to the fact that many of the specimens showed no measurable dimpling effect, it was not possible to make any meaningful correlations between dimpling geometry and crack geometry.

Table V. 5 summarizes the pertinent data for observed threshold levels of back surface dimpling. It is important to note that the specimens not included in the table showed no signs of back surface dimpling up to the maximum tensile load applied

Figure V. 5 illustrates the effect of the crack geometry on the stress intensity factor for threshold back surface dimpling. The figure contains data from the 0. 1 and 0. 2 inch thickness Fe-3Si specimen series, and from the 0. 1 inch thickness Ti-6Al-4V specimen series The Kobayashi & Moss stress intensity factor is used in the correlations. The threshold stress intensity factor appears to be inversely related to the flaw depth ratio a/t , indicating that deeper flaws promote through-thickness yielding at lower stress levels than do more shallow cracks

Scatter in the data is attributed both to the difficulty in visually perceiving the precise onset of back surface dimpling, and to the approximate nature of the Kobayashi & Moss model for deep flaws with large scale yielding. The data from the 0.1 inch Fe-3Si specimens are widely scattered from the remaining data While the reason for this is not clear, it is likely that the high temperature heat treatment and rapid quench given to this specimen group had a significant effect in altering the yield characteristics, and therefore in the dimpling disposition The validity of the dimpling data for the 0 1 inch Fe-3Si specimens may, therefore, be open to some question.

Figure V.6 compares the same back surface dimpling threshold data with theoretical predictions of yield zone penetration into the back surface The curves were derived from the Kobayashi & Moss model by crossplotting Figure IV 3; these curves corroborate the shown point predicted by Ayres from Figure IV.7. The fact that the data, despite the inherent scatter, all lie beneath the curves shows that observable back surface dimpling develops at stress levels considerably lower than those needed to cause yield zone penetration by the Kobayashi & Moss, and Ayres models.

TABLE V.5

BACK SURFACE DIMPLING THRESHOLDS AND ASSOCIATED PLASTIC ZONE SIZE AT $\phi = \pi/2$ AT MAXIMUM LOAD

Spec. No.	t	a	Threshold σ/σ_y	Max Load σ/σ_y	Max measured plastic zone dimension
68	0.230	0.099	0.544	0.554	0.031
69	0.230	0.145	0 341	0.496	0.028
70	0.230	0.127	0.596	0.684	0.044
71	0.230	0 166	0.121	0.670	0.032
85	0.230	0 122	0.524	0.622	0.021
89	0.230	0 141	0.530	0 631	0.044
91	0.230	0.161	0.314	0 564	0.037
94	0.230	0.153	0.416	0.554	0.017
95	0 230	0.183	0.386	0.640	0.052
96	0.230	0.153	0.468	0.468	0.020
97	0.230	0 157	0.525	0.563	0.061
98	0.230	0 166	0.462	0.628	0.065
99	0.230	0.175	0.392	0.553	0.044
100	0.230	0.180	0.313	0 625	*

Spec No.	t	a	Threshold σ/σ_y	Max. Load σ/σ_y	Max. measured plastic zone dimension
109	0.104	0.086	0.134	0.649	---
110	0.104	0.082	0.104	0.104	---
111	0.101	0 087	0.0576	0.0576	---
112	0.105	0.088	0.0842	0.692	---
113	0.102	0.086	0.0736	0.0736	---
114	0.101	0.094	0.0451	0.0451	---
115	0.103	0 094	0.0608	0.746	---
116	0.104	0.095	0.0255	0.0255	---
117	0.103	0.098	0.0239	0.0239	---

* Specimen cracked through back surface at maximum load, no metallography was done in transverse section due to extensive plastic deformation.

C-2. Front Surface Dimpling

The Michelson interferometric apparatus, as described in Section III. D-2, was used to map the surface contours of the residual deformation near the crack tips after tensile testing. This method can provide fine-scale topological features in small regions, and it is possible to resolve the residual dimple depth and extent with high accuracy

Table V. 6 summarizes the data obtained from the 0. 2 inch Fe-3Si and the 0. 1 inch Ti-6Al-4V specimens as to the dimple depth on the front surface in the unloaded state. In the table, the dimple depths have been taken to be the average depth as measured at each end of the front surface crack. In Figure V. 7, these data have been plotted against the length parameter $(K/\sigma_y)^2$, where K is the plane stress stress intensity factor $\sigma\sqrt{\pi c}$. From the considerable scatter in these data it is evident that the parameter $(K/\sigma_y)^2$ is not a strong correlating factor. The Fe-3Si data appear to be relatively insensitive to this factor, and the Ti-6Al-4V data, while exhibiting an increasing trend with $(K/\sigma_y)^2$, lie quite outside the Fe-3Si data. Several other parameters were tested in an attempt to find a stronger correlation, but none were found. Among these were the ratio of the dimple depth to linear expanse, and the ratio σ/σ_y.

There was a very definite difference between the symmetry and degree of definition of the interferograms of the Fe-3Si and Ti-6Al-4V

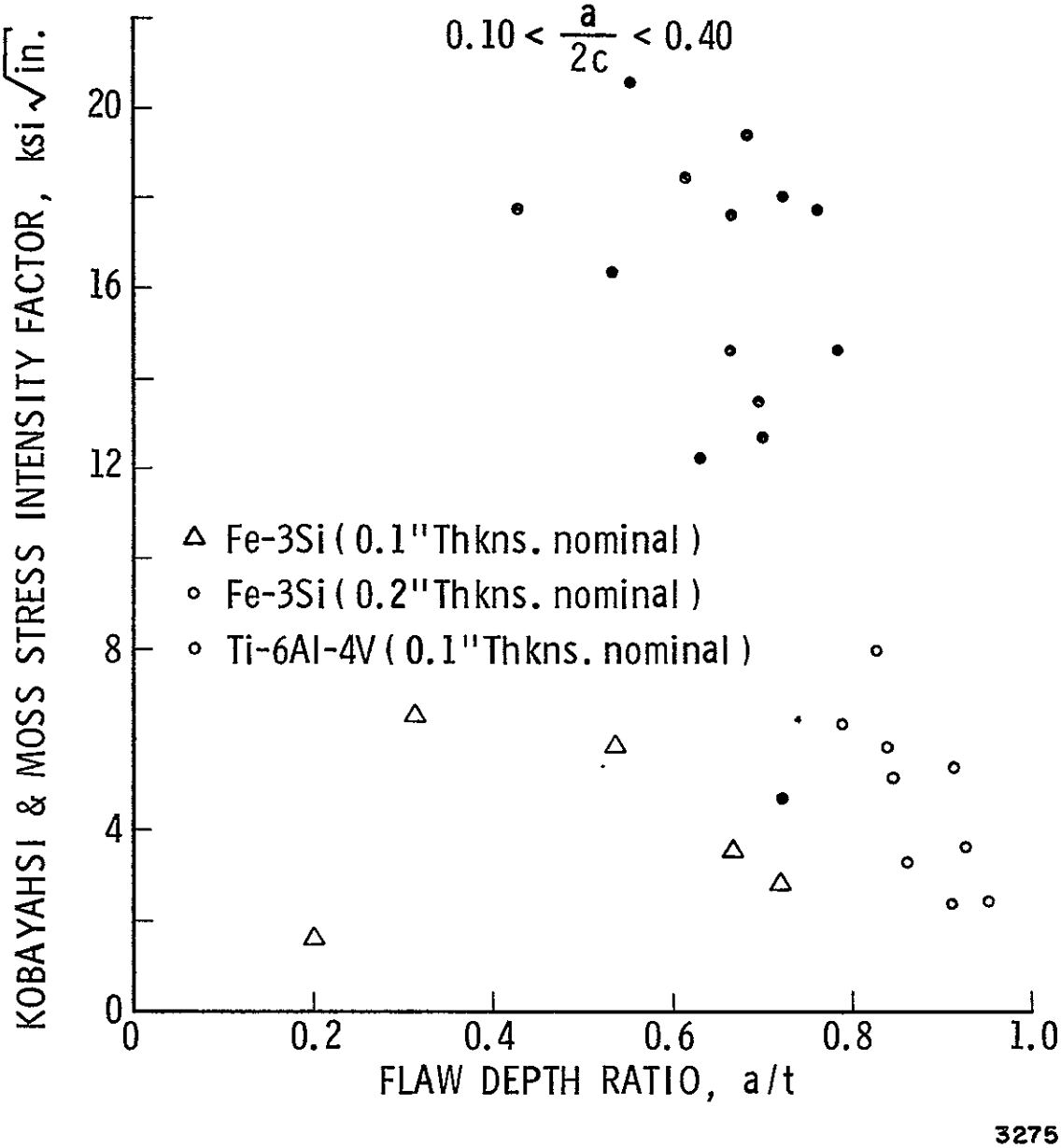

Figure V.5 Back Surface Dimpling Thresholds for Fe-3Si and Ti-6Al-4V

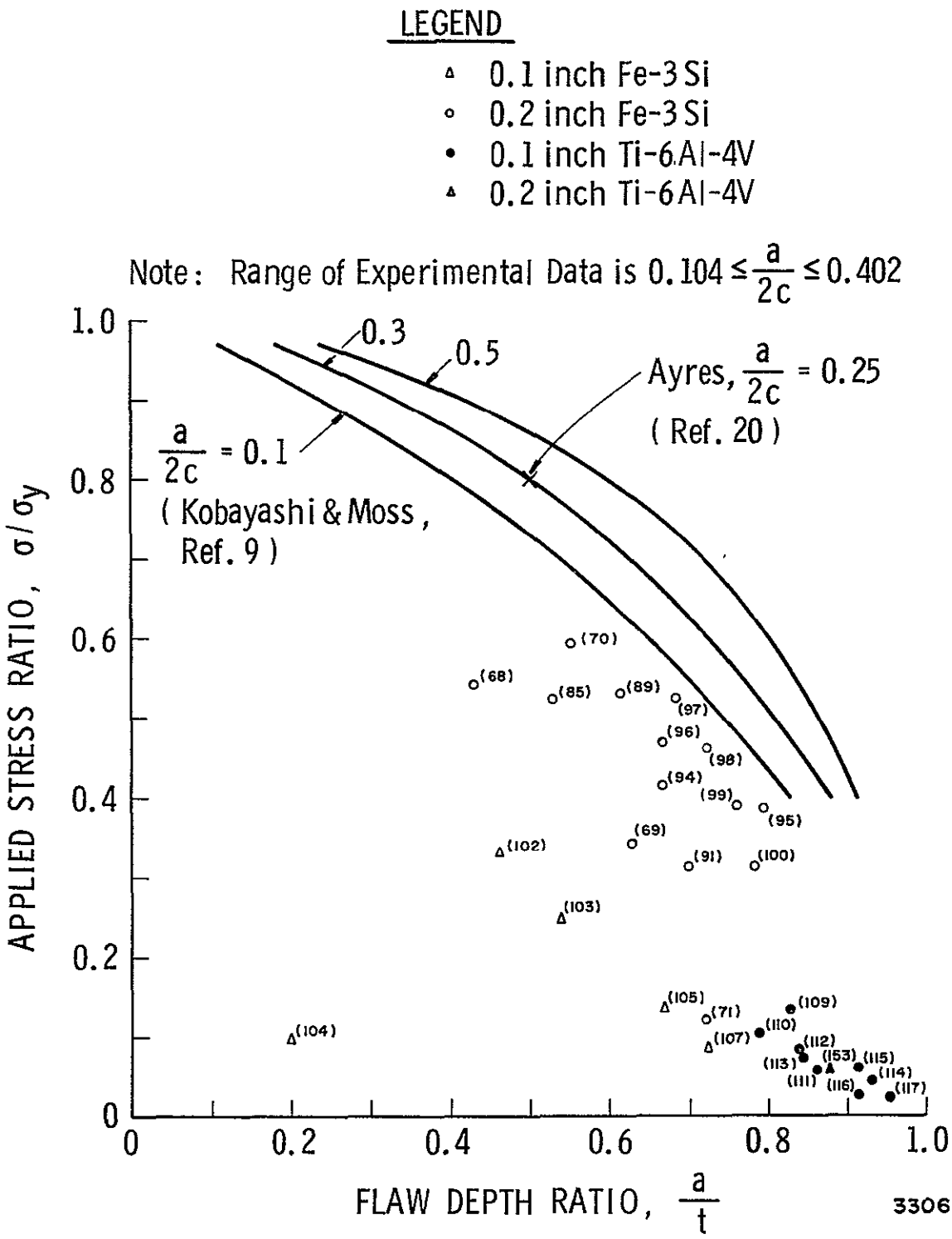

Figure V.6 Comparison of Incipient Back Surface Dimpling Data with Theoretical Models of Plastic Strain Penetration

TABLE V.6

FRONT SURFACE RESIDUAL DIMPLE DEPTHS

Spec. No.	σ/σ_y	a/2c	Depth, microinches
65	0.576	0.308	81.0
66	0.662	0.318	87.2
68	0.554	0.185	68 5
69	0.496	0.258	81.0
70	0.684	0.239	62.2
71	0.670	0.308	87.2
84	0.466	0.339	74.7
85	0.622	0.313	56.0
86	0.560	0.348	56.0
87	0.555	0.272	56.0
88	0.474	0.236	43.6
89	0.631	0.275	56 0
90	0.486	0.209	49.8
91	0.564	0.216	49.8
92	0.626	0.174	37.4
94	0.554	0.324	62.2
95	0.640	0.401	93.5
96	0.468	0.254	43.6
97	0.563	0.216	81.0
98	0.628	0.276	74.7
99	0.553	0.197	62.2
109	0.649	0.402	124.7
112	0.692	0.316	249.4
115	0.746	0.231	274.0

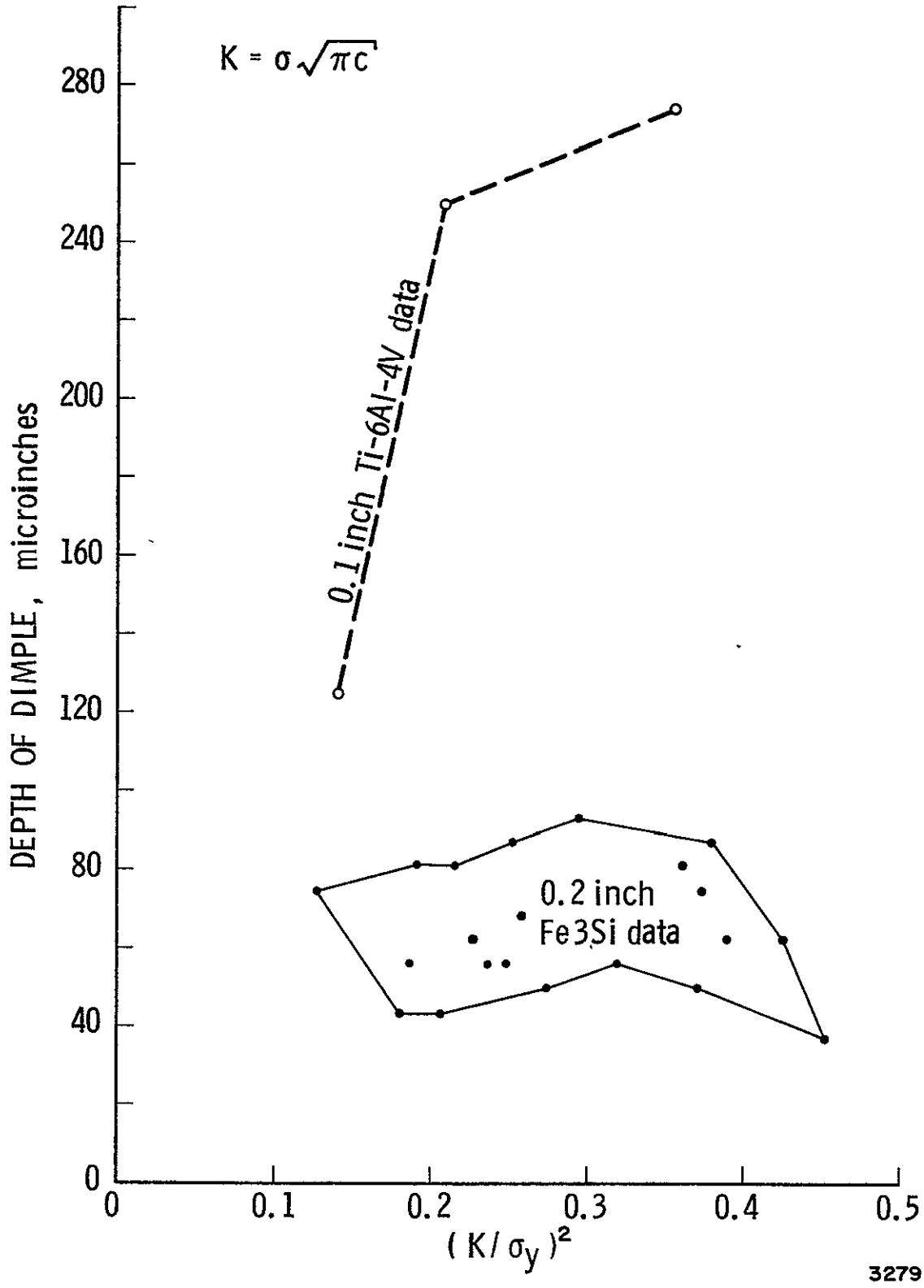

Figure V.7 Residual Dimple Depth at Front Surface Crack Tips

specimens. The silicon iron specimens displayed much more complex and irregular dimple contours, and the difficulty in characterizing their depth in a consistent fashion undoubtedly is responsible for much of the scatter in Figure V. 7 By comparison, the dimple contours of the titanium specimens were much more regular and repeatable There was no bifurcation of the crack tips as there was in many of the Fe-3Si specimens. Also, there was very little difference in fringe patterns on either end of the crack, unlike the silicon iron specimens which frequently displayed quite different dimple geometry. Some typical photographs of the dimple contours from these two groups of specimens are shown in Figures V. 8 through V. 11. It is worth emphasizing that since these interferograms were taken from relaxed specimens after prior tensile loading, the dimples represent residual displacement fields, and no information is available regarding the magnitude of the associated elastic fields that were removed on unloading

Figures V. 8 and V. 9 show surface and interferogram photos typical of those found in the 0. 2 inch Fe-3Si specimens. Some interferograms were much clearer than these, others less so. These figures reveal the difficulty in accurately characterizing the small dimple depth in these specimens. They show also how the surface edges of the EDM notch were rounded off in the metallurgical polishing. Figure V. 10 shows typical results from the 0. 1 inch Fe-3Si specimens. These specimens underwent large scale yielding and cracked through the back surface at relatively low net section stresses. The amount of surface deformation is difficult to characterize due to the high density of the fringe lines (on the order of 100). Figure V. 11 shows results typical of those obtained from the 0. 1 inch titanium series. The fringe pattern is quite regular and in general agreement with what one would expect from the highlighted surface appearance. In connection with the titanium series, it is important to point out that at net section stresses just sufficient for the onset of back surface dimpling, no residual front surface crack tip dimpling was found. That is, for deep surface cracks in Ti-6Al-4V back surface dimpling preceeds front surface dimpling.

V. D Plastic Zone Configuration

The series of Fe-3Si specimens was designed and conducted to reveal information regarding the plastic zone configuration as influenced by applied stress level, crack geometry (a/c), and proximity of the back surface (a/t). The Fe-3Si specimens were designed in three thickness groups, 0. 1, 0. 2, and 0. 5 inch (nominal). Most of the specimens

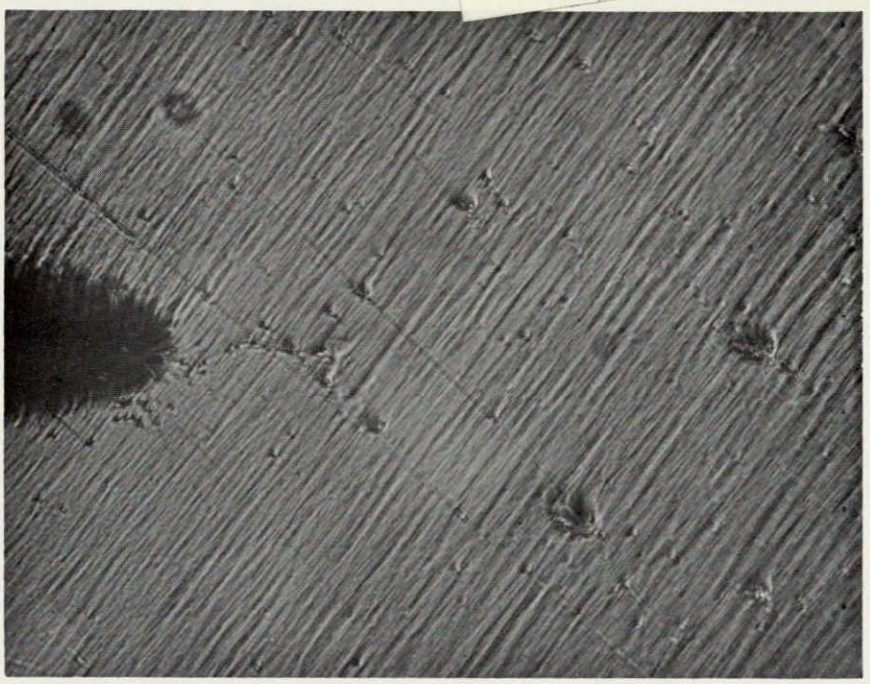

Laser Illuminated Photograph, 50X

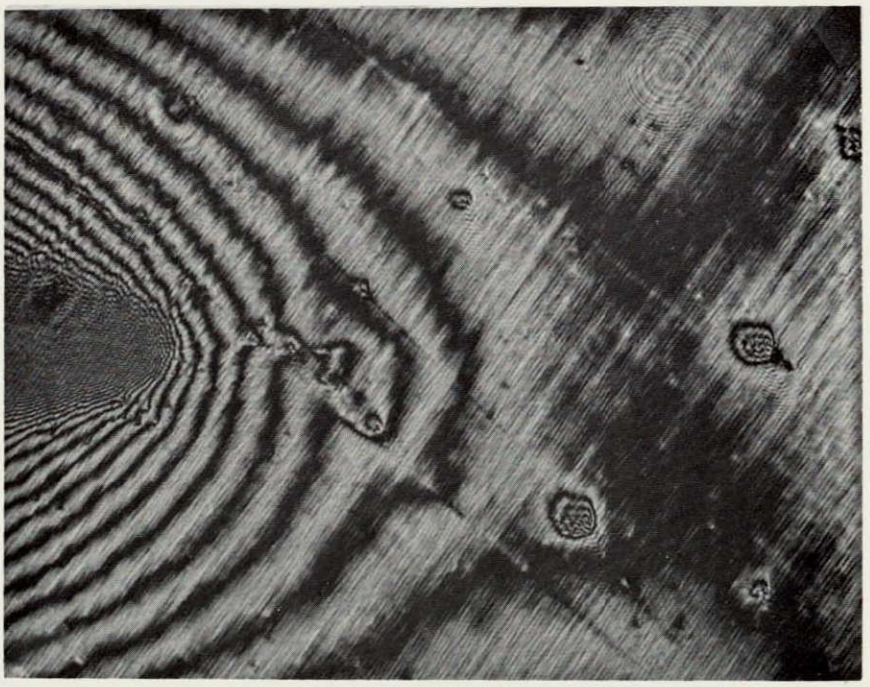

Interferogram, 50X

Figure V. 8 Front Surface of Specimen 90 (0. 2" Fe-3Si) Showing Crack Tip and Dimple

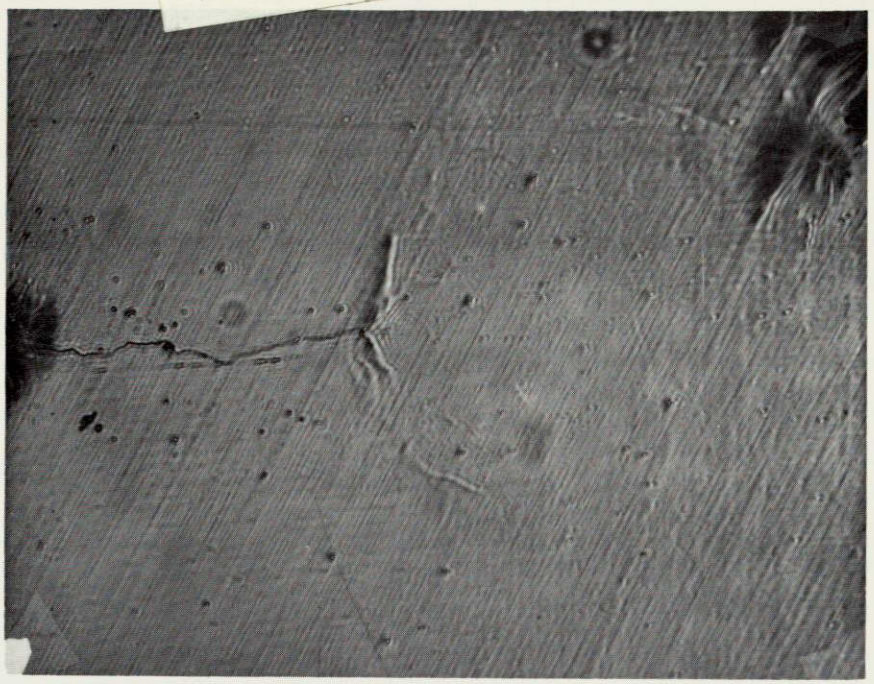

Laser Illuminated Photograph, 50X

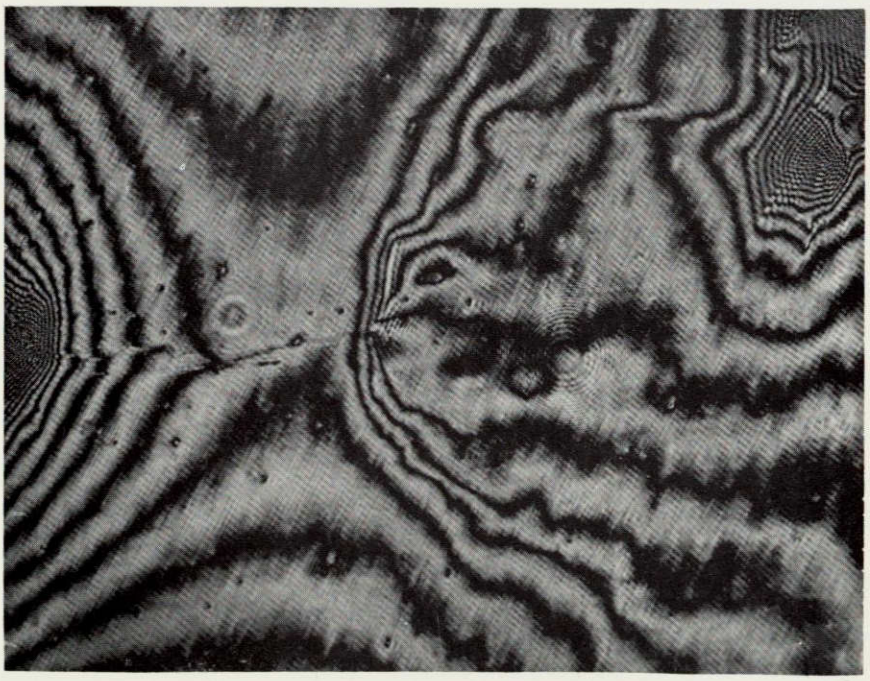

Interferogram, 50X

Figure V.9 Front Surface of Specimen 94 (0.2" Fe-3Si) Showing Crack Tip and Dimple

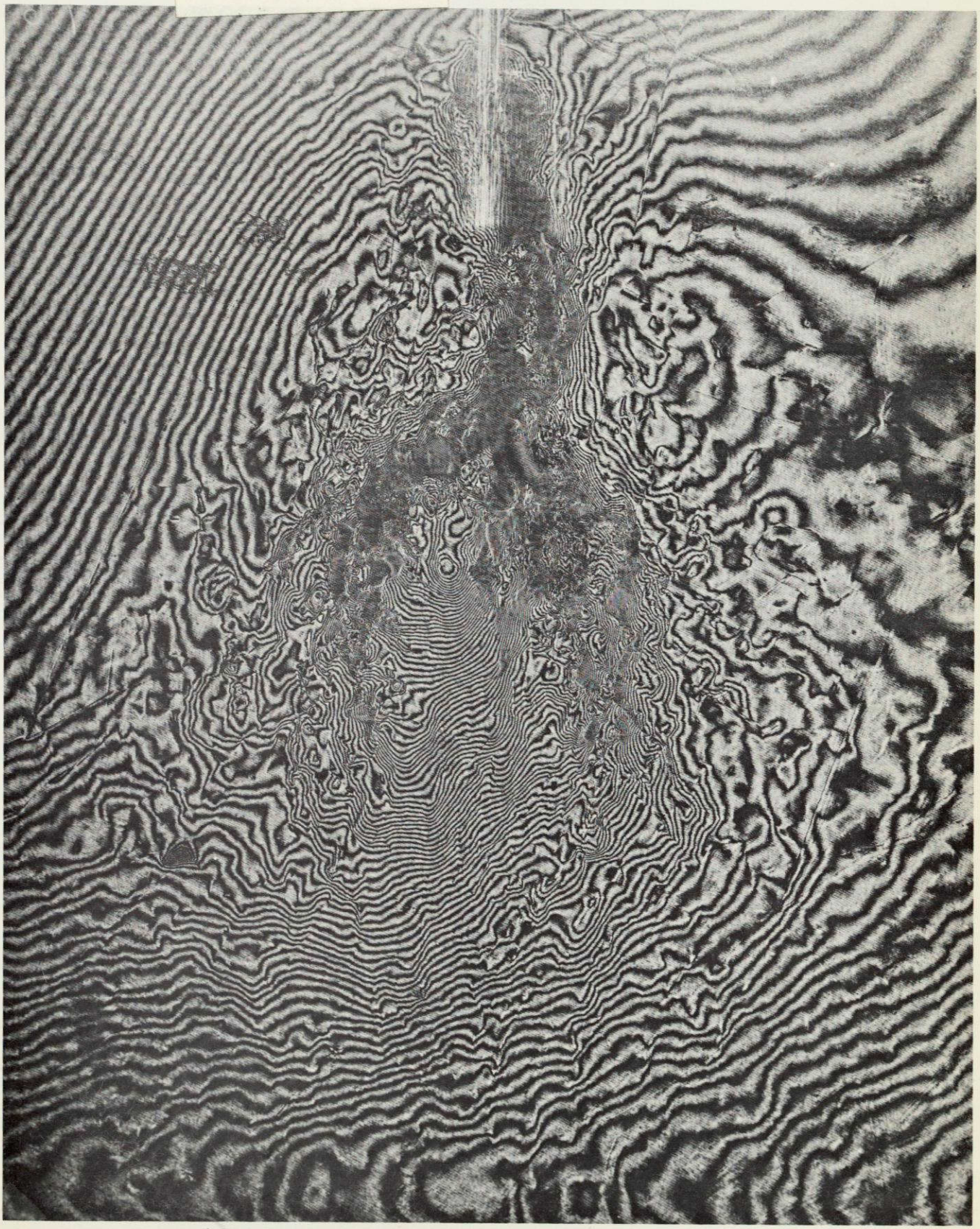

Figure V. 10 Interferogram of Front Surface of Specimen 103 (0. 1" Fe-3Si) Showing Crack Tip and Dimple, 22 1/2 X

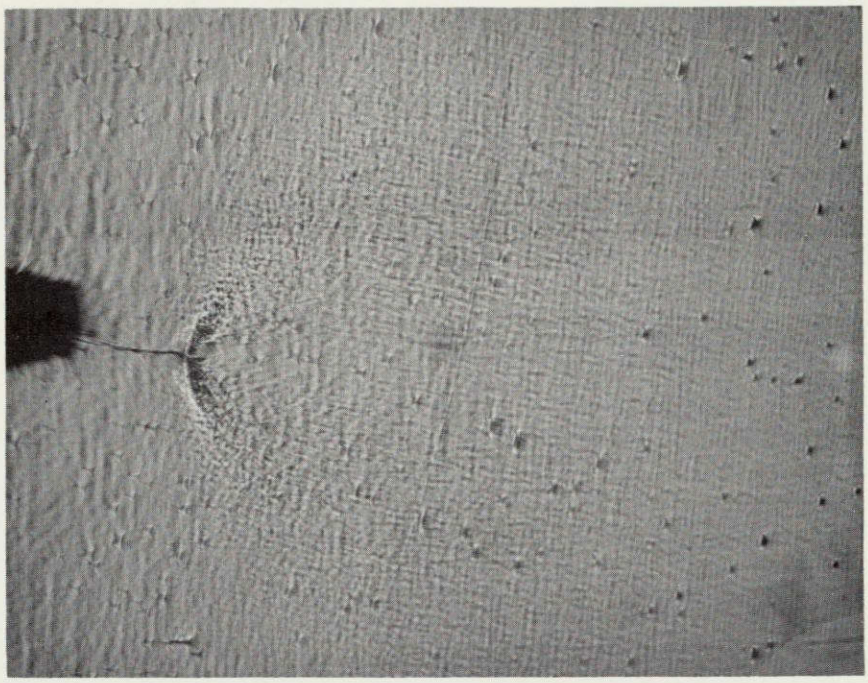

Laser Illuminated Photograph, 30X

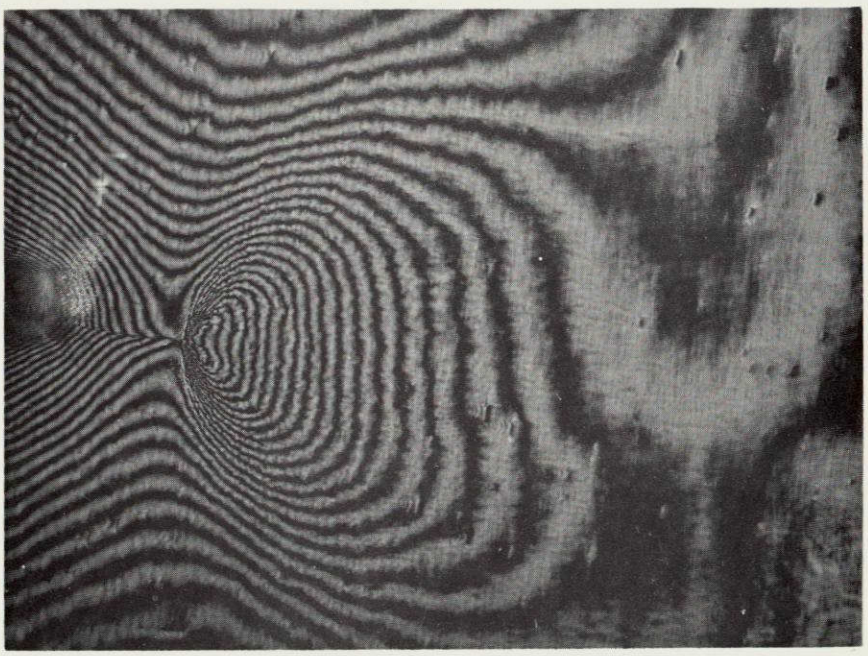

Interferogram, 30X

Figure V.11 Front Surface of Specimen 112 (0.1" Ti-6A1-4V) Showing Crack Tip and Dimple

were concentrated in the 0.2 inch group. Difficulties (explained in Section III.B) were experienced in achieving good etch response from the 0.1 and 0.5 inch specimens. The high heat treatment temperature and fast quench needed for acceptable etching response clearly altered the mechanical behavior. There was a strong tendency toward intergranular fracture, and some evidence of an intergranular precipitate film, which acted together to promote premature fracture in these two specimen groups. Nearly all of the 0.1 and 0.5 inch Fe-3Si specimens either cracked through to the back surface during loading, or fractured during heat treatment. As a result, no meaningful description of the plastic zone configuration for these specimens could be made. Thus, in this report, the discussion of the plastic zone configuration is confined to the 0.2 inch thickness group of silicon iron specimens, where the results were far more gratifying. As discussed in Section IV.B, the state of deformation at the crack front varies from one of plane strain at the full crack depth ($\phi = \pi/2$ in Figure IV.1) to plane stress where the crack front intercepts the front surface. Since a plane strain state tends to inhibit plastic deformation as compared to a plane stress state, it is expected that the yield zone would be smaller at the crack depth than at the front surface. This tendency is also modified by the fact that the stress intensity factor, to which the plastic zone is related for small scale yielding, varies with position along the crack front, in accordance with the ratio a/c. These, of course, are qualitative considerations, supported by our general interpretation of the deformation process. What is needed is some more specific knowledge as to the region of the crack front over which plane strain prevails, and as to the depth of the plane stress effect at the front surface. In addition, it would be useful to know how the plastic zone configuration is influenced by the proximity of the back surface.

Figures V.12 - V.14 provide an overall view of the extent of plastic deformation around the crack front for Specimen 71. This specimen had the following geometry and loading parameters:

$$a/c = 0.615$$
$$a/t = 0.720$$
$$\sigma/\sigma_y = 0.670$$

Figures V.12 and V.13 show the etched microstructure at the crack plane and 0.006 inch below the crack plane, respectively. Regions of distinct plastic strain can be seen near the front surface (ground 0.008 inch from original front surface during metallography) and at the full crack depth. Figure V.14 shows a composite drawing of the plastic zone extent at two parallel surfaces 0.006 and 0.012 inch

Figure V.12. Specimen 71, Through Plane of Crack

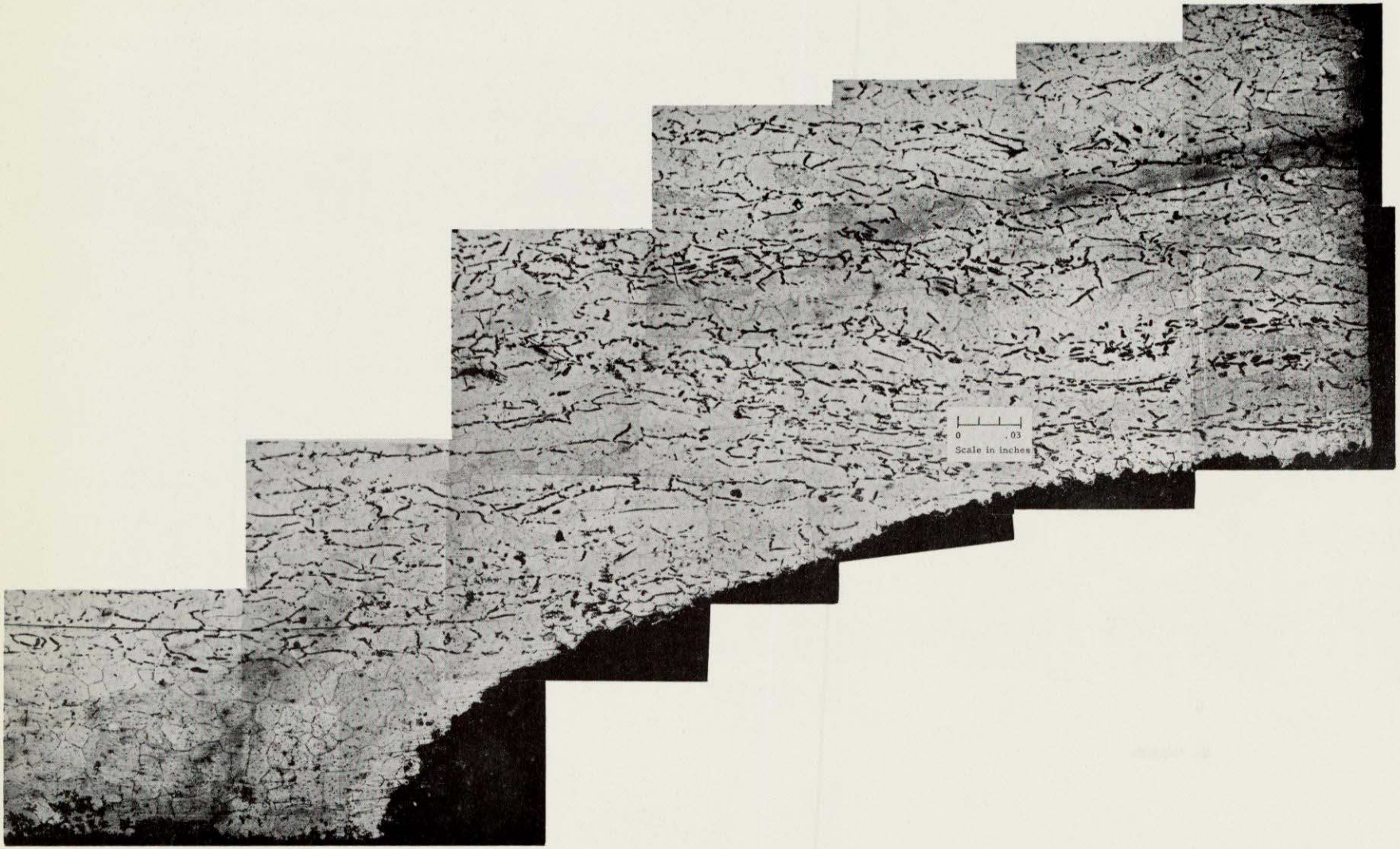

Figure V.13. Specimen 71, 0.006 Inches Below Plane of Crack

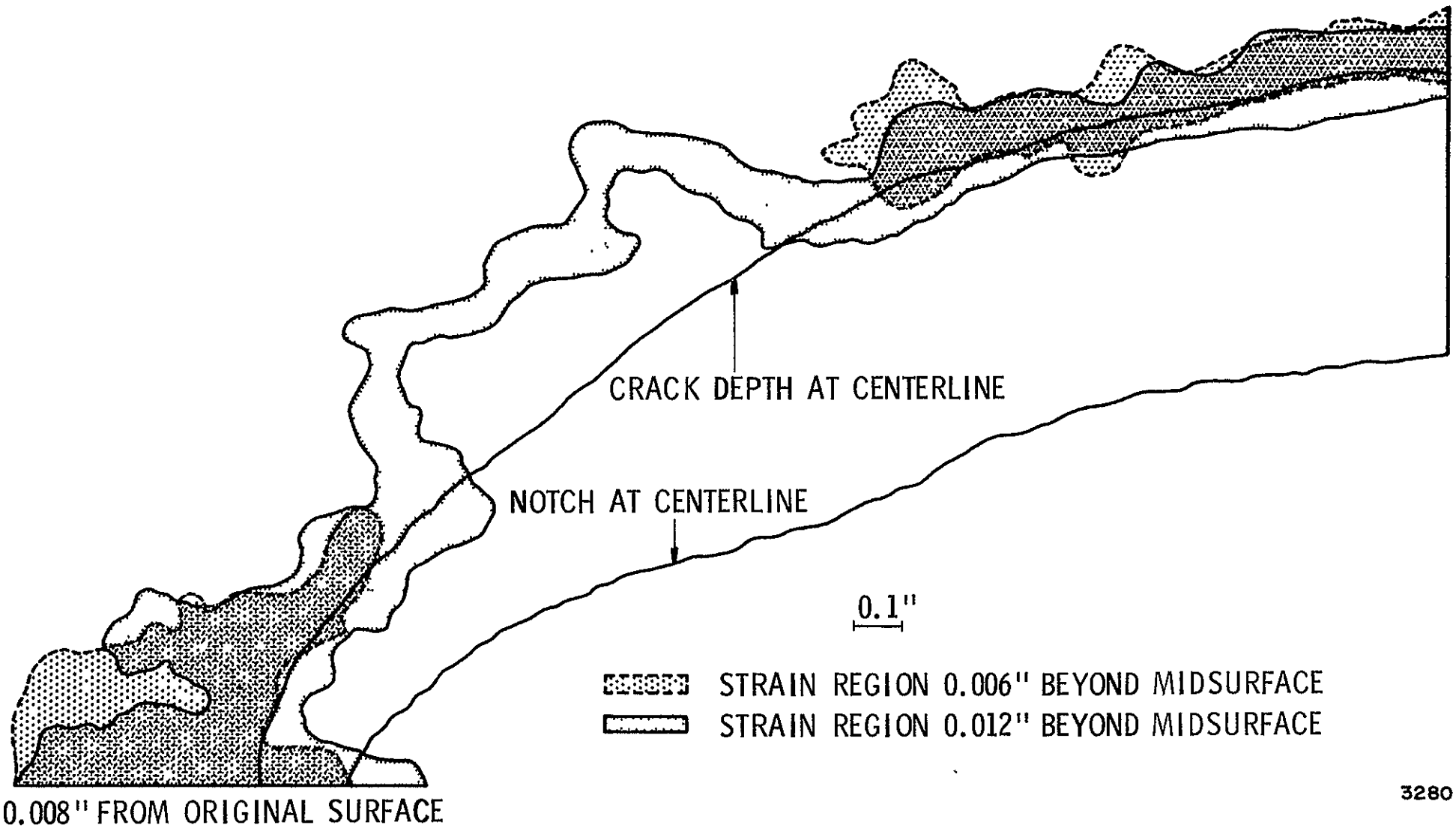

Figure V.14 Plastic Zones Circumscribing Crack Front, Specimen #71

from the nominal crack plane. From this figure one can see that the plastic zone would appear to be relatively extensive and compact at the front surface, "C" shaped in cross section over the central third of the crack front, and more compact toward the back of the crack due to the back surface influence. Figure V. 14 would suggest that the region of plane stress behavior is shallow, and that plane deformation prevails over most of the crack front. Further photomicrographs of Specimen 71, as well as other specimens from the 0. 2 inch Fe-3Si group, are included in the Appendix.

In order to make the results from the plastic zone etching somewhat quantitative, overlay tracings were made of the plastic zone in each photomicrograph. This not only permitted calculation of extent and area of plastic deformation, but also provided a good visual indication of the overall shape. In the remainder of this section, the size of the plastic zone is discussed from etched metallographic observations made at the front surface, at an "angle section" midway along the crack perimeter, and at the "cross section", i. e., at the full crack depth The geometry of these sections is discussed and illustrated in Section III. B of this report. The calibration of the etching response to plastic strain is given in Section III. C. The reader is referred to the Appendix where a large number of photomicrographs have been included which show the plastic zone configuration at the front surface, angle section, and cross section for specimens in the 0. 2 inch Fe-3Si group.

Figure V. 15 shows the relationship between plastic zone size and stress intensity factor, as calculated both by the Paris & Sih, and the Kobayashi & Moss models. The plastic zone sizes were measured from photomicrographs of polished and etched transverse (cross-section) sections in the nominally 0. 2 inch thickness Fe-3Si specimens. Thus, the measured plastic zone sizes, characterized both by their maximum linear dimension and by the diameter of the circle having equivalent area, represent a state approximating plane strain. There is somewhat less scatter when the plastic zone size is characterized by the diameter of the equivalent area, than by the maximum dimension. Also, the Kobayashi & Moss stress intensity factor appears to lessen the scatter in the data as compared with the Paris & Sih model. It should be pointed out that the data shown in Figure V. 15 cover a range of $0.43 < a/t < 0.80$ and $0.17 < a/2c < 0.40$, which undoubtedly accounts for much of the scatter present.

Superimposed on the data shown in these two figures are three analytical models for plastic zone sizes which have been proposed. The Irwin plane strain model consistently underestimates the plastic zone

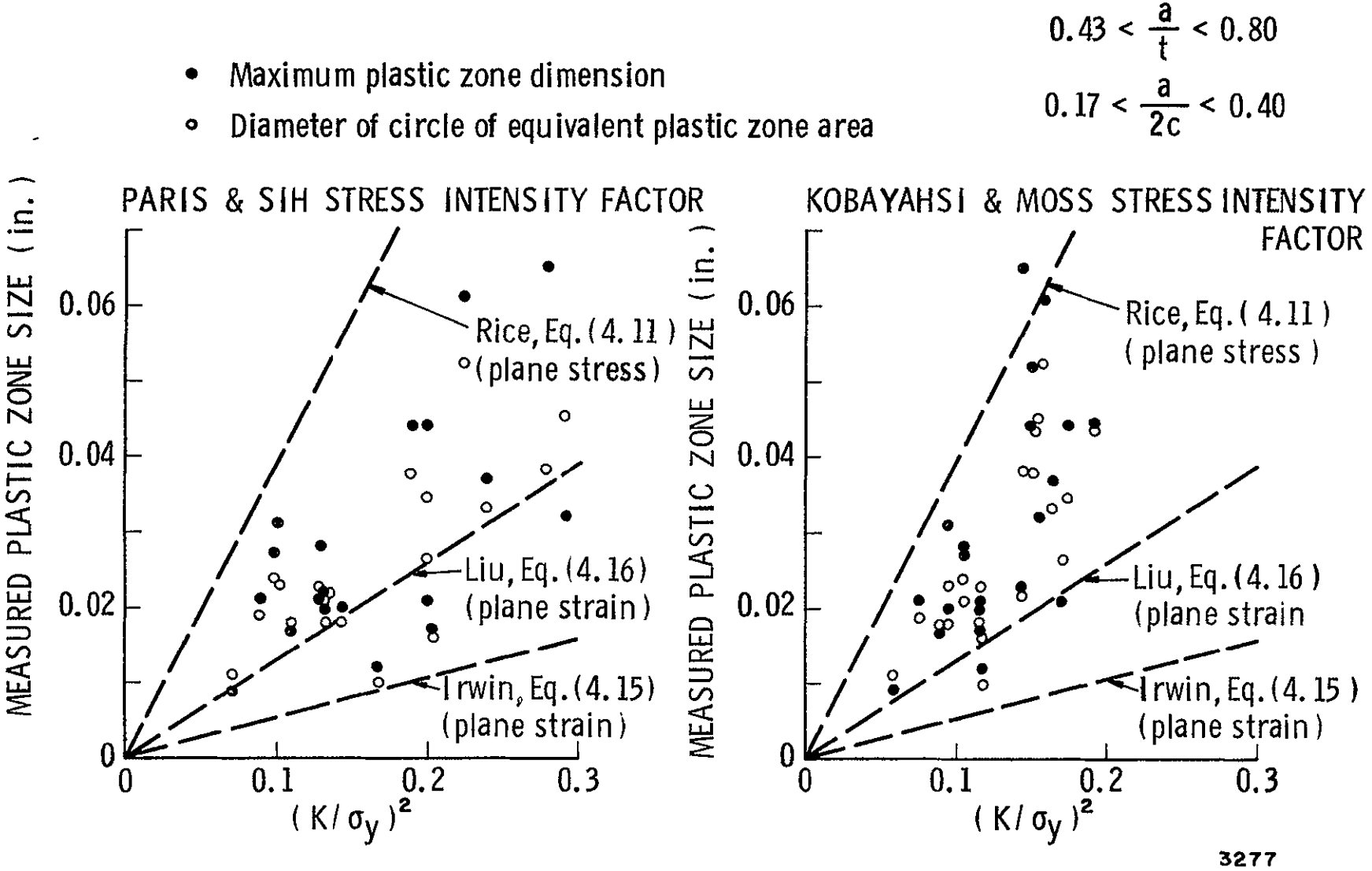

Figure V.15 Transverse Section Plastic Zone Sizes
Nominally 0.2 in. thick Fe-3Si Specimens

size, while the plane stress model, discussed by Rice, tends to overestimate the size, as should be expected since the state of deformation in the transverse section of the crack approaches plane strain. The model proposed by Liu reasonably correlates the data when presented on the basis of the Paris & Sih stress intensity factor, but underestimates somewhat the data trend as presented on the basis of the Kobayashi & Moss model The two stress intensity factor models differ considerably in their ability to correlate these data. The Paris & Sih model displays more scatter, although the trend of the plastic zone size is linear in $(K/\sigma_y)^2$ as calculated from the model. The Kobayashi & Moss model, on the other hand, results in less scatter, although the plastic zone size trend is not linear in $(K/\sigma_y)^2$. Rather, based on the Kobayashi & Moss model, the plastic zone size is more nearly proportional to $(K/\sigma_y)^4$

Figure V. 16 presents plastic zone size data from the angle sections in the same terms as was done in Figure V. 15 for the transverse sections. The same remarks hold relative to the Paris & Sih and the Kobayashi & Moss stress intensity factors as correlates.

The extent of the plastic zone size at the free front surface of the specimen is illustrated in Figure V. 17. These data also were taken from the nominally 0. 2 inch series of Fe-3Si specimens, and the plastic zone sizes were characterized by the diameter of the circle having an area equivalent to the measured area of the plastic zone. Thus, the maximum observed extent of the plastic zone generally was somewhat larger than as represented in the figure. Circles touching or connected by vertical lines are data pairs taken from either end of the crack, with two or three exceptions there was little scatter between data pairs, as shown. Other sources of scatter include the fact that a range of a/t and a/2c parameters are included in the data, and that the plastic zones revealed by the etch were actually some 0. 005 - 0. 010 inch from the free surface due to the surface removal during polishing. Thus, while very close to the free surface, these measured plastic zones did not represent a pure plane stress mode.

The data shown are compared with two analytical models for plane stress plastic zone sizes. The Bilby & Swinden model consistently overestimates the plastic zone size. The model discussed by Rice, while predicting smaller plastic zone sizes than the Bilby & Swinden model, also overestimates the measured data in all but one isolated case.

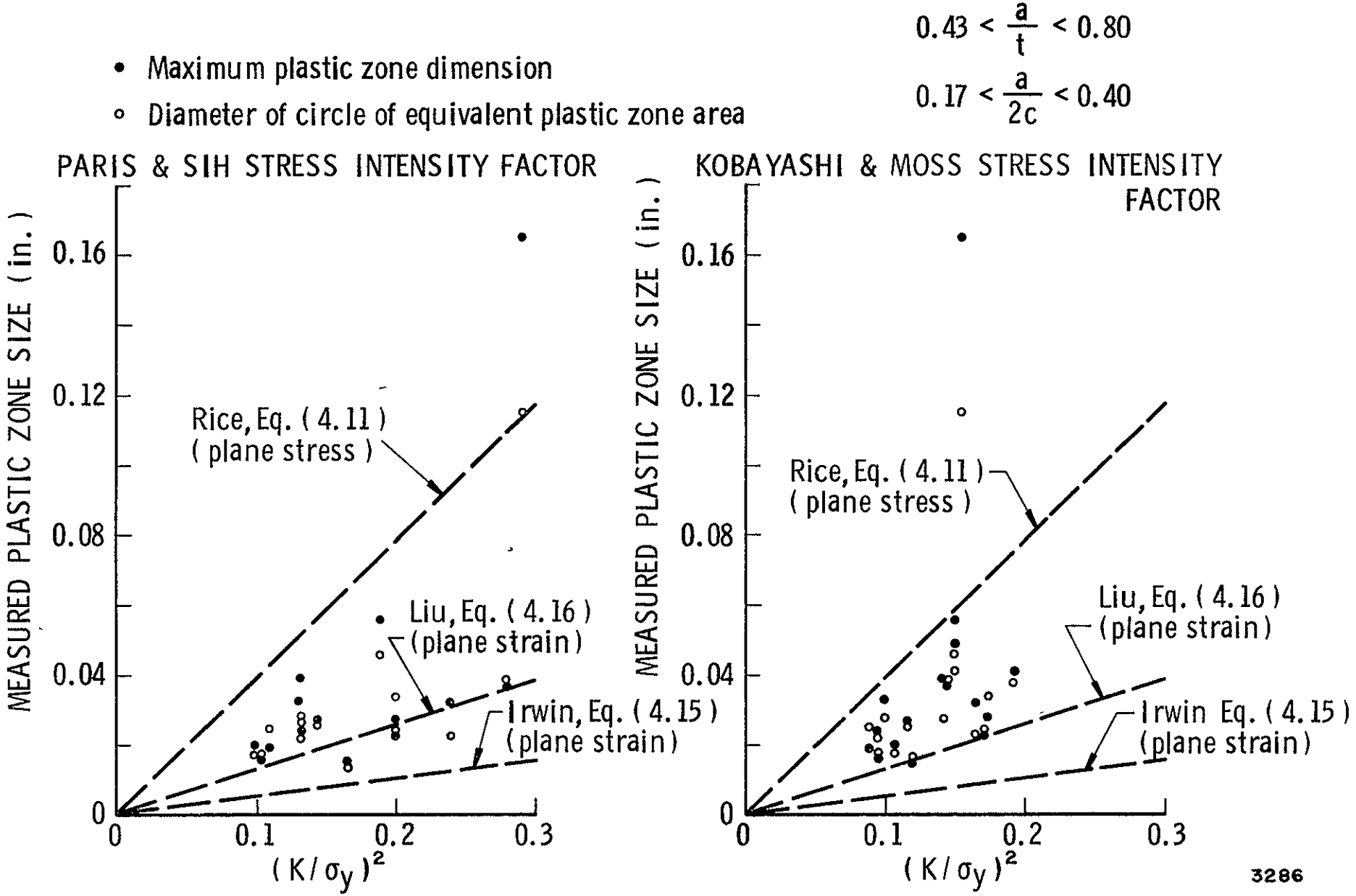

Figure V.16 Angle Section Plastic Zone Sizes
Nominally 0.2 in. Thick Fe-3Si Specimens

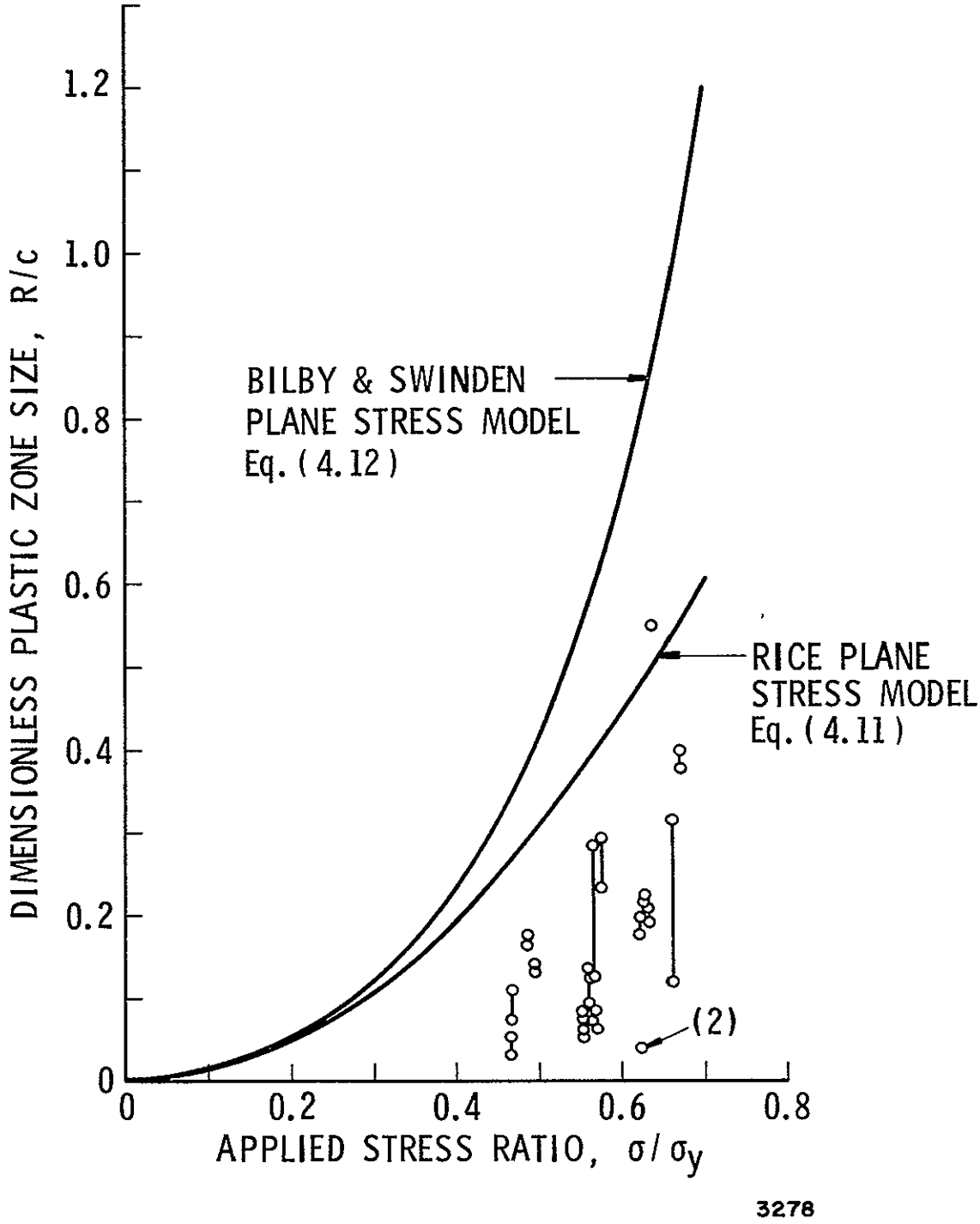

Figure V.17 Front Surface Plastic Zone Sizes
Nominally 0.2 in. thick Fe3Si specimens

VI. REFERENCES

REFERENCES

1. Morris, C. E., "Electropolishing of Steel in Chrome-Acetic Acid Electrolyte," Metal Progress, Vol. 56, No. 5, 696ff (1949).

2. Hibbard, W. R., and Dunn, C. G , "A Study of 112 Edge Dislocations in Bent Silicon-Iron Single Crystals," Acta Metallurgica, Vol. 4, No. 3, 306-315, (1956).

3. Rosenfield, A. R., Dai, P. K., and Hahn, G. T., "Crack Extension and Propagation Under Plane Stress," Proceedings of the 1st International Conference on Fracture, Sendai, Edited by T. Yokobori, T. Kawasaki, and J. L. Swedlow, Vol. 1, 223-257, Japanese Society for Strength and Fracture of Materials, Tokyo (1965).

4. Hahn, G. T., and Rosenfield, A. R., "Plastic Zones Generated by Cracks Growing Under Load," International Journal of Fracture Mechanics, Vol. 4, No. 2, 78-88 (1968).

5. Hahn, G. T., Mincer, P. N., and Rosenfield, A. R., "The Fe-3Si Steel Etching Technique for Local Strain Measurement," Experimental Mechanics (to appear).

6. Irwin, G. R., "Crack-Extension Force for a Part-Through Crack in a Plate," Journal of Applied Mechanics, Trans. ASME, Series E, Vol. 29, No. 4, 651-654 (1962).

7. Paris, P. C., and Sih, G. C. M., "Stress Analysis of Cracks," ASTM STP No. 381, 30-83 (1965).

8. Smith, F. W., "Stress Intensity Factors for a Semi-Elliptical Surface Flaw," The Boeing Co., SDRM No. 17, August, 1966.

9. Kobayashi, A. S., and Moss, W. L., "Stress Intensity Magnification Factors for Surface-Flawed Tension Plate and Notched Round Tension Bar," Address to 2nd International Conference on Fracture, Brighton, April 13-18, 1969.

10. Orange, T W., "A Semiempirical Fracture Analysis for Small Surface Cracks," NASA TN D-5340, July, 1969.

11. Rice, J. R., and Levy, N., "The Part-Through Surface Crack in an Elastic Plate," Tech. Rept. NASA NGL 40-002-080/3, Division of Engineering, Brown University, September, 1970 (submitted to Trans. ASME, Journal of Applied Mechanics for publication).

12. Gross, B., and Srawley, J. E., "Stress Intensity Factors for Single Edge Notch Specimens in Bending or Combined Bending and Tension by Boundary Collocation of a Stress Function," NASA TN D-2603, 1965.

13. Anderson, R. B., Holms, A. G., and Orange, T. W., "Stress Intensity Magnification for Deep Surface Cracks in Sheets and Plates," NASA TN D-6054, October, 1970.

14. Smith, F. W., Emery, A. F., and Kobayashi, A. S., "Stress Intensity Factors for Semicircular Cracks· Part 2 - Semi-Infinite Solid," Journal of Applied Mechanics, Trans. ASME, Series E, Vol. 34, No. 4, 953-959 (1967).

15. Rice, J. R., "Mathematical Analysis in the Mechanics of Fracture," Chapter 3 of FRACTURE, Vol. 2, Edited by H. Liebowitz, Academic Press, Inc., New York (1969).

16. Bilby, B. A , and Swinden, K. H., "Representation of Plasticity at Notches by Linear Dislocation Arrays," Proceedings of the Royal Society, Series A, Vol. 285, 22-33 (1965).

17. Keer, L. M., and Mura, T., "Stationary Crack and Continuous Distributions of Dislocations," Proceedings of the 1st International Conference on Fracture, Sendai, Edited by T. Yokobori, T. Kawasaki, and J. L. Swedlow, Vol. 1, 99-116, Japanese Society for Strength and Fracture of Materials, Tokyo (1965).

18. Irwin, G. R., "Dimensional and Geometric Aspects of Fracture," FRACTURE OF ENGINEERING MATERIALS, ASM, p. 211 (1964).

19. Liu, H. W., Discussion to: "The Effect of Size and Stress History on Fatigue Crack Initiation and Propagation," Proceedings of the Cranfield Crack Propagation Symposium, Vol. 2, p 514 (1962).

20. Ayres, D. J., "A Numerical Procedure for Calculating Stress and Deformation Near a Slit in a Three-Dimensional Elastic-Plastic Solid," NASA TN D-4717, August, 1968. Also in Engineering Fracture Mechanics, Vol. 2, No. 2, 87-106 (1970).

21. Randall, P. N., Discussion in: "Plane Strain Crack Toughness Testing of High Strength Metallic Materials," by W. F. Brown, Jr., and J. E. Srawley, ASTM STP No. 410, 88-126 (1966).

22. Bixler, W. D., and Masters, J. N., "Fracture Characteristics of Structural Aerospace Alloys Containing Deep Surface Flaws," Monthly Progress Report No. 6 prepared by the Boeing Co. under Contract NAS3-14341 for NASA, Lewis Research Center, January 20, 1971.

SUPPLEMENTARY BIBLIOGRAPHY

S-1 Cammett, J., Rosenfield, A. R., and Hahn, G. T., "Residual Strains and Displacements Within the Plastic Zone Ahead of a Crack," Ship Structure Committee Rept. No. SSC-179, November, 1966.

S-2 Hahn, G. T., and Rosenfield, A. R., "Local Yielding and Extension of a Crack Under Plane Stress," Ship Structure Committee Rept. No. SSC-165, December, 1964.

S-3 Hahn, G. T., and Rosenfield, A. R., "Experimental Determination of Plastic Constraint Ahead of a Sharp Crack Under Plane-Strain Conditions," Ship Structure Committee Rept. No. SSC-180, December, 1966.

S-4 Hahn, G. T., Rosenfield, A. R , Hulbert, L. E., and Kannien, M F., "Elastic-Plastic Fracture Mechanics," AFML-TR-67-143, September, 1968.

S-5 Hahn, G. T., and Rosenfield, A. R., "Plastic Flow in the Locale on Notches and Cracks in Fe-3Si Steel Under Conditions Approaching Plane Strain," Ship Structure Committee Rept. No. SSC-191, November, 1968.

S-6 Hall, L. R., "Plane-Strain Cyclic Flaw Growth of 2014-T62 Aluminum and 6Al-4V (ELI) Titanium," Final Report, NASA-CR-72396, November, 1968.

S-7 Hoeppner, D. W., Pettit, D. E., Feddersen, C. E., and Hyler, W. S., "Determination of Flaw Growth Characteristics of Ti-6Al-4V Sheet in the Solution-Treated and Aged Condition," NASA CR-65811, Final Report prepared by Battelle Memorial Institute for NASA, Manned Spacecraft Center, Under Contract NAS9-6969, January, 1968.

S-8 Rice, J. R., and Johnson, M. A., "The Role of Large Crack Tip Geometry Changes in Plane Strain Fracture," Tech. Rept. NYO-2394-38, prepared for the U. S. AEC under Contract No. AT (30-1) -2394, Division of Engineering, Brown University, September, 1969

S-9 Smith, F. W., and Alavi, M. J., "Stress-Intensity Factors for a Part-Through Surface Flaw," Proceedings, ASME Conference on Pressure Vessel Technology, First, Part II, 793-800 (1969).

S-10 Wilhem, D. P., "Fracture Mechanics Guidelines for Aircraft Structural Applications," AFFDL-TR-69-111, February, 1970.

APPENDIX

Angle Section

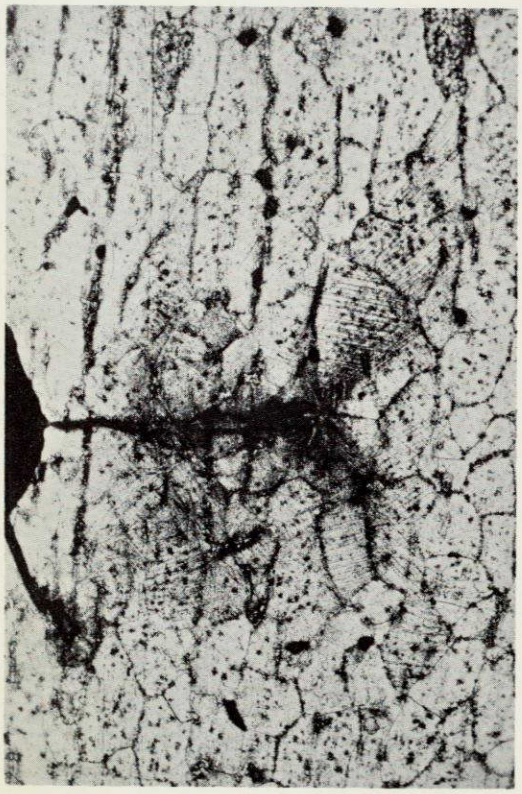

Cross Section

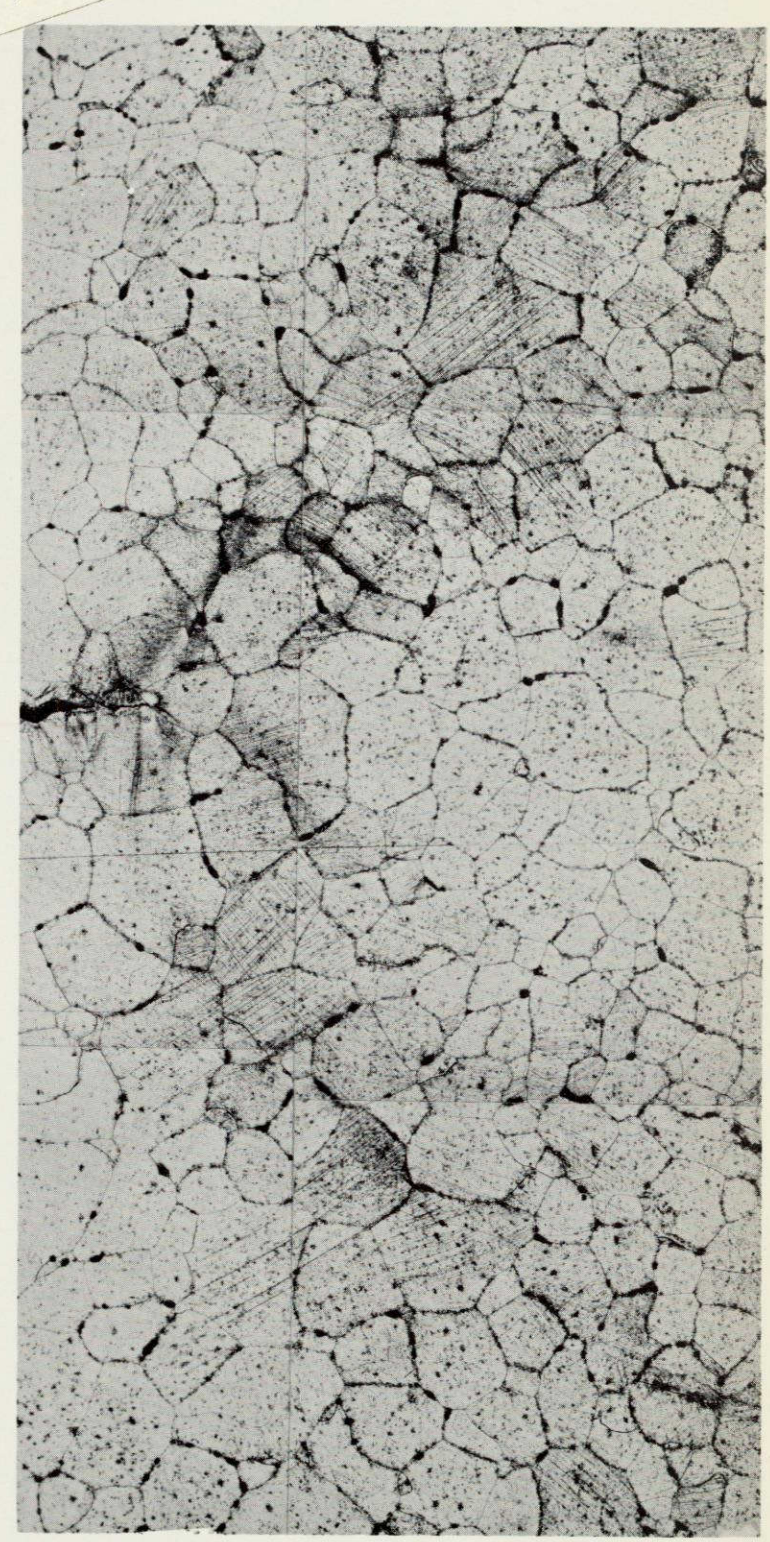

Front Surface

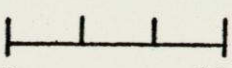

Scale in inches

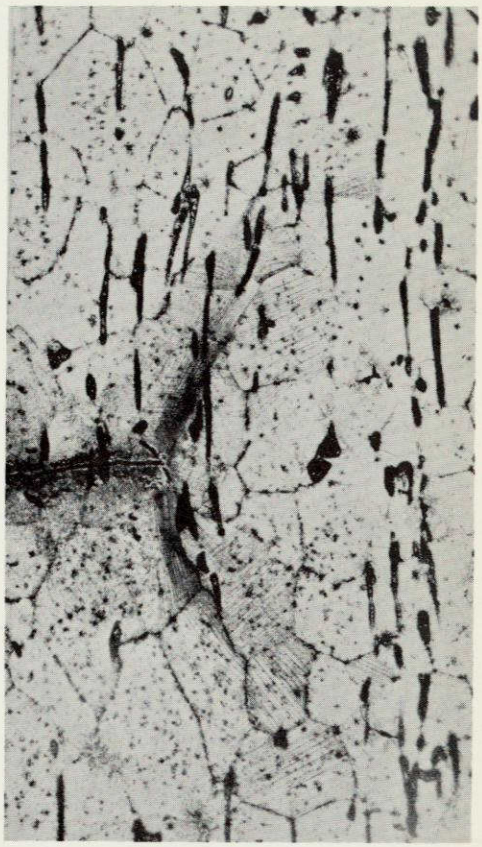

Angle Section, 75X

Specimen No. 69

Cross Section, 75X

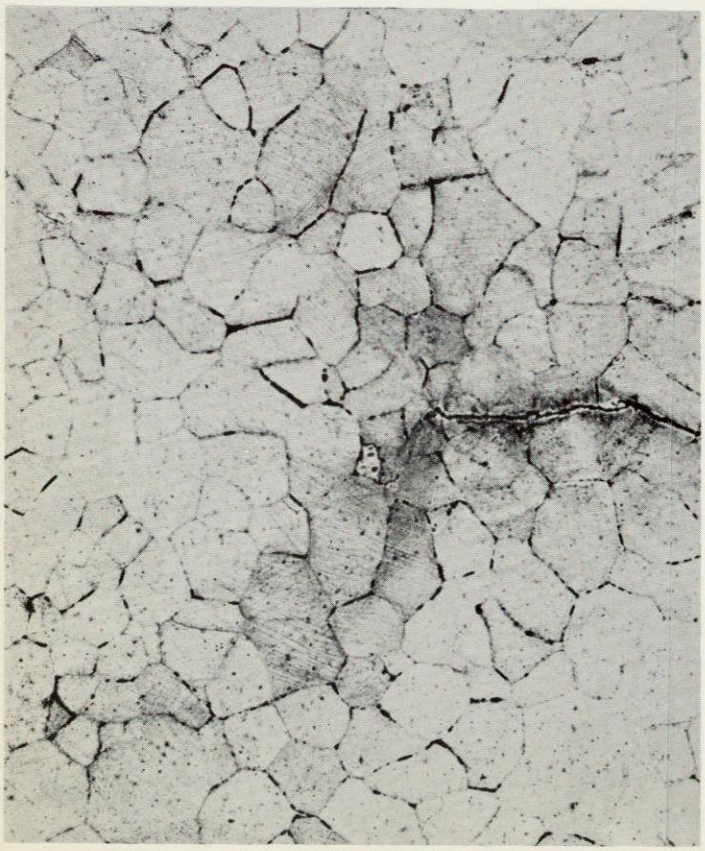

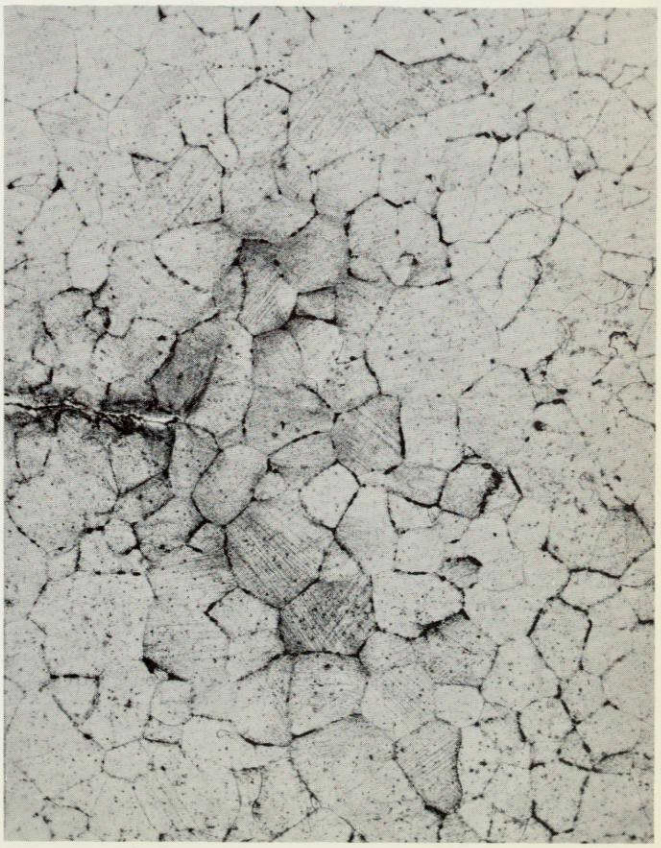

Front Surface, 75X

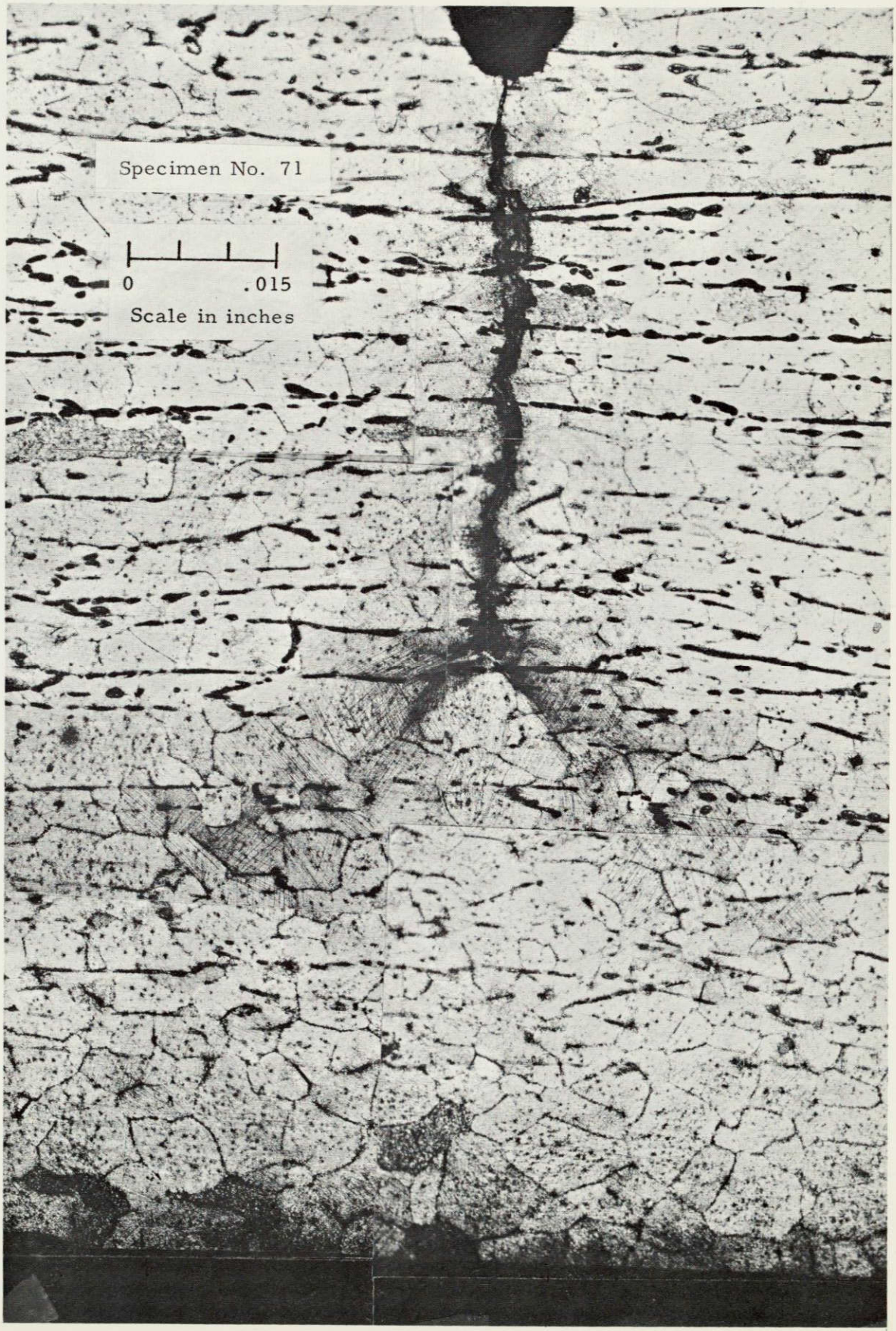

Cross Section Showing Back Surface

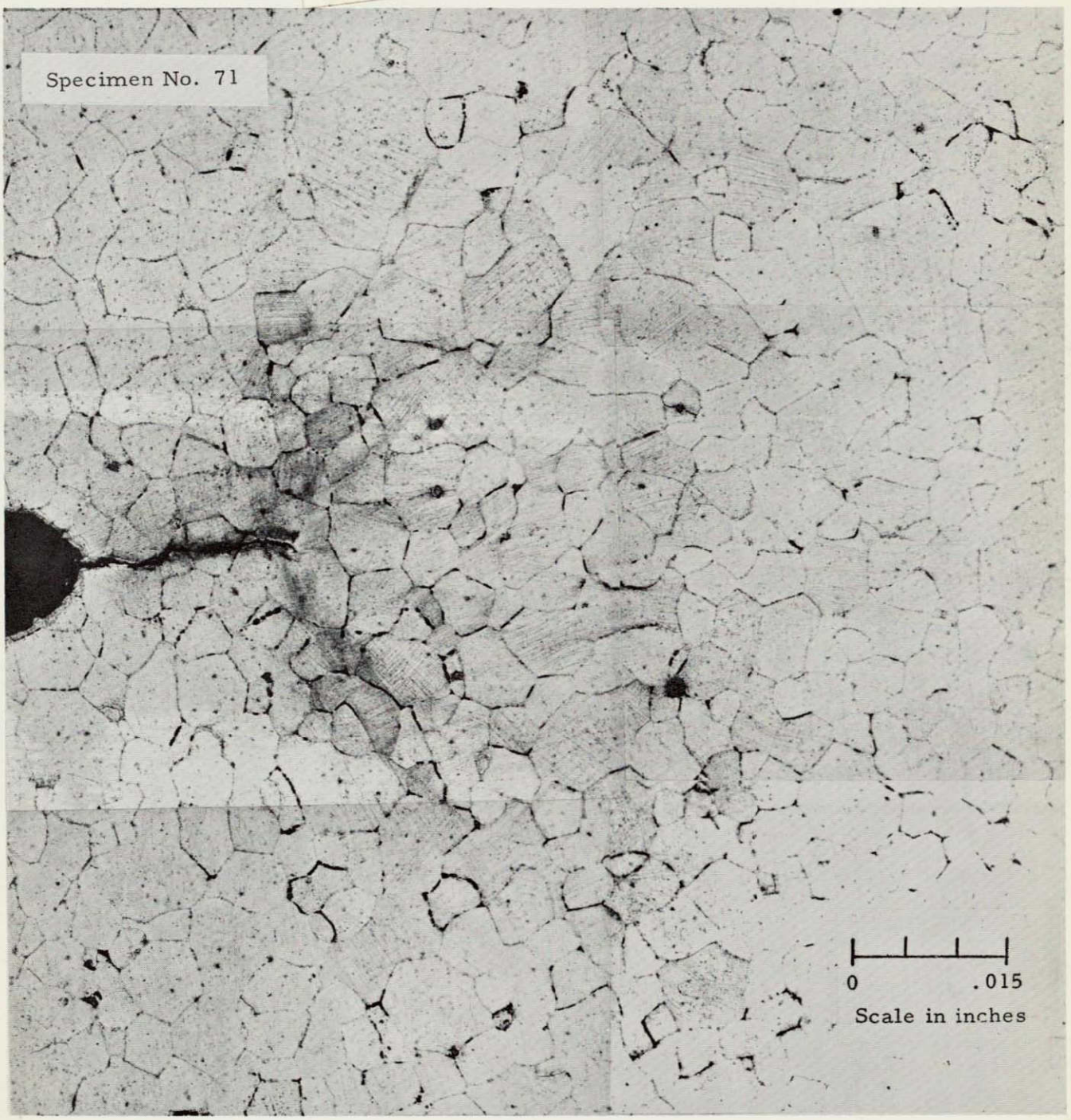

Front Surface, 0.033" Removed

Specimen No. 71

0 .015

Scale in inches

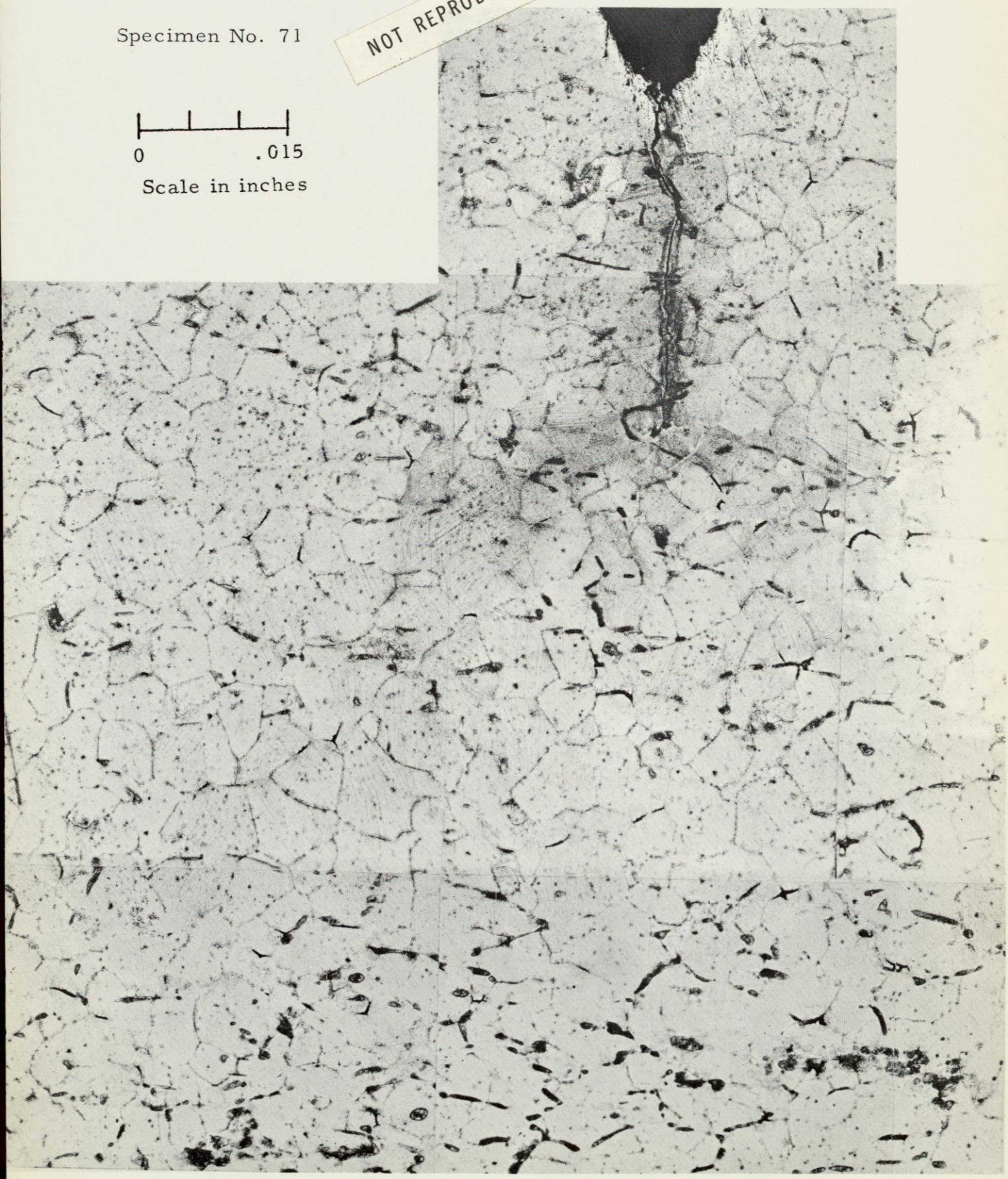

Front Surface, 0.033" Removed

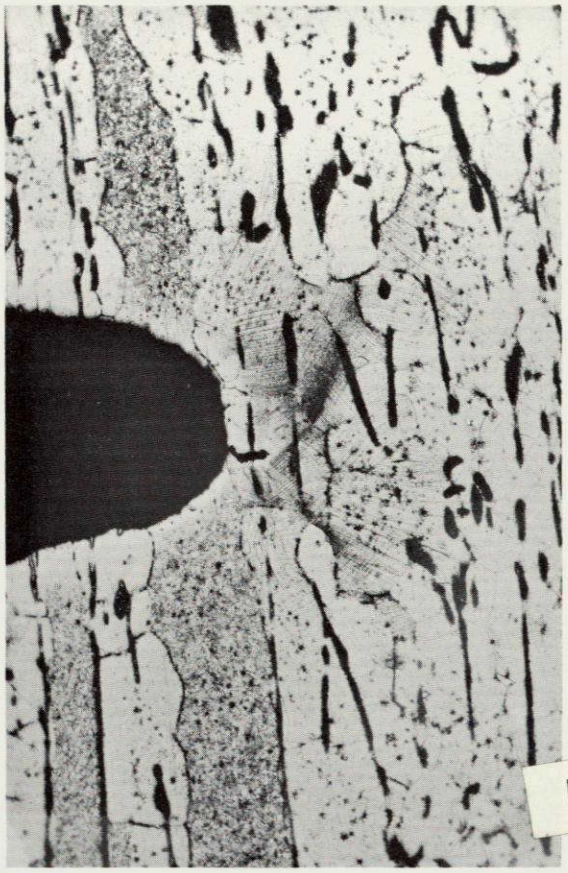

Cross Section, 75X Specimen No. 85

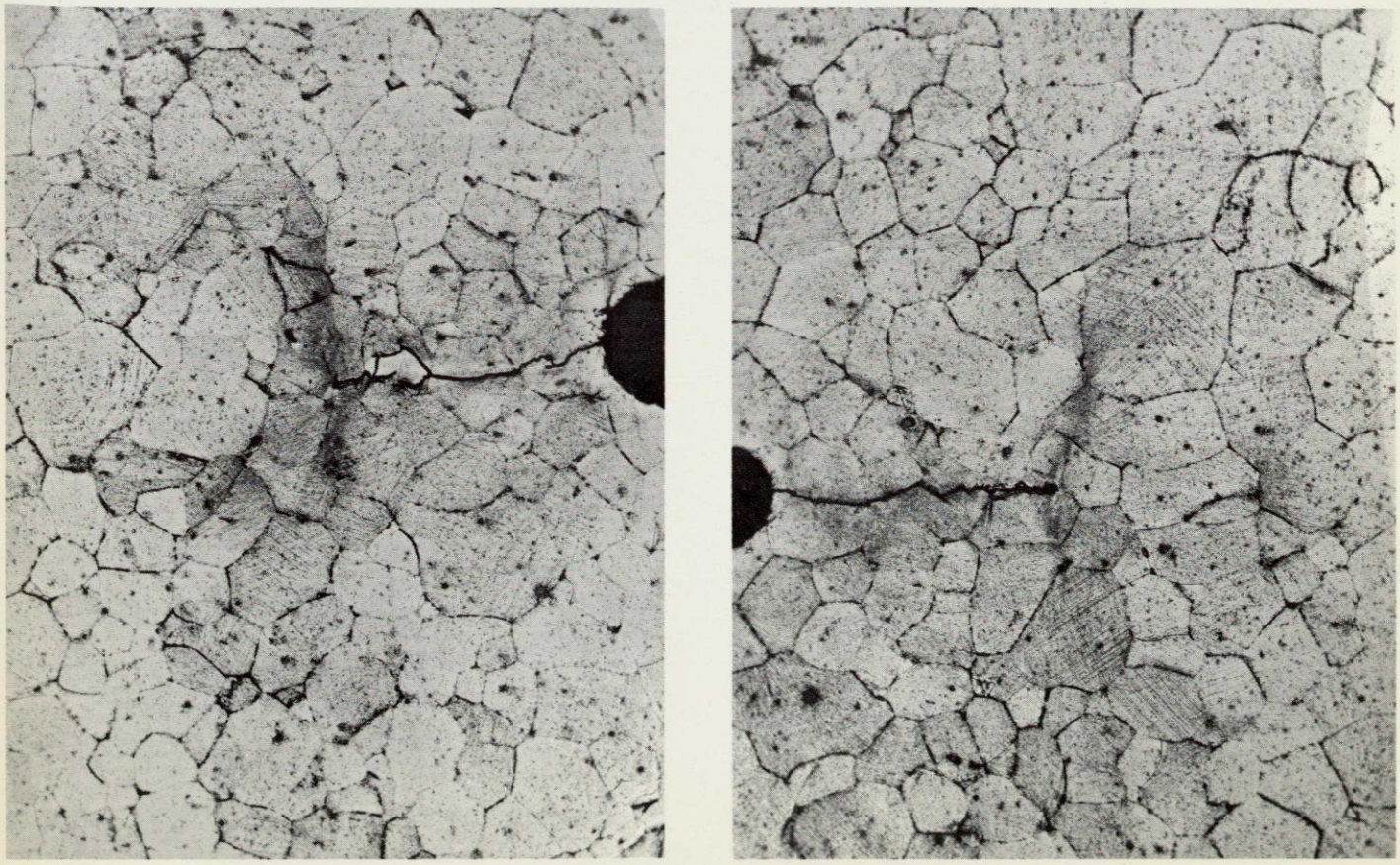

Front Surface, 75X

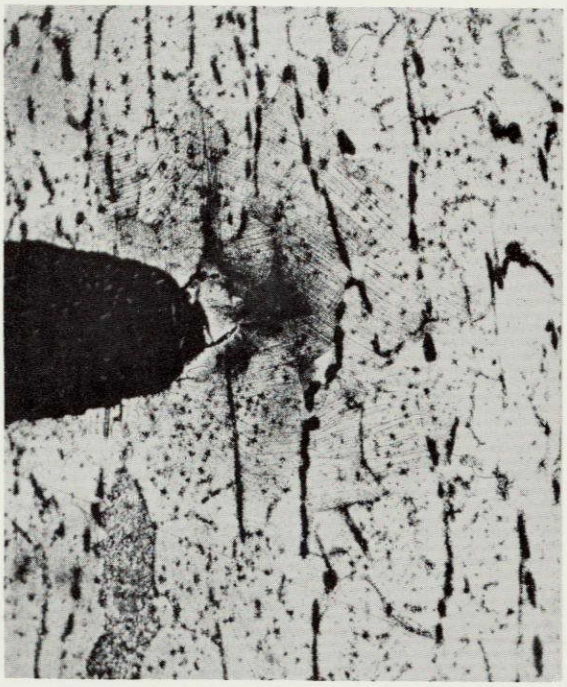

Angle Section, 75X

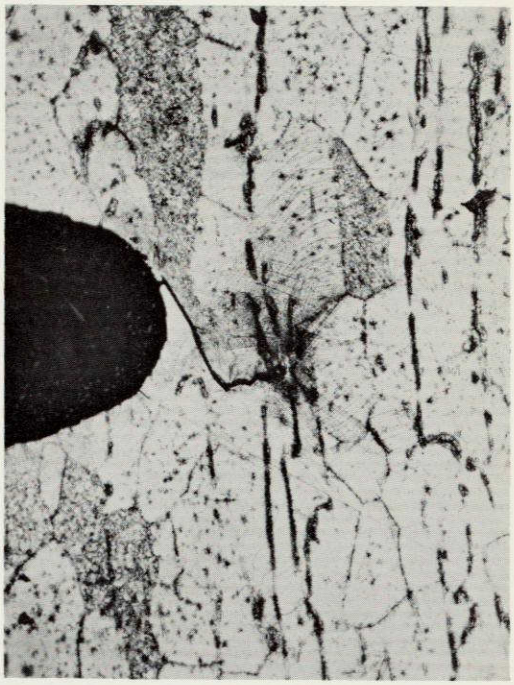

Cross Section, 75X

Specimen No. 86

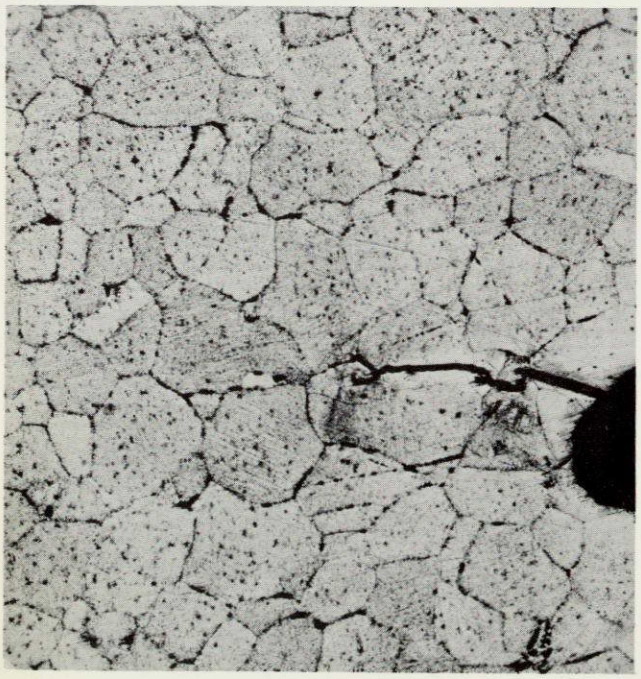

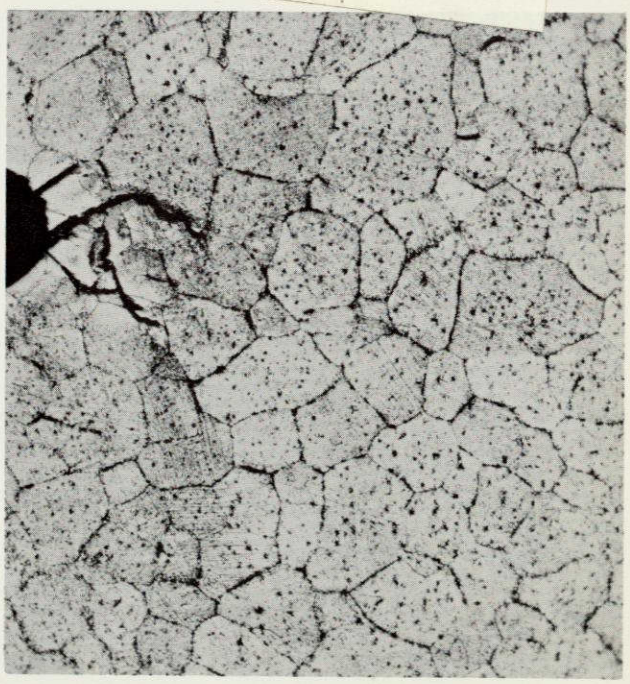

Front Surface, 75X

Angle Section

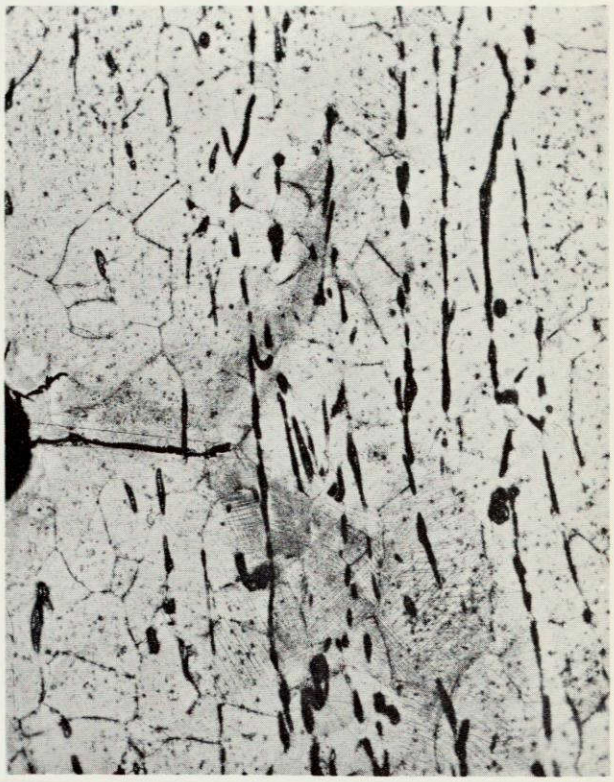

Cross Section

Specimen No. 89

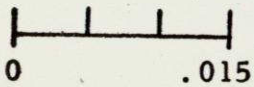

Scale in inches

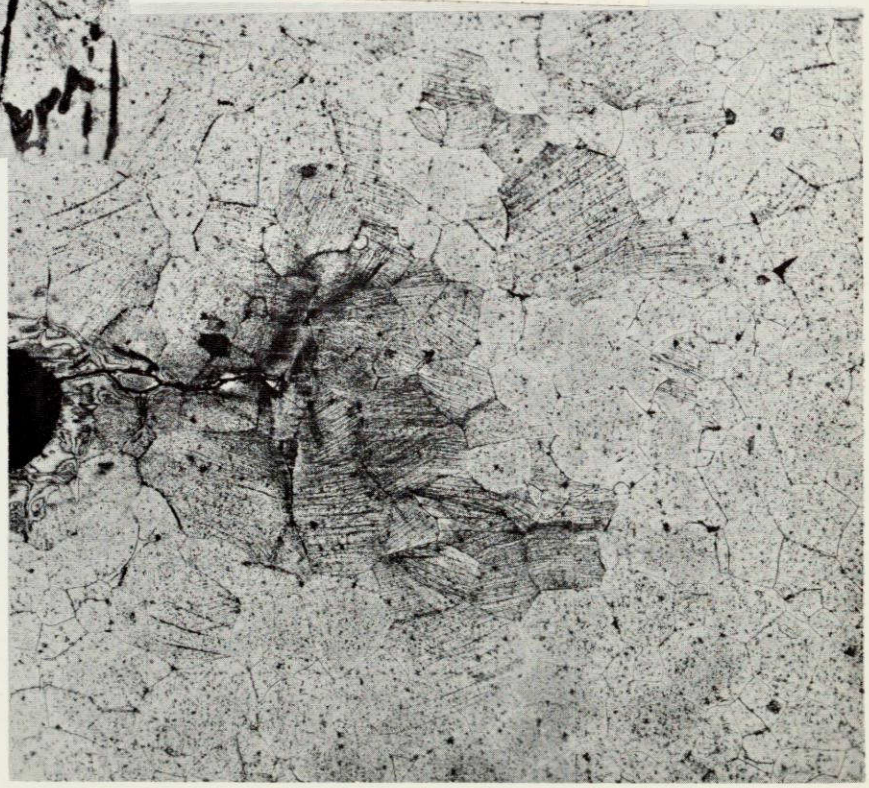

Front Surface

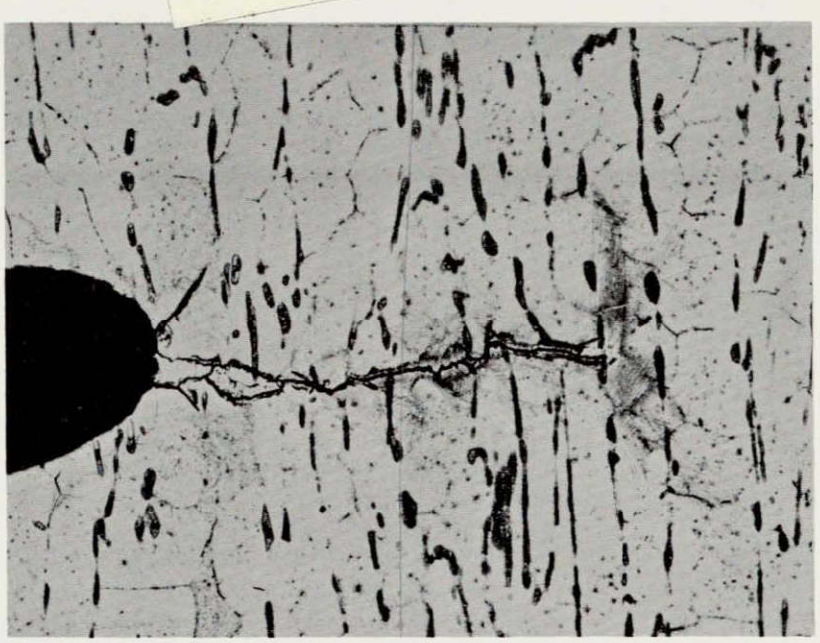

Cross Section, 75X

Specimen No. 90

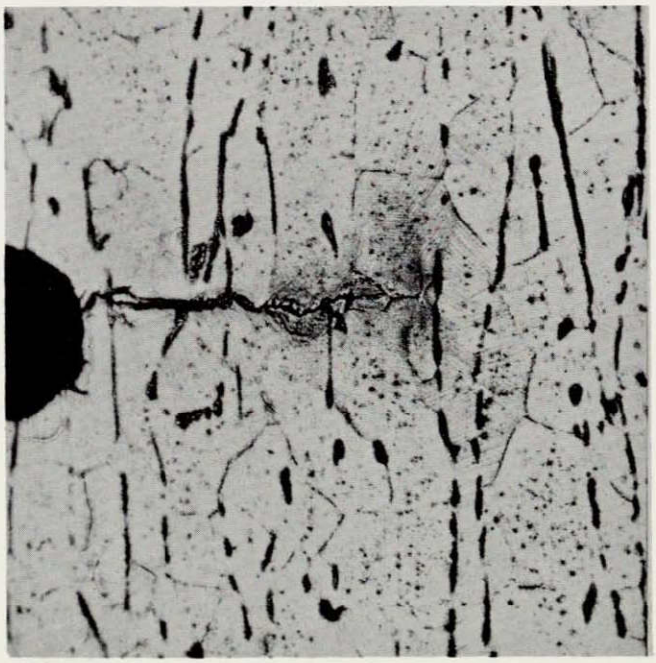

Angle Section, 75X

Angle Section, 75X

Cross Section, 75X

Specimen No. 91

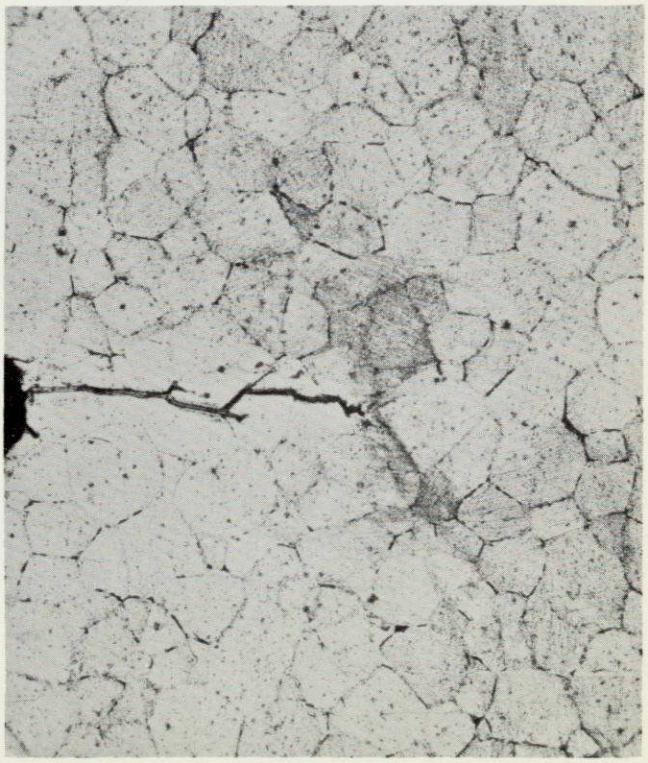

Front Surface, 75X

Angle Section, 75X

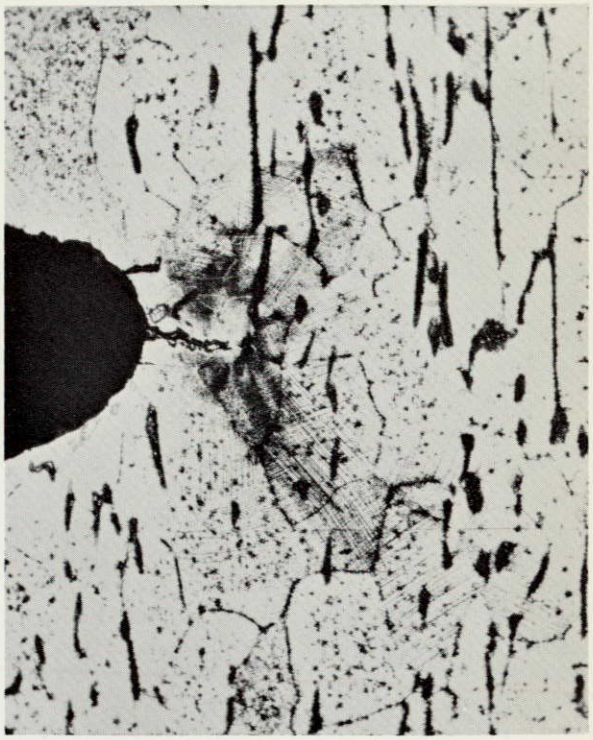

Cross Section, 75X

Specimen No. 92

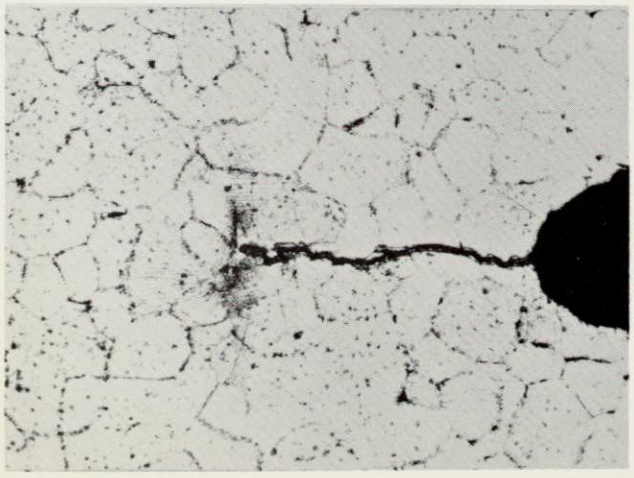

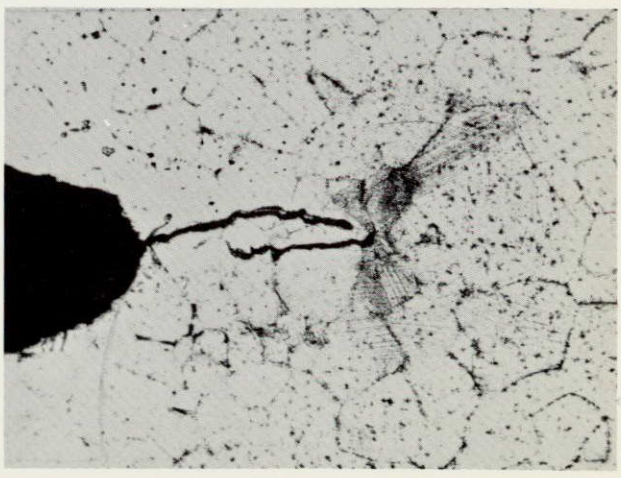

Front Surface, 75X

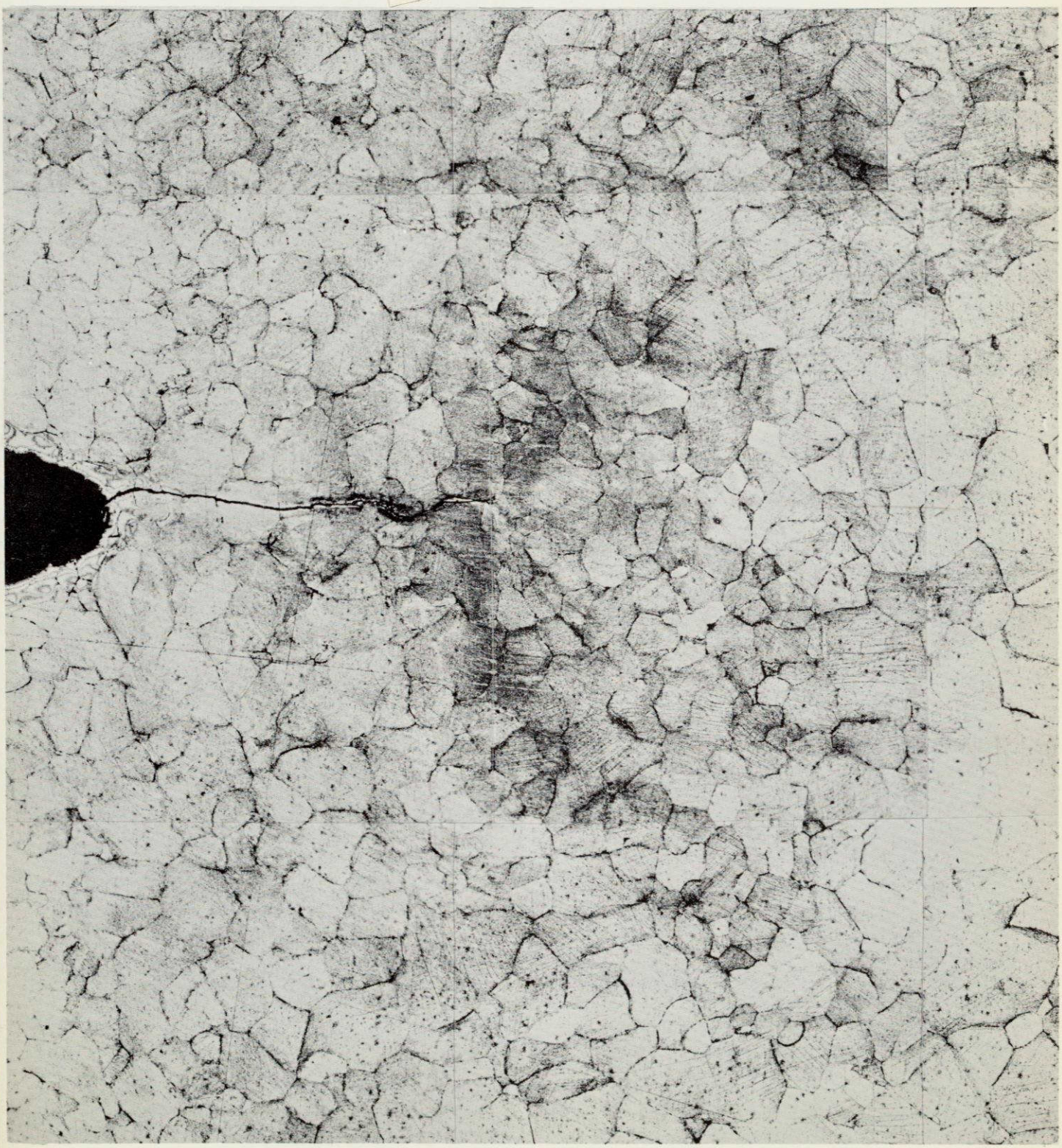

Front Surface, 75X Specimen No. 94

(Note light strain lines over entire surface)

Specimen No. 95

0 .015

Scale in inches

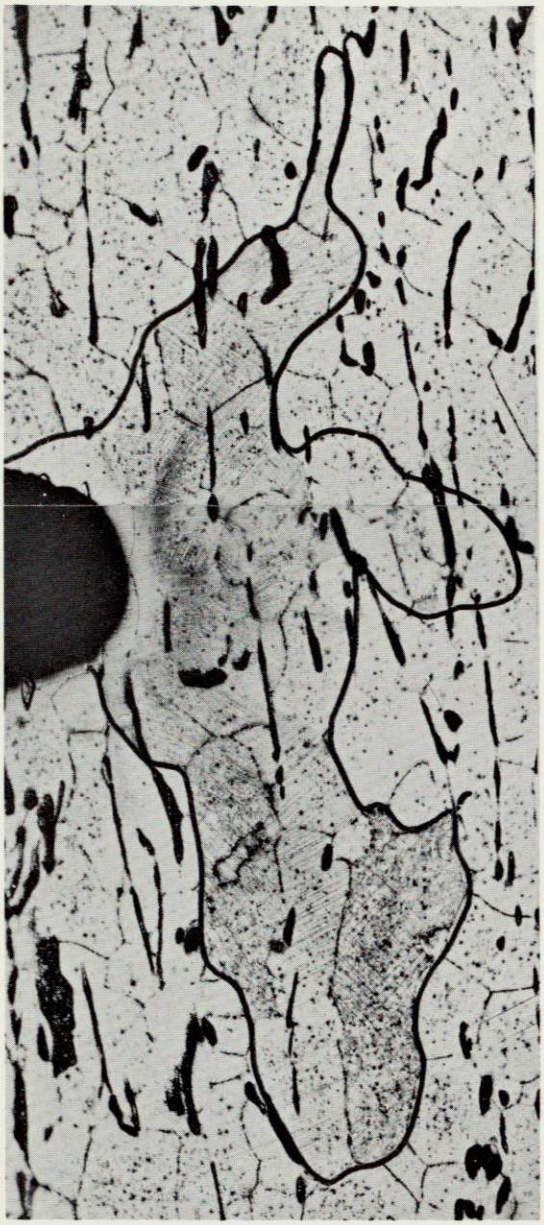

Angle Section

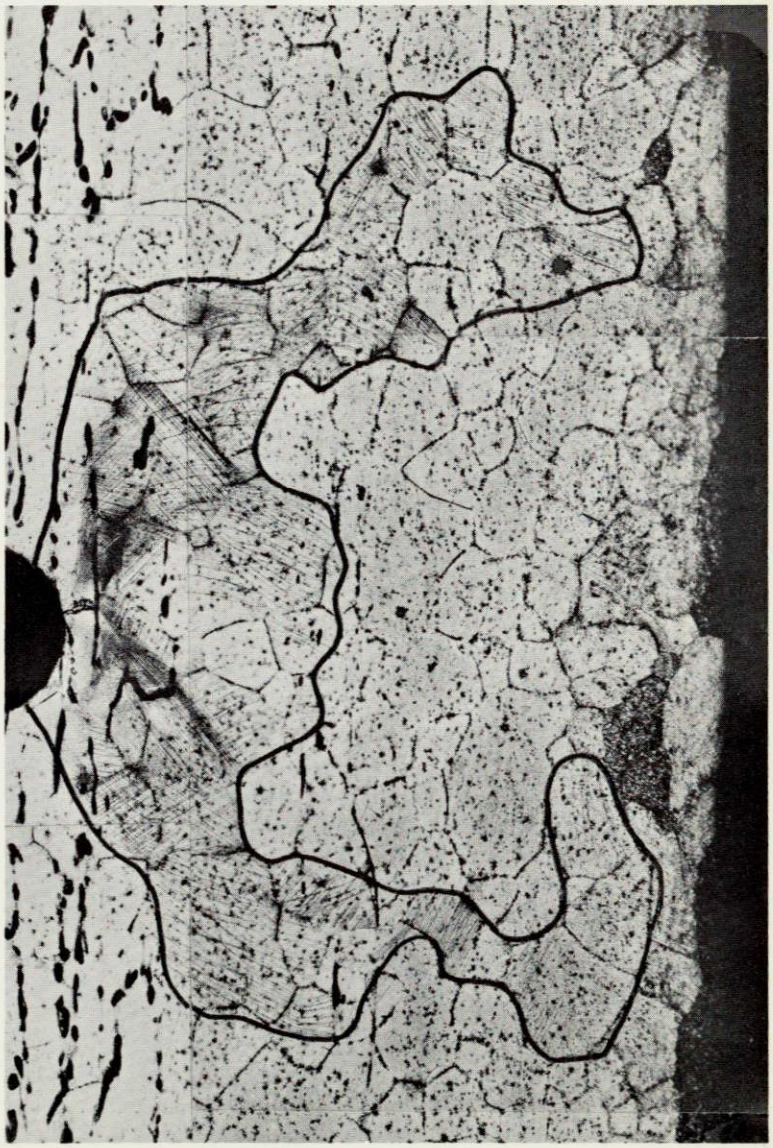

Cross Section Showing Back Surface

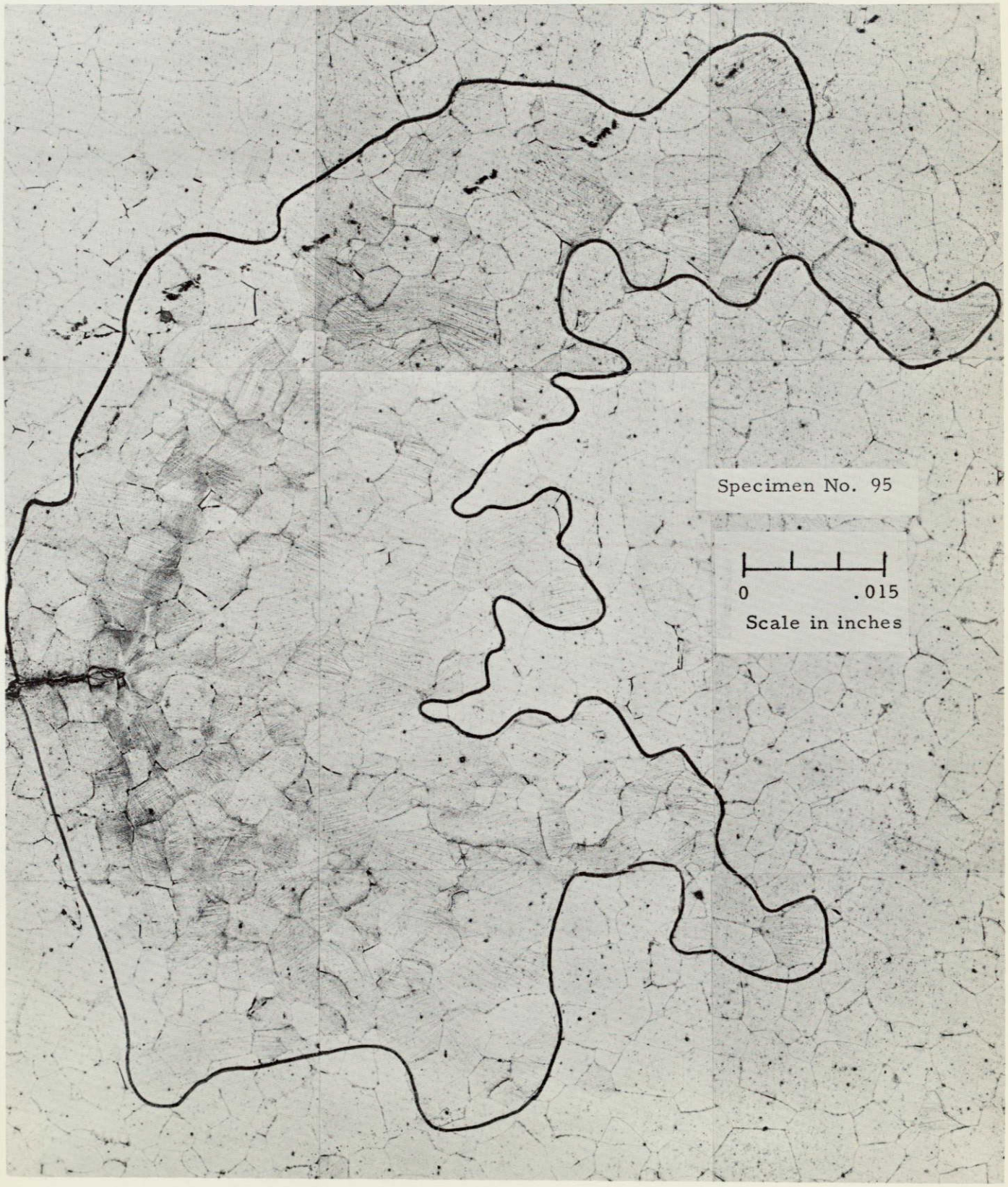

Front Surface

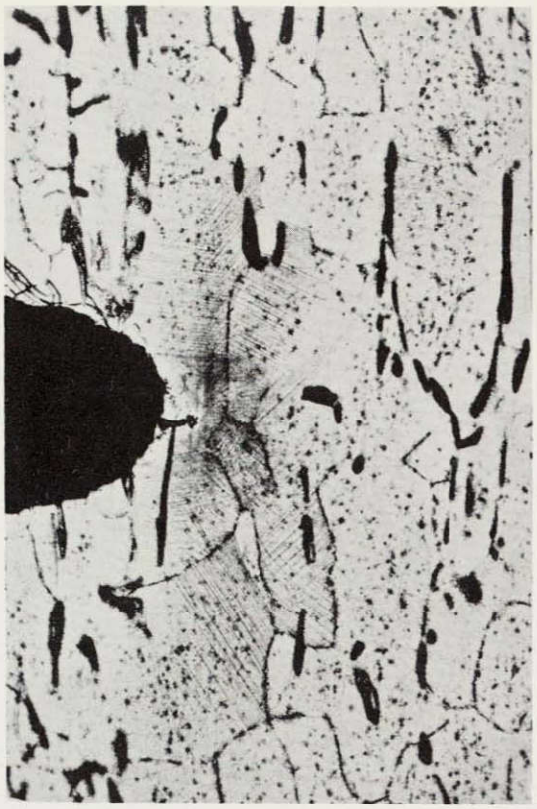

Angle Section, 75X

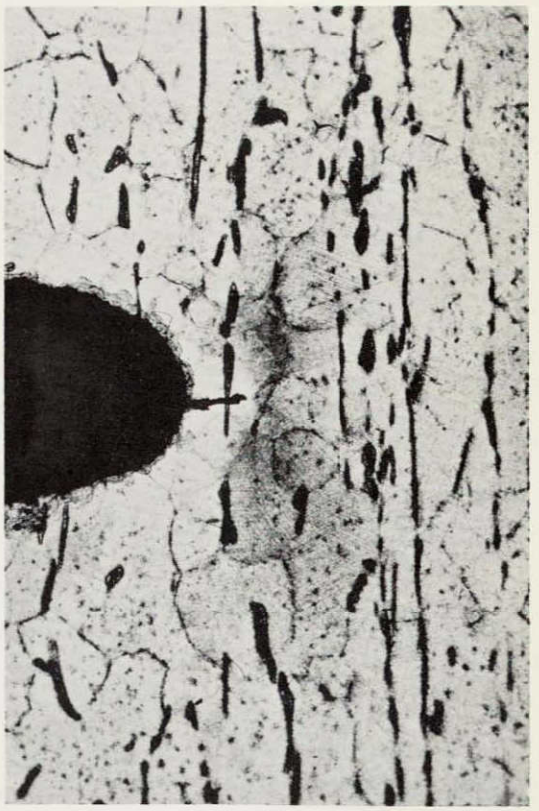

Cross Section, 75X

Specimen No. 96

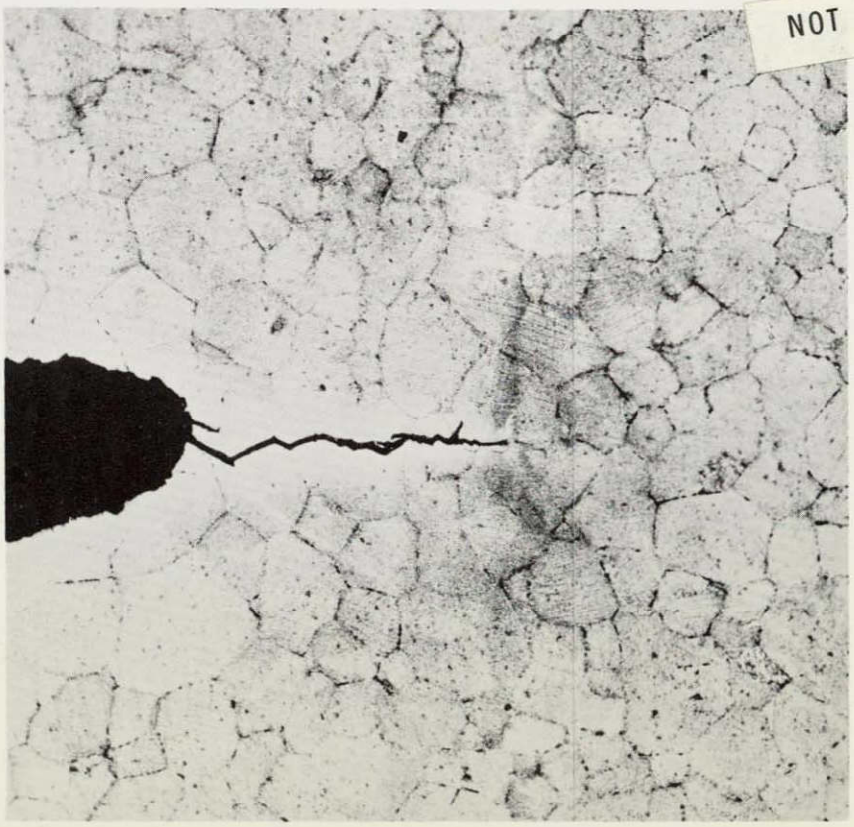

Front Surface, 75X

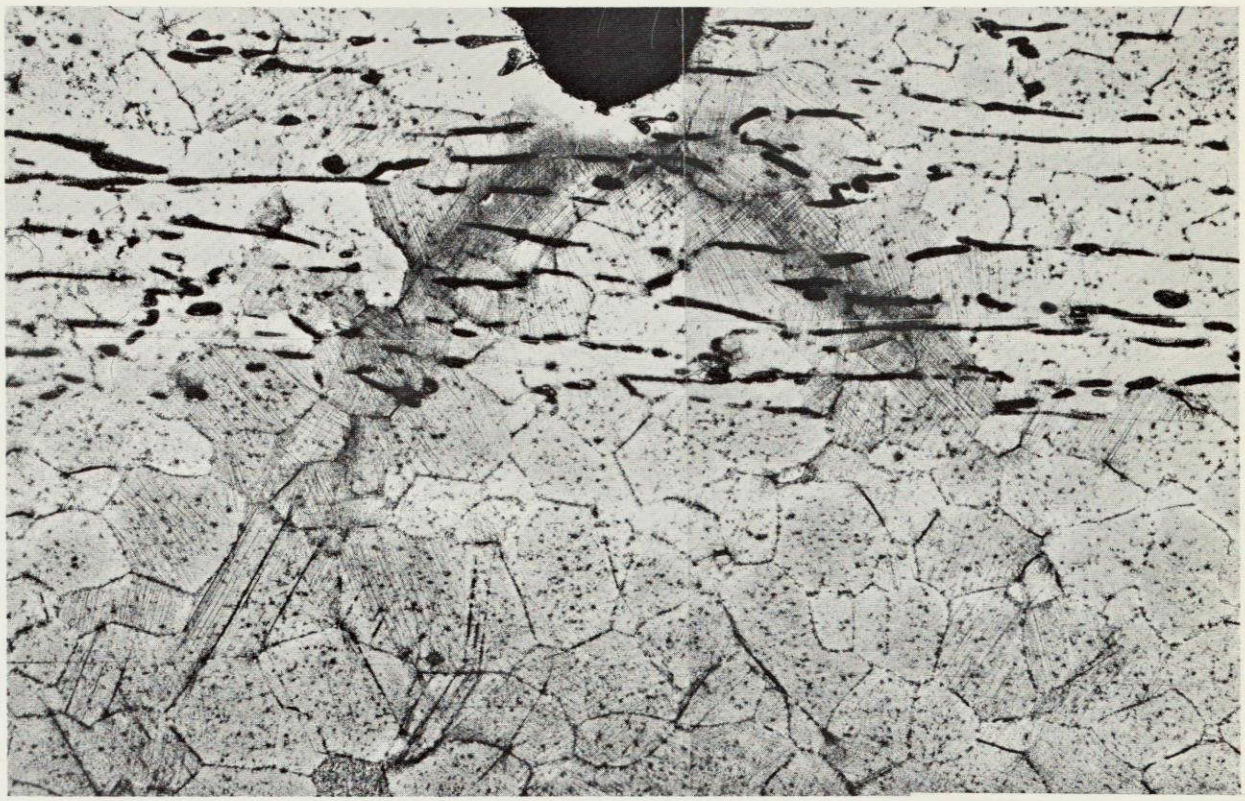

Specimen No. 97

Cross Section

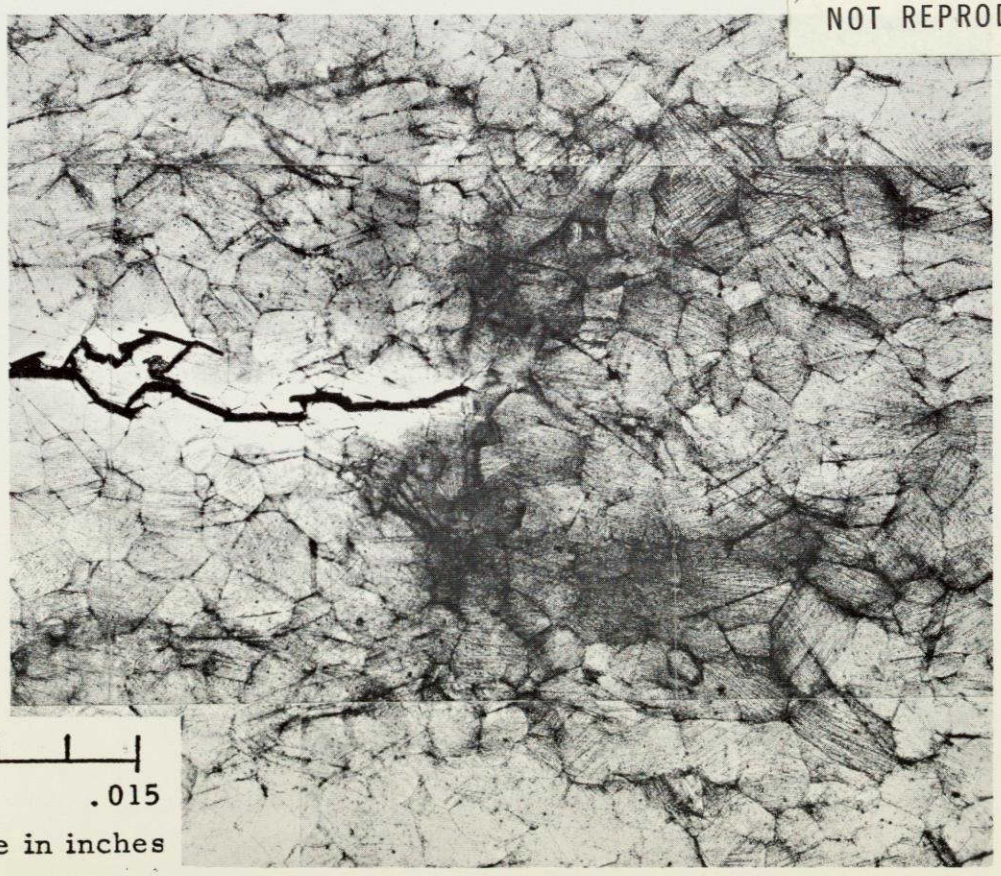

Front Surface

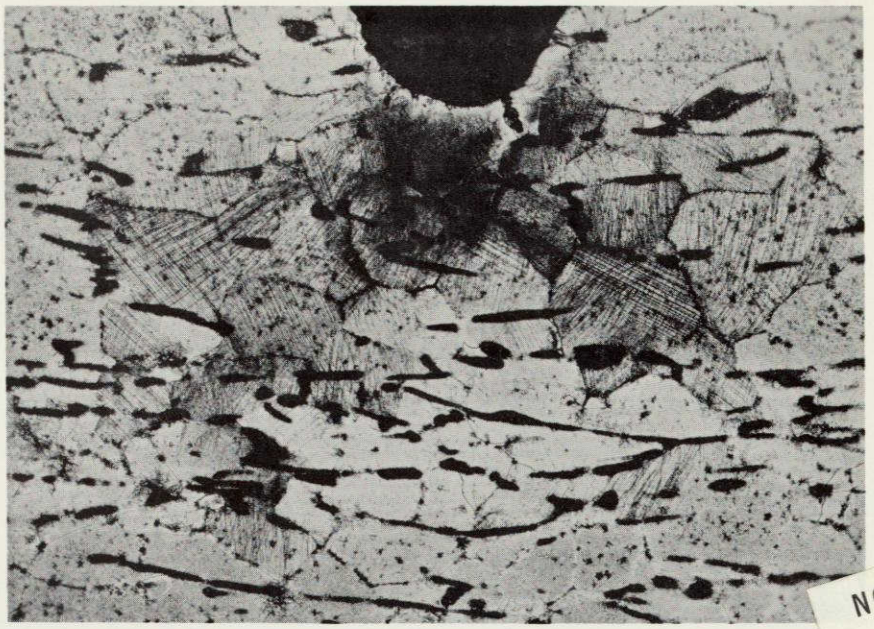

Angle Section, 75X Specimen No. 98

Cross Section Showing Back Surface, 75X

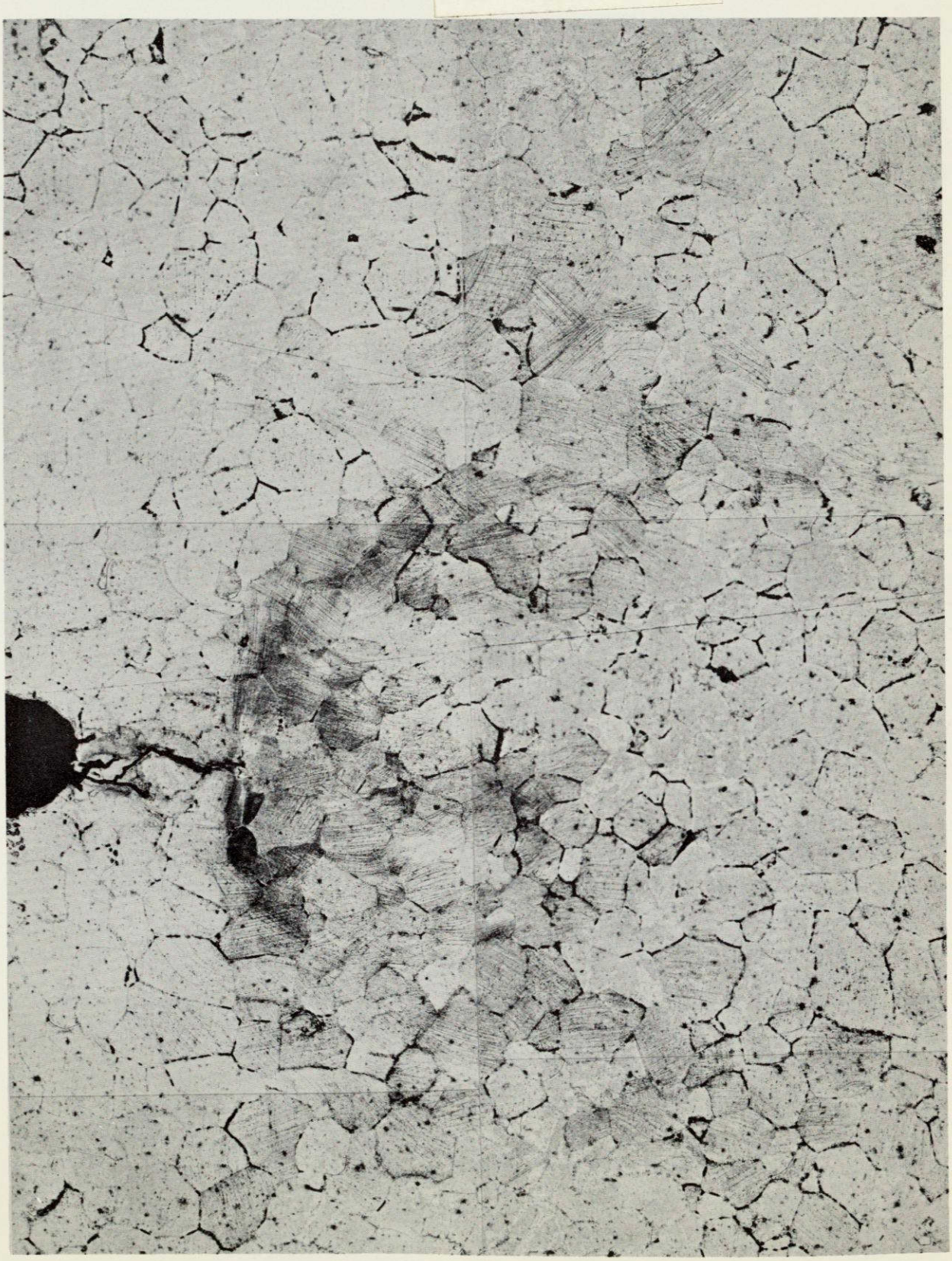

Front Surface, 75X

Specimen No. 98

Cross Section, 75X Specimen No. 99

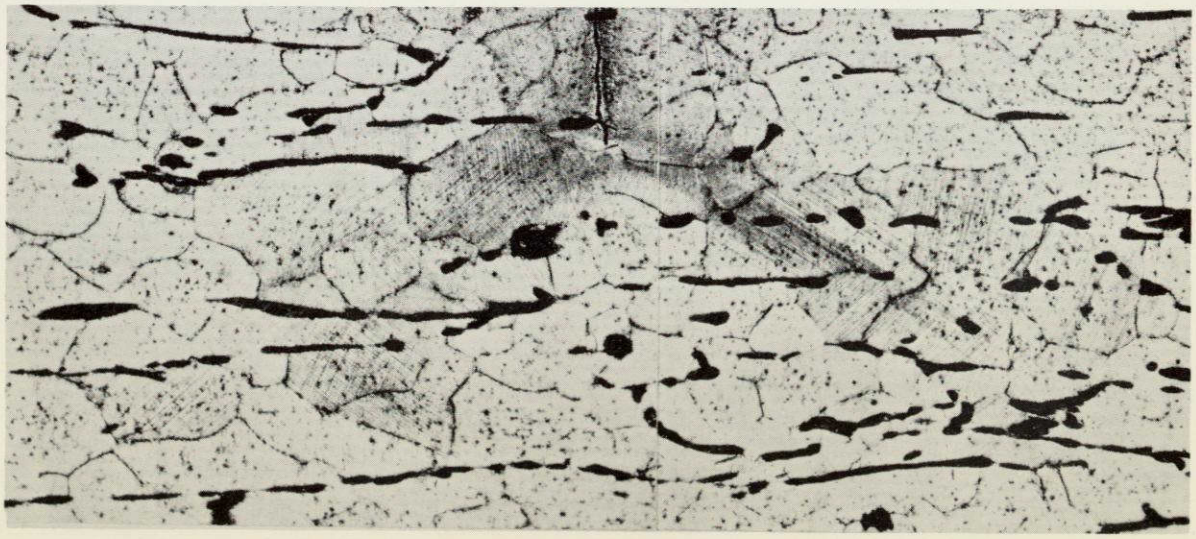

Angle Section, 75X